ДОКЛАДЫ
АКАДЕМИИ НАУК СССР

SOVIET PHYSICS

"Doklady"

VOLUME 2 NUMBER 3

A Translation
of the
"Physics Section"
of the

Proceedings of the Academy of Sciences of the USSR

(RUSSIAN ORIGINAL VOL. 114, NOS. 1-6)

Published by the
AMERICAN INSTITUTE OF PHYSICS
INCORPORATED

SOVIET PHYSICS
"Doklady"

A translation of the "Physics Section" of the Proceedings of the Academy of Sciences of the USSR.

A publication of the

AMERICAN INSTITUTE OF PHYSICS

Governing Board

ALLEN V. ASTIN
WALTER S. BAIRD
JESSE W. BEAMS
HANS A. BETHE
RAYMOND T. BIRGE
RICHARD H. BOLT
FRANKLIN D. DEXTER
IRVINE C. GARDNER
SAMUEL A. GOUDSMIT
CHARLES KITTEL
HUGH S. KNOWLES
WINSTON E. KOCK
R. BRUCE LINDSAY
WILLIAM F. MEGGERS
WALTER C. MICHELS
R. RONALD PALMER
ROBERT F. PATON
JOSEPH B. PLATT
RALPH A. SAWYER
HENRY D. SMYTH
MARK W. ZEMANSKY

Officers and Staff

FREDERICK SEITZ
Chairman, Governing Board
ELMER HUTCHISSON
Director
HENRY A. BARTON
Associate Director
WALLACE WATERFALL
Executive Secretary
MARK W. ZEMANSKY
Treasurer
THEODORE VORBURGER
Advertising Manager
RUTH F. BRYANS
Publication Manager
KATHRYN SETZE
Assistant Treasurer
ALICE MASTROPIETRO
Circulation Manager
EUGENE H. KONE
Director of Public Relations

American Institute of Physics Advisory Board on Russian Translations

ROBERT T. BEYER, *Chairman*

FREEMAN DYSON, DWIGHT GRAY, MORTON HAMERMESH, VLADIMIR ROJANSKY

Advisory Editor, Soviet Physics—"Doklady": VLADIMIR ROJANSKY, Ramo-Wooldridge Corporation, Los Angeles, California

SOVIET PHYSICS—"Doklady" is a bi-monthly journal published by the American Institute of Physics for the purpose of making available in English reports of current Soviet research in physics as contained in the "Physics Section" of the Proceedings of the Academy of Sciences of the USSR. The Proceedings appears thirty-six times per year and the "Physics Sections" are accumulated and English translations of them are published in six issues per year.

Transliteration of the names of Russian authors follows the system employed by the Library of Congress.

This translating and publishing project was undertaken by the Institute in the conviction that dissemination of the results of research everywhere in the world is invaluable to the advancement of science. The National Science Foundation of the United States encouraged the project initially and is supporting it in large part by a grant. Translation and printing are being handled by Consultants Bureau, Inc.

The American Institute of Physics and its translators propose to translate faithfully all of the scientific material in the "Physics Section" of the Proceedings of the Academy of Sciences of the USSR appearing after January 1, 1956. The views expressed in the translated material, therefore, are intended to be those expressed by the original authors, and not those of the translators nor of the American Institute of Physics.

One volume is published annually. Volume 2 will consist of six issues and will contain all scientific material published in the "Physics Section" of the original Russian journal during the 1957 calendar year.

Subscription Prices:

Per year (6 issues)	
United States and Canada	$25.00
Elsewhere	27.50
Back Numbers	
Single copies	$ 5.00

Subscriptions should be addressed to the American Institute of Physics, 335 East 45th Street, New York 17, New York.

Copyright by American Institute of Physics 1958

SOVIET PHYSICS

"Doklady"

VOLUME 2, NUMBER 3 MAY-JUNE 1957

THE INFLUENCE OF CHEMICAL BONDS ON THE FINE STRUCTURE OF TITANIUM Kβ LINES IN COMPOUNDS

E. E. Vainshtein and Iu. N. Vasil'ev

(Presented by Academician A. P. Vinogradov December 25, 1956)

We shall make a comparative study of the fine structure of the K radiation of titanium in titanium dioxide (rutile) and simple and complex titanium-tungsten carbide, nitride and hydride. The findings are of interest both for the theory of x-ray emission and the problem of the nature of chemical binding forces in these compounds.

Titanium carbide was produced by heating titanium dioxide and carbon black in a stream of hydrogen at ~2000° inside a furnace. 19.1% of carbon was bound in the carbide. The structure and lattice constant of the compound as determined by x-ray study were in good agreement with [1]. The investigated complex carbide $TiWC_2$ was an industrial sample containing 24.05% Ti and 9.5% of bound carbon.*

The titanium nitride was obtained by the method described in [2]; titanium metal was heated in a nitrogen stream inside a porcelain furnace tube at 1200°. For the removal of oxygen the nitrogen gas passed through bubblers containing an alkali solution of pyrogallol and copper chips heated to 600°. The crystal structure of the nitride was studied by x-rays. We confirmed earlier studies [3] and proved that the structure remains unchanged under the conditions arising at the anode of the x-ray tube during primary excitation of the titanium spectrum.

The method of [4] was used to prepare titanium hydride by heating degassed titanium metal powder in a hydrogen stream in a tubular furnace at ~ 400°.

The structure of the samples before and after the x-ray spectrum studies was checked by x-rays.

The x-ray spectra were obtained from an RSD-2 vacuum x-ray spectrograph [5] with a quartz crystal as analyzer. The reflecting planes were $(10\bar{1}0)$. Johanson focusing [6] was used in the spectrograph. For the purpose of increasing the resolving power of the instrument at small angles of reflection the surface of the bent crystal was cut to form a small angle (~10°) with the reflecting planes of the crystal [7]. The bent crystal surface had the dimensions 10 x 50 mm. The crystal was bent in a special crystal holder [5] where the crystal plate was bent elastically on four supports. Second order reflection spectra were photographed on a film which was placed perpendicular to the direction of the diffracted x-ray beam. The dispersion of the instrument in the studied region of the spectrum was ~6 XU/mm. Each sample was placed on the copper anode of the x-ray tube, which was operated at 55 ma and 12 kv. The spectrograms were studied with a MF-2 photometer in three sections and the data were averaged. Each substance gave three well reproduced microphotograms. The $K\beta''$ and $K\beta_5$ lines were on the descending curve with respect to the much more intense $K\beta_1$ line. Weak x-ray lines were resolved as in previous work [8]. This is illustrated by the curves for titanium metal in Fig. 1. *

---

*The sample was kindly supplied by E. A. Shchetilina.

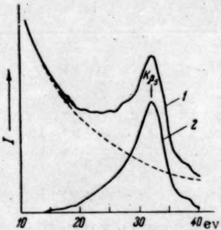

Fig. 1. Intensity of titanium metal $K\beta_5$ line (according to [8]): 1) Total experimental curve; 2) $K\beta_5$ line after allowance for $K\beta_1$ intensity.

Figs. 2 and 3 give the experimental results which characterize the relative positions, shape and intensities of the $K\beta''$, $K\beta_5$, $K\beta_1'''$ and $K\beta_2'''$ lines of titanium in the different compounds.** At the same time we studied the position and shape of the $K\beta_1$ titanium line in these compounds. The $K\alpha_{1,2}$ doublet of vanadium was used as a reference line in the study of the positions of titanium $K\beta_1$ and $K\beta_5$. The positions of the other titanium lines were determined with respect to $K\beta_5$.

The following conclusions can be drawn from the data:

1. The shape and position of some of the emitted Kβ lines ($K\beta_1$ and $K\beta'''$) in the investigated compounds is practically unvaried; their relative intensity is also unchanged. For example, the intensity of titanium $K\beta_2'''$ in all of the compounds is about 1/3 of the $K\beta_5$ intensity.***

2. Unlike the $K\beta_1$ and $K\beta'''$ lines the titanium $K\beta_5$ line was considerably influenced by the chemical bond. In the oxide and both carbides (Fig. 2) its position remains unchanged. In the nitride a long-wave shift of the $K\beta_5$ peak is observed (~ 1.6 ev), which indicates that the corresponding energy bands in the compounds are less completely filled by electrons. In the hydride an even greater shift of the $K\beta_5$ peak is observed. A check showed that such is the case despite the provisional character of the data for the hydrides, which were obtained by primary excitation and thus showing the effects of distortions resulting from chemical decomposition of the original substance and the accumulation**** during the investigation of the phase with the smaller hydrogen content. The $K\beta_5$ band of titanium in the hydride has a complex structure under these conditions. It is characterized by two pronounced peaks whose relative intensity varies with the length of the exposure and the experimental procedure, that is, it depends on the degree of decomposition of the original substance and the relative amounts of the resultant components with different hydrogen content. The energy position of both peaks remains unchanged. By comparison with the titanium $K\beta_1$ peak in the carbide the short-wave $K\beta_5$ peak in the hydride is shifted in the short-wave direction by 1.6 ev, and the long-wave peak is shifted in the opposite direction by 3.9 ev.

3. The $K\beta''$ line of the metal shows an especially marked effect of the chemical bond. A change of the anion results in considerable shifting of these lines and change of their shape as well as a strong effect on their relative intensity. In TiO_2, TiC, $TiWC_2$, TiN and TiH the relative intensity of the $K\beta''$ line is gradually reduced until it practically disappears from the hydride. The ratio of the integral intensities of the $K\beta''$ and

---

*Taken from [8].

**$K\beta_1'''$ and $K\beta_2'''$ of titanium in $TiWC_2$ were not measured because the more intense tungsten emission was superimposed.

***The appearance of a $K\beta'''$ satellite in the x-ray emission spectra of elements is sometimes explained by electron transmissions in multiply-ionized atoms. In this connection it is significant that the relative intensities and energy difference of the two lines $K\beta_2'''$ and $K\beta_1'''$ which we observed are very similar to the case for $K\beta_5$ and $K\beta''$. It is therefore possible that each of these pairs of lines results from analogous transitions in titanium atoms that are in different excited states. This hypothesis would enable us to understand the practically unchanged position of the K_1''' and K_2''' lines with respect to the first group of lines in different compounds and makes it probable that the relative intensity of these lines depends on the method of exciting the x-ray spectra.

****This is evidenced by the x-ray structural analysis of the original sample and of the hydride that was removed from the x-ray tube after the titanium spectra were studied.

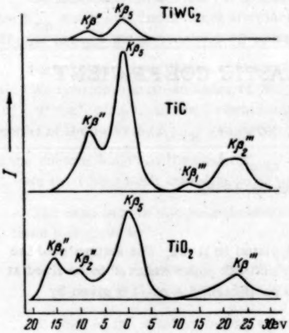

Fig. 2. Relative positions and shapes of the Kβ lines of titanium in $TiWC_2$, TiC and TiO_2.

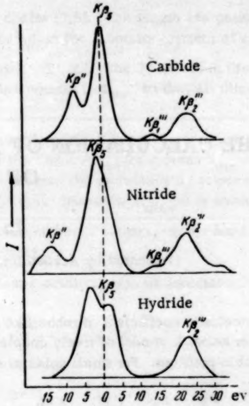

Fig. 3. Relative positions and shapes of the Kβ lines of titanium in the simple carbide, nitride and hydride.

$K\beta_5$ lines in titanium spectra in the compounds was 0.52 for rutile, 0.4 for simple and complex carbide and 0.18 for the nitride. This is in good qualitative agreement with the mechanism for the production of this satellite which we proposed previously [8], the verification of which was one of the most important purposes of the present investigation.

The relatively high resolution of the instrument permitted clearer resolution than in [8] of the two components of the Kβ '' line in the emission spectra of titanium and rutile. It is significant that for the compounds which we studied the separation of the Kβ '' and $K\beta_5$ lines in the titanium spectrum is smallest in the carbides, in which these two lines are essentially a single emission band with two characteristic peaks. Titanium dioxide (especially with regard to the titanium spectrum in brookite and anatase [8]) and nitride differ qualitatively from the carbide in this respect.

The authors thank K. I. Tobelko for the x-ray structural analysis of the materials used in this investigation.

LITERATURE CITED

[1] Ia. S. Umanskii and S. S. Khidekel', J. Phys. Chem. (USSR) 15, 9 (1941).

[2] C. Agte and K. Moers, Z. anorg. allgem. Chem. 198, 233 (1931).

[3] A. Kh. Breger, J. Phys. Chem. (USSR) 13, 272, 1482 (1939).

[4] L. Kirschfeld and A. Sieverts, Z. phys. Chem., A 145, 227 (1929).

[5] K. I. Narbutt, E. E. Vainshtein, A. B. Gil'varg and L. M. Beliaev, Bull. Acad. Sci. USSR, Phys. Ser. 1956, 20, 152.

[6] T. Johanson, Z. f. Phys. 82, 507 (1933).

[7] V. N. Protopopov, Factory Lab. (USSR) 14, 196 (1948).

[8] E. E. Vainshtein, I. B. Staryi and M. N. Brill', Bull. Acad. Sci. USSR,Phys. Ser. 1956, 20, 784.

V. I. Vernadskii Institute for Geochemistry and
Analytic Chemistry, Academy of Sciences, USSR

Received December 22, 1956

ON THE CALCULATION OF THE PHOTOELASTIC COEFFICIENT OF POLYMERS

Iu. Ia. Gotlib

(Presented by Academician A. F. Ioffe November 23, 1956)

The photoelastic coefficient of rubberlike polymers has been calculated in [1-3]. The authors used the Gaussian polymer network model of freely coupled chains with the inner network points assumed to be fixed at their most probable positions. For small uniaxial strains the photoelastic coefficient $B = \Delta n/t$ is given by

$$B = \frac{2\pi}{27}\,\frac{(\overline{n}^2 + 2)^2}{\overline{n}}\,\Delta A, \tag{1}$$

where $\Delta n = n_1 - n_2$; n_1 and n_2 are the refractive indices for light polarized in the direction of the strain and in the plane perpendicular to this direction; $\overline{n} = {}^1/_2\,(n_1 + n_2)$; ΔA is the mean anisotropy of the polymer chain in the coordinate system associated with the chain; $\underline{t}$ is the stress per unit area of the specimen cross section.

In this note we shall show that (1) can be applied to any polydisperse Gaussian network consisting of chains with quenched internal rotations, taking account of the oscillations of the internal network points. We shall use the theory of the mechanical properties of Gaussian networks which was developed by Guth and James and is based on the same assumptions [4-6].

Let us consider birefringence in a unit cube of a block polymer whose sides are parallel to the axes of the laboratory Cartesian coordinates X, Y, Z. The dimensions of the specimen after deformation are L_x, L_y, L_z and constancy of volume requires $L_x L_y L_z = 1$. The coordinates of the network points on the surface of the specimen ("fixed" points [5,6]) are denoted by the Greek letters α, β, γ,...; the coordinates of all points (fixed and internal so-called free points) will be denoted by the Latin letters m, n, ...

For a uniaxial strain along the Z axis ($L_y = L_x$) in Gaussian networks of chains with quenched internal rotation [4,6] the following relations hold between the stress $t_z = t$ per unit of actual cross section normal to the strain axis and the relative strain L_z:

$$t_z = kKT\left(L_z^2 - \frac{1}{L_z}\right), \tag{2}$$

where $\underline{k}$ is Boltzmann's constant; T is the absolute temperature; K is a constant which for an isotropic network is

$$K = \frac{1}{l_{\text{eff}}^2}\sum_{\alpha>\beta}\sum\frac{(r_\alpha^{(0)} - r_\beta^{(0)})^2}{N'_{\alpha\beta}} = \frac{3}{l_{\text{eff}}^2}\sum_{\alpha>\beta}\sum\frac{(u_\alpha^{(0)} - u_\beta^{(0)})^2}{N'_{\alpha\beta}}; \tag{3}$$
$$u_\alpha - x_\alpha,\ y_\alpha,\ z_\alpha;$$

$r^{(0)}$ and $r_\beta^{(0)}$ are the radius-vectors of the fixed ponts in an undeformed specimen; N'_β are complicated functions of all N_m, i.e. of the numbers of links in all chains of the specimen. The mean square length $\overline{h^2}$ of a Gaussian chain consisting of N_{mn} links is expressed in terms of the parameter l_{eff}^2 as follows:

$$\overline{h_{mn}^2} = N_{mn} l_{\text{eff}}^2 + g + o(\lambda^{N_{mn}}), \quad |\lambda| < 1, \quad g \sim 1. \tag{4}$$

The values of l^2_{eff} are determined by the internal structure of the chains [7,8]. The length and position of the chain uniting two neighboring points $\underline{m}$ and $\underline{n}$ is given by the vector $\mathbf{h}_m$ in the laboratory system of coordinates.

We introduce the auxiliary molecular system of coordinates X', Y', Z'. The Z' axis is in the direction of the vector $\mathbf{h}_{mn}$ and the X' and Y' axes are placed anywhere in the plane normal to $\mathbf{h}_{mn}$, so that all directions perpendicular to $\mathbf{h}_{mn}$ are physically equivalent.

For a given h_{mn} a chain can assume many configurations, each of which has a characteristic polarizability. We consider the mean value of the polarizability tensor of the chain $A_{u'v'}$ for a given $h_{mn} = h(u'; v' - x', y', z')$. In the Gaussian region it is possible to decompose the polarizability tensor components in powers of the ratio (h/h_{max}) just as for freely linked chains [1,2,4,9]. Instead of h_{max} it is convenitent to take the contour length of the chain $h'_{max} = N_{mn} l$, where N_{mn} is the number of links; $\underline{l}$ is the bond length C–C. We shall here limit ourselves to chains of the type $(-CH_2-CHR-)_n$.

The expansion of the polarizability tensor of a chain in the molecular system of coordinates X', Y', Z' with fixed $\underline{h}$ is given by

$$A_{u'u'} = A_{00} + \Gamma_{u'u'}\left(\frac{h}{N_{mn}l}\right)^2 + \ldots; \quad u' - x',\ y',\ z'. \tag{5}$$

Because of the axial symmetry of the tensor A_{ik} we can write $A_{x'x'} = A_{y'y'} = A_\perp$; $\Gamma_{x'x'} = \Gamma_{y'y'} = \Gamma_\perp$; $A_{z'z'} = A_\|$ and $\Gamma_{z'z'} = \Gamma_\|$. The nondiagonal components of the averaged tensor vanish when averaged over all angles of rotation of the chain around the Z' axis. Since the polarizability tensor of the chain is an additive quantity the coefficients $\Gamma_\|$ and $\Gamma_\perp$ can be represented as $\Gamma_\| = N_{mn}\gamma_\|$ and $\Gamma_\perp = N_{mn}\gamma_\perp$, where $\gamma_\|$ and $\gamma_\perp$ represent the contribution of a single monomeric unit. We shall now write the expression for the average tensor of a given chain in the laboratory system:

$$P^{(mn)} = A_{00}^{(mn)} \cdot I + (A_\|^{(mn)} - A_\perp^{(mn)}) \cdot S, \tag{6}$$

Where I is the unit tensor; $S_{uu} = \cos^2(\mathbf{z}',\mathbf{u}) - {}^1/_3$; $S_{uv} = \cos(\mathbf{z}',\mathbf{u})\cos(\mathbf{z}',\mathbf{v})$, u, v − X, Y, Z.

Inserting (5) in (6) and summing over all chains in a unit volume we obtain an expression for the tensor of the mean polarizability of a unit volume for given positions of all internal points and outer fixed points:

$$P = P_{00} + (\gamma_\| - \gamma_\perp)\, R, \tag{7}$$

where

$$R_{uv} = \sum_{m>n}\sum \frac{(u_m - u_n)(v_m - v_n)}{N_{mn}l^2} - \frac{1}{3}\delta_{uv} \sum_{m>n}\sum \frac{(\mathbf{r}_m - \mathbf{r}_n)^2}{N_{mn}l^2};$$
$$u_m,\ v_m - x_m,\ y_m,\ z_m.$$

In deriving (7) we use the fact that $h_{mn}\cos(\mathbf{z}', \mathbf{u}) = u_m - u_n$.

Equation (7) must be averaged over all positions of the internal points. The probability of a given distribution of all points of a Gaussian network is given by [6]

$$W(\ldots \mathbf{r}_m,\ \mathbf{r}_n \ldots) = C \exp\left\{-(3/2\, l^2_{\text{eff}}) \sum_{m>n}\sum [(\mathbf{r}_m - \mathbf{r}_n)^2 / N_{mn}]\right\}. \tag{8}$$

Then the average of the sum $\sum_{m>n}\sum [(u_m - u_n)^2 / N_{mn}l^2] \equiv \sum_{uu}$ over all positions of internal points using the distribution function (8) will be

$$\overline{\sum_{uu}} = (l_{\text{eff}}^2/l^2)\left[\int \sum_{uu} \cdot w\, d\gamma_{\text{int}}\right] \Big/ \left[\int w\, d\gamma_{\text{int}}\right]. \tag{9}$$

The integration in (9) is carried out over all positions of internal points. In [5] it was shown that

$$\int \cdots \int \exp\left\{-\frac{3}{2l_{\text{eff}}^2}\sum_{m>n}\sum \frac{(u_m-u_n)^2}{N_{mn}}\right\} d\gamma_{\text{int}} = C_u \exp\left\{-\frac{3}{2l_{\text{eff}}^2}\sum_{\alpha>\beta}\sum \frac{(u_\alpha-u_\beta)^2}{N'_{\alpha\beta}}\right\}. \tag{10}$$

Here u_α and u_β are the coordinates of the outer fixed points in the deformed specimen; $N''_{\alpha\beta}$ are the same constants as in (3); C_u is a complicated function of all N_{mn} and l^2_{eff}.

We introduce the auxiliary parameter τ ; then

$$\overline{\sum_{uu}} = -\frac{2}{3}\frac{l_{\text{eff}}^2}{l^2}\lim_{\tau\to 1}\left\{\frac{d}{d\tau}\ln\left[\int \exp\left(-\frac{3}{2l_{\text{eff}}^2}\tau\sum_{m>n}\sum\frac{(u_m-u_n)^2}{N_{mn}}\right) d\gamma_{\text{int}}\right]\right\}. \tag{11}$$

If in the direction u the specimen is deformed by the factor L_u we have $u_\alpha = u_\alpha^{(0)} L_u$ and using (10) and (11) we obtain

$$\overline{\sum_{uu}} = \frac{l_{\text{eff}}^2}{l^2}\{\lim_{\tau\to 1}\ln C_u(\tau) + {}^1/_3 L_u^2 K\}, \quad u - x,\ y,\ z. \tag{12}$$

C_u does not depend on the coordinates of the outer fixed points or on the degree of strain $L_x = L_y$ and L_z. Because of the isotropy of the network before deformation

$$C_x = C_y = C_z. \tag{13}$$

In order to calculate Δn we use the condition $L_y^2 L_z = 1$, the Lorentz-Lorenz equation for the refractive indices n_1 and n_2 and the smallness of $\Delta n = n_1 - n_2$ compared with n_1 and n_2. The light beam is parallel to the X axis. The Lorentz-Lorenz equation gives

$$= \frac{n_2^2-1}{n_2^2+2} \text{ and } \frac{4}{3}\pi P_{zz} = \frac{n_1^2-1}{n_1^2+2}.$$

After some simple manipulations we obtain the following expressions for Δn and B:

$$\Delta n = n_1 - n_2 = \frac{2\pi}{27}\frac{(\bar{n}^2+2)}{\bar{n}}\frac{l_{\text{eff}}^2}{l^2} K\left(L_z^2 - \frac{1}{L_z}\right)(\gamma_\parallel - \gamma_\perp), \tag{14}$$

$$B = \frac{\Delta n}{t_z} = \frac{2\pi}{27}\frac{(\bar{n}^2+2)^2}{\bar{n}kT}\frac{l_{\text{eff}}^2}{l^2}(\gamma_\parallel - \gamma_\perp). \tag{15}$$

(15) if very important for what follows: the photoelastic coefficient of an arbitrary isotropic Gaussian network is independent of the structure of the network (on functionality and polydispersity), i.e., on N_{mn}, $r_\alpha^{(0)}$ and $r_\beta^{(0)}$, and is determined only by the anisotropy and structure of the individual polymer chains (through the parameters l^2_{eff} and $\gamma_\parallel - \gamma_\perp$).

We express the photoelastic coefficient (15) in terms of the average anisotropy of an individual chain. The average anisotropy ΔA of an individual Gaussian polymer chain is obtained from (4) and (5) as follows:

$$\Delta A = \overline{A_\parallel(h) - A_\perp(h)} = \frac{l_{\text{eff}}^2}{l^2}(\gamma_\parallel - \gamma_\perp) + O\left(\frac{1}{N}\right). \tag{16}$$

Inserting (16) in (15) we obtain the desired expression (1) for the photoelastic coefficient.

In conclusion the author sincerely thanks Professor M. V. Vol'kenshtein for his interest in this work.

LITERATURE CITED

[1] W. Kuhn and F. Grün, Koll. Z. 101, 248 (1942).

[2] A Isichara, A. Hashitsume and M. Tatibana, J. Appl. Phys. 28, 3, 308 (1952).

[3] L. R. G. Treloar, The Physics of Rubber Elasticity (Foreign Lit. Press. 1953) (Russian translation).

[4] Iu. Ia. Gotlib, Dissertation. Leningr. State Ped. Inst., 1956.

[5] H. James, J Chem. Phys. 15, 651 (1947).

[6] H. James and E. Guth, J. Polymer Sci. 4, 153 (1949). J. Chem. Phys. 1953, No. 21, 527.

[7] M. V. Vol'kenshtein and O. B. Ptitsyn, J. Phys. Chem. (USSR) 26, 1061 (1951).

[8] T. M. Birshtein and O. B. Ptitsyn, J. Phys. Chem. (USSR) 28, 213 (1954).

[9] Iu. Ia. Gotlib, M. V. Vol'kenshtein and E. K. Biutner, Dokl. Akad. Nauk SSSR 49, 935 (1954).

A. I. Herzen Leningrad State Pedagogical Institute Received November 15, 1956

ENERGY LEVEL SHIFT OF SPIN ½ PARTICLES IN A COULOMB FIELD

G. A. Zaitsev

(Presented by Academician N. N. Bogoliubov December 15, 1956)

Let a spin $^1/_2$ particle with negative charge, such as a $\mu-$ meson or electron be in a field represented by the potential $\varphi = Ze/r$, $A_k = 0$. The charge of the particle will be denoted by $-e$ ($e > 0$). From the fundamental equation for a spin $^1/_2$ particle in an electromagnetic field, which was discussed in [1], we obtain the appropriate energy levels.

We shall assume that the particle is in a stationary state so that

$$\hbar i \frac{\partial}{\partial t} \xi = E\xi, \quad \xi = [\exp(-iEt/\hbar)]\,\xi_0. \tag{1}$$

Equation (7) of [1] gives

$$\hat{H}\xi_0 = 0,$$

$$\hat{H} = \frac{1}{r^2}\left(\frac{\partial}{\partial r} r^2 \frac{\partial}{\partial r}\right) + \frac{1}{\hbar^2 c^2}\left[\left(E + \frac{Ze^2}{r}\right)^2 - m_0^2 c^4\right] + \frac{\nabla^2_{\vartheta\varphi} + iZ\alpha(1+\delta)\,\sigma_{(r)}}{r^2}, \tag{2}$$

where

$$\alpha = \frac{e^2}{\hbar c}, \quad \sigma_{(r)} = \frac{\sum\limits_k x^k \sigma_k}{r}, \quad \nabla^2_{\vartheta\varphi} = \frac{1}{\sin\vartheta}\frac{\partial}{\partial\vartheta}\left(\sin\vartheta \frac{\partial}{\partial\vartheta}\right) + \frac{1}{\sin^2\vartheta}\frac{\partial^2}{\partial\varphi^2}.$$

We can separate variables by setting

$$\xi_0 = f(r)\begin{pmatrix} y_1(\vartheta, \varphi) \\ y_2(\vartheta, \varphi) \end{pmatrix},$$

with the equation

$$-[\nabla^2_{\vartheta\varphi} + iZ\alpha(1+\delta)\,\sigma_{(r)}]\begin{pmatrix} y_1 \\ y_2 \end{pmatrix} = \hat{L}y = \lambda y. \tag{3}$$

Then the energy levels will be determined from

$$\left\{\frac{\partial^2}{\partial r^2} + \frac{2}{r}\frac{\partial}{\partial r} + \frac{1}{\hbar^2 c^2}\left[\left(E + \frac{Ze^2}{r}\right)^2 - m_0^2 c^4\right] - \frac{\lambda}{r^2}\right\} f(r) = 0. \tag{4}$$

It is easily verified that $\widehat{H}$ and $\widehat{L}$ commute with the operators

$$\hat{M}_k = h\left(-i\sum_{j,s=1}^{3}\varepsilon_{kjs}x^{j}\frac{\partial}{\sigma x^{s}}+\frac{1}{2}\sigma_k\right). \tag{5}$$

The operators $\widehat{L}$, $\widehat{M}_k$ and $\widehat{M}^2 = \widehat{M}_1^2 + \widehat{M}_2^2 + \widehat{M}_3^2$ also commute with each other. Therefore we can select y_1 and y_2 such that $\underline{y}$ and thus ξ_0 also will simultaneously be an eigenfunction of the operators $\widehat{L}$, $\widehat{M}_3$ and $\widehat{M}_2$:

$$\hat{M}_3 y = hmy, \tag{6}$$
$$\hat{M}^2 y = h^2 j(j+1)y, \tag{7}$$

and the state of the particle will be characterized by the quantum numbers λ, m, j and the radial quantum number which we shall introduce later.

We know that it follows from the commutation relations between the $\widehat{M}_k$ that for a given j the following values can be assumed by m: $-j, -j+1, \ldots, j-1, j$. It is easily verified that (6) and (7) give

$$y = \begin{pmatrix} y_1 \\ y_2 \end{pmatrix} = \begin{pmatrix} \left(C_{j-{}^1/_2}P_{j-{}^1/_2,\ m-{}^1/_2} + C_{j+{}^1/_2}P_{j+{}^1/_2,\ m-{}^1/_2}\right)e^{i(m-{}^1/_2)\varphi} \\ \left(-\sqrt{\frac{j-m}{j+m}}\,C_{j-{}^1/_2}P_{j-{}^1/_2,\ m+{}^1/_2} + \sqrt{\frac{j+m+1}{j-m+1}}\,C_{j+{}^1/_2}P_{j+{}^1/_2,\ m+{}^1/_2}\right)e^{i(m+{}^1/_2)\varphi} \end{pmatrix}, \tag{8}$$

where $C_{j-1/2}$, $C_{j+1/2}$ are arbitrary constants;

$$P_{j-{}^1/_2,\ m-{}^1/_2} = \sqrt{j\,\frac{(j-m)!}{(j+m-1)!}}\,(1-x^2)^{\frac{m-{}^1/_2}{2}}\,\frac{1}{2^{(j-{}^1/_2)}(j-{}^1/_2)!}\times$$
$$\times\frac{d^{j+m-1}}{dx^{j+m-1}}(x^2-1)^{j-{}^1/_2}, \quad x = \cos\vartheta. \tag{9}$$

From the properties of the P(see, for example, [2], pp. 383-384), (3) gives the ratio $C_{j+1/2} : C_{j-1/2}$ and the third quantum number λ:

$$\lambda = (j+{}^1/_2)^2 \mp \sqrt{(j+{}^1/_2)^2 - \alpha^2(1+\delta)^2} \tag{10}$$

(for simplicity we assume here and in subsequent formulas that Z = 1).

We see that the quantum number λ for given j and m can assume only two values corresponding to the two possible signs in (10). If we neglect α^2 and in (10) assume $\alpha^2 = 0$ we can for this limiting case introduce instead of the quantum number λ another quantum number l defined by

$$\lambda = l(l+1), \quad l = j \mp {}^1/_2. \tag{11}$$

For consistency with the terminology of spectroscopy we can characterize the state of a spin $^1/_2$ particle by the number l (in addition to $\underline{j}$ and $\underline{m}$) even when we do not neglect the value of α^2. For this purpose we set $l = j - {}^1/_2$ or $l = j + {}^1/_2$, depending on the sign in (10). Then the quantum number λ can be expressed in terms of $\underline{j}$ and $\underline{l}$ as follows:

$$\lambda = (j + {}^1/_2)^2 + 2\,(l - j)\,\sqrt{(j + {}^1/_2)^2 - \alpha^2\,(1 + \delta)^2}\,. \tag{12}$$

We shall now consider the equation for the radial function (4) written in the form

$$\left(\frac{\partial^2}{\partial r^2} + \frac{2}{r}\,\frac{\partial}{\partial r} - A + \frac{2B}{r} - \frac{C}{r^2}\right) f\,(r) = 0, \tag{13}$$

where

$$A = \frac{m_0^2c^2}{\hbar^2}\left[1 - \left(1 + \frac{\mathcal{E}}{m_0c^2}\right)^2\right],\ \mathcal{E} = E - m_0c^2,\ B = \frac{m_0e^2}{\hbar^2}\left(1 + \frac{\mathcal{E}}{m_0c^2}\right),$$

$$C = \lambda - \alpha^2 = (j + {}^1/_2)^2 \mp \sqrt{(j + {}^1/_2)^2 - \alpha^2\,(1 + \delta)^2} - \alpha^2 = l'\,(l' + 1),\ \ l' > 0. \tag{14}$$

The solution of this equation is well known (see, for example, [3], p. 438). In particular, in order to obtain the discrete energy levels $\mathcal{E}$ we must introduce the radial quantum number k in accordance with the formula

$$B\,/\,\sqrt{A} = l' + k + 1. \tag{15}$$

k can assume the values 0,1,2. . . . The energy levels are obtained from

$$1 + \frac{\mathcal{E}}{m_0c^2} = \left[1 + \frac{\alpha^2}{(l' + k + 1)^2}\right]^{-1/2} = \left[1 + \frac{\alpha^2}{(k + {}^1/_2 + \sqrt{{}^1/_4 + \lambda - \alpha^2})^2}\right]^{-1/2}. \tag{16}$$

Expanding the right-hand side of (16) in powers of α^2 and limiting ourselves to terms of the order α^4 we shall have

$$\frac{\mathcal{E}}{h} = -\frac{R}{n^2}\left[1 + \frac{\alpha^2}{n^2}\left(\frac{n}{j + {}^1/_2} - {}^3/_4\right) \mp \frac{\alpha^2\,(\delta + {}^1/_2\delta^2)}{n\,(j + {}^1/_2)\,(j + {}^1/_2 \mp {}^1/_2)}\right], \tag{17}$$

where

$$R = \frac{m_0e^4}{4\pi\hbar^3} = \frac{\alpha^2 m_0c^2}{2h},\ \ n = j + 1 \mp {}^1/_2 + k = l + k + 1.$$

Thus the difference δ between the magnetic moment of the particle and the corresponding magneton results in a shift of the energy levels from those obtained through the Dirac equation with neglect of this difference. In particular the separation of the levels $2^2S_{1/2}$ and $2^2P_{1/2}$ according to (17) is now given by

$$h\,[\nu\,(2^2S_{1/2}) - \nu\,(2^2P_{1/2})] = \frac{h}{3}\,R\alpha^2\,(\delta + {}^1/_2\,\delta^2). \tag{18}$$

LITERATURE CITED

[1] G. A. Zaitsev, Dokl. Akad. Nauk SSSR 113, 6, 1248 (1957) [Soviet Physics - Doklady, p. 199].

[2] H. Bethe, The Quantum Mechanics of One- and Two-Particle Systems (1935) (Russian translation).

[3] A. A. Sokolov and D. D. Ivanenko, Quantum Theory of Fields (1952) (in Russian).

Received October 28, 1954

TEMPERATURE DEPENDENCE OF THE g-FACTOR AND RELAXATION TIME IN FERROMAGNETIC RESONANCE OF SOME FERRITES

Academician A. P. Komar (Academy of Sciences,
Ukrainian SSR) and N. I. Krivko

We know that the study of ferromagnetic resonance makes it possible to investigate the behavior of electron spins in a lattice under different conditions. Experiment leads to a determination of the spectroscopic splitting factor g and the relaxation time T from the absorption curves of electromagnetic vibrations of frequency ω^2 10^{10} cps and the dispersion of the effective magnetic permeability in varying magnetic fields accompanied by a steady magnetizing field.

On the basis of the general theory of L. D. Landau and E.M. Lifshits [1] for the behavior of ferromagnetic materials in varying magnetic fields various authors [2] have proposed "resonance" formulas connecting g, ω, H, I and T, where I is the saturation magnetization. According to A. I. Pil'shchikov [3] the important resonance parameters g and T can be determined quite accurately from absorption and dispersion extrema. The relaxation time can also be evaluated from the half width of the absorption curves.

For the calculation of g and T we have used the familiar equations which are adapted to our experimental method:

$$\omega^2 = g^2 \left(\frac{e}{2mc} \right)^2 H \, [H \, (N_y - N_z) I] + \frac{1}{T^2}, \tag{1}$$

$$\frac{1}{T} = g^2 \left(\frac{e}{2mc} \right)^2 \frac{[H_2 - H_1] \, [H_2 - H_1 (N_y - N_z) \, I]}{4\omega}. \tag{2}$$

We have determined g and T for two groups of technical ferrites of the compositions $NiO \cdot ZnO \cdot Fe_2O_3$ and $Li_2O \cdot ZNO \cdot Fe_2O_3$. The ferrites were prepared by sintering with fragments of the oxides on the grain boundaries. Measurements were obtained at 290° and 4.2° K with the frequency 9.4×10^9 cps.

We obtained magnetization curves and determined the saturation magnetization for all of the ferrites. The latter was obtained in relatively weak fields (H < 1400 oersteds). Ferromagnetic resonance was investigated with two rectangular and coaxial waveguides. The planes of the ferrite disks placed in the waveguides were normal to the axis of the latter. The steady magnetic field was perpendicular to the varying magnetic field. The ferrite disks were of 8 mm diameter with thickness varying from 0.2 to 1.15 mm. Each disk had a circular aperture of 2 mm diameter. Both the calculations and measurements showed that the apertures in the thin disks did not seriously affect the demagnetizing factors N_x and N_y. The steady magnetic field could be varied from 0 to 26,000 oersteds. For the generation and measurement of the electromagnetic field we used standard apparatus covering the range 8600-9600 Mc. The gilt measuring line with controlled probe load was supplemented by two gages which enabled us to measure the probe position with 0.005 mm accuracy. The signal from the silicon detector was fed to a galvanometer of 9×10^{-11} amp/mm sensitivity or a 28I amplifier. The inner surface of both the rectangular and coaxial waveguides was silvered. The outer cylinder of the coaxial waveguide was made of quartz. Fig. 1 is a block diagram of the apparatus.

TABLE 1

Composition of ferrites	I in gauss/cm³		N_x		$\frac{\text{Diameter}}{\text{Thickness}}$
	290° K	4,2° K	Exper.	Calc.	
18% Li_2O, 2% ZnO, 80% Fe_2O_3	265	361	1.67	1.79	5.52
18% Li_2O, 2% ZnO, 80% Fe_2O_3	265	361	1.20	1.19	8.27
20% Li_2O, 80% Fe_2O_3	264	357	1.63	1.93	5.12
20% Li_2O, 10% ZnO, 70% Fe_2O_3	289	367	1.88	2.09	4.77
16,7% NiO, 37,3% ZnO, 46% Fe_2O_3	282	544	1.63	2.17	4.55
18% NiO, 42% ZnO, 40% Fe_2O_3	277	525	1.76	2.18	4.52

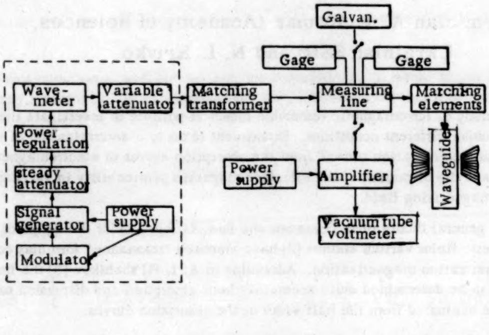
Galvan.
Gage
Gage
Wave-meter
Variable attenuator
Matching transformer
Measuring line
Matching elements
Power regulation
steady attenuator
Power supply
Amplifier
Waveguide
Signal generator
Power supply
Vacuum tube voltmeter
Modulator

Fig. 1.

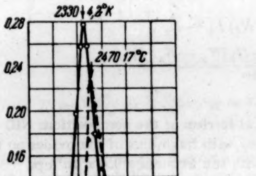

Fig. 2.

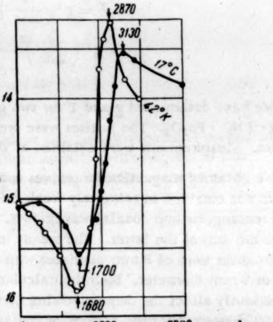

Fig. 3.

TABLE 2

Ferrites	g		$T\cdot10^{10}$, sec	
	290° K	4,2° K	290° K	4,2° K
18% Li_2O, 2% ZnO, 80% Fe_2O_3	2.07	2.04	4.8	4.5
20% Li_2O, 80% Fe_2O_3	2.03	1.84	5.1	3.8
20% Li_2O 10% ZnO, 70% Fe_2O_3	2.05	2.03	4.8	5.6
16,7% NiO, 37,3% ZnO, 46% Fe_2O_3	2.23	1.86	11.0	4.0
18% NiO, 42% ZnO, 40% Fe_2O_3	2.06	1.73	4.3	4.8

The absorption curves (in relative units) and the dispersion curves (in scale units of the measuring line) are shown in Figs. 2 and 3.

The data in Table 2 show that for some of the ferrites the g-factor is reduced at low temperatures to a value that lies outside the limits of random experimental errors, which are estimated at 4%. No general tendency was detected in the variation of the relaxation time. The variation of g at low temperatures cannot be explained by existing microscopic theories.

LITERATURE CITED

[1] L. Landau and E. Lifshitz, Phys. Z. Sowjetunion 8, 153 (1935).

[2] Ferromagnetic Resonance, A Collection, (Foreign Lit. Press, 1952) (Russian translation).

[3] A. I. Pil'shchikov, J. Exptl. Theoret. Phys. (USSR) 29, 798 (1955).

Physicotechnical Institute, Academy of Sciences USSR

Received December 24, 1956

ON THE RELATION BETWEEN THE ELECTRICAL PROPERTIES OF CRYSTALS AND THE LATTICE PARAMETERS

V. A. Presnov and V. I. Haman

(Presented by Academician A. F. Ioffe December 28, 1956)

In [1-4] it was shown experimentally that there is a relation between the electrical properties of crystals and the lattice parameters. In particular, a relation was established between the electrical strength and loss angle on the one hand and the lattice energy on the other hand. In the present article we present a preliminary calculation of the relation between the electrical strength and lattice parameters of crystals.

In a strong electric field the average energy of an electron interacting with a phonon gas is [5]

$$\varepsilon \sim mv^2 \sim eEl\frac{v}{a} \sim eE\frac{l}{a}\sqrt{\frac{kT}{m}},$$

where m is the electron mass; k is the Boltzmann constant, T is the absolute temperature; E is the electric field strength; l is the electron mean free path; and a is the phonon speed of propagation (in this instance we are considering the beginning of the acoustical branch). A crystal is punctured when the electron energy is greater or equal to the width of the forbidden band; the breakdown condition can be written as

$$eE_{\mathrm{br}}\frac{l}{a}\sqrt{\frac{kT}{m}} \simeq u_0, \tag{1}$$

where u_0 is the width of the forbidden zone of the crystal. The speed of phonon propagation [6] is

$$a = r_0\sqrt{\frac{\alpha}{2(M_1+M_2)}},$$

where α is the quasi-elastic force constant; M_1 and M_2 are the masses of the particles which form the crystal; and r_0 is the lattice constant. Inserting a in (1) we obtain

$$E_{\mathrm{br}} \simeq \frac{u_0}{el}\sqrt{\frac{m}{kT}}\,r_0\sqrt{\frac{\alpha}{2(M_1+M_2)}};$$

but $l = Br_0$ [5], so that

$$E_{\mathrm{br}} \simeq \frac{u_0}{Be}\sqrt{\frac{m}{kT}}\sqrt{\frac{\alpha}{2(M_1+M_2)}}. \tag{2}$$

We shall calculate E_{br} for NaCl from (2); the value of α is given by T.A. Kontorova [7] as $3.45 \cdot 10^4$; B can be set equal to 10. Then $E_{\mathrm{br}\,\mathrm{NaCl}} \simeq 1.92 \cdot 10^6$ v/cm. The calculated value is in quite good agreement with the experimental value.

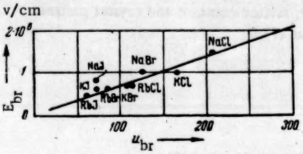

Fig. 1.

TABLE 1

Crystal	$E_{br}\cdot 10^{-6}$ v/cm	
	Experim.	Theoret.
NaCl	1,5	1,92
NaBr	1	1,15
KCl	1	1,54
KBr	0,7	1,02
KJ	0,6	0,65
RbCl	0,7	1,00
RbBr	0,6	0,8
RbJ	0,5	0,55
NaJ	0,8	0,65

The force constant is given by [7]

$$\alpha = \frac{mnU}{r_0^2}\,, \tag{3}$$

where U is the lattice energy per ion pair; m = 1; n for alkali halides varies within different limits according to different authors. Inserting (3) in (2) and replacing all constants by their values we obtain

$$E_{br} \simeq 30{,}85\,\frac{n^{1/2}U^{1/2}u_0}{r_0\sqrt{2\,(M_1+M_2)}}\,. \tag{4}$$

The curve representing E_{br} vs $u_{br} = \dfrac{n^{1/2}U^{1/2}u_0}{r_0\sqrt{2\,(M_1+M_2)}}$ must be a straight line. Fig. 1 shows that von Hippel's values of E_{br} approximately fit a straight line. (2) or (4) can be used for a theoretical calculation of the breakdown potentials of alkali halide crystals.

Table 1 gives the calculated and experimental values of E_{br}. The values of u_0 are taken from [8]. We see that the calculated values of E_{br} for the different alkali halide crystals are in good agreement with experiment [1].

Another important electrical characteristic of a crystal is the electrical field strength at which the electrical conductivity begins to depart from Ohm's law. Experiments show that the field E_r at which such a departure from Ohm's law begins is not the same for all crystals [9]. In this instance also it is possible to establish the relation between E_r and the lattice parameters.

It is known [10] that the spherical portion of the electron distribution function in an electrical field is given by

$$n_0 = A\exp\left[-\frac{1}{kT}\int\frac{b\,d\varepsilon}{b+{}^2/_3\,\tau(eEv)^2}\right], \tag{5}$$

where $b = \overline{\Delta\epsilon^2}/2t$ ($\overline{\Delta\epsilon^2}$ is the mean square energy transferred per collision; t is the energy transfer time); ϵ is the mean electron energy; τ is the mean free time.

For a semiconductor or dielectric $\Delta\epsilon^2 = {}^2/_3\,\epsilon\, ma^2$.

Inserting b in (5) we have

$$n_0 = A_{\exp}\left[-\frac{1}{kT}\int\frac{\varepsilon\, d\varepsilon}{\varepsilon+\dfrac{2\tau^2}{ma^2}\,(eEv)^2}\right]. \tag{6}$$

If we neglect the second term in the denominator of the integrand the relation between the electrical conductivity and the field is given by Ohm's law; on the other hand, if we neglect the first term we obtain a departure from Ohm's law [10]. Thus the critical field (at which the departure from Ohm's law begins) can be estimated from the relation

$$\varepsilon \simeq \frac{2\tau^2}{ma^2}\,(eE_r v)^2\,.$$

Substituting $\tau = l/v$, ϵ, a and considering that $l = Br_0$, we obtain

$$E_r \simeq \frac{\sqrt{kTm}}{2Be}\sqrt{\frac{\alpha}{2\,(M_1+M_2)}} = \frac{\sqrt{kTm}}{2Be}\,\frac{n^{1/2}U^{1/2}}{r_0\sqrt{2\,(M_1+M_2)}}\,. \tag{7}$$

Thus in accordance with experimental findings the electrical strength of crystals and the critical field at which the departure from Ohm's law begins depend on the lattice energy, lattice constant and crystal particle masses. The functional relationship of these quantities is given by (4) and (7).

LITERATURE CITED

[1] A. V. Hippel, Zs. f. Phys. 88, 358 (1934).

[2] A. A. Vorob'ev and E. K. Zavadovskaia, Dokl. Akad. Nauk SSSR 81, No. 3 (1951).

[3] A. A. Vorob'ev, J. Tech. Phys. (USSR) 26, 2, 330 (1956). [Soviet Physics - Technical Physics, p. 324.]

[4] A. A. Vorob'ev, K. A. Vodop'ianov and M. A. Krivov, Dokl. Akad. Nauk SSSR 106, No. 6 (1954).

[5] L. Z. Gurevich, Elements of Physical Kinetics (in Russian), 1940, p. 178.

[6] K. F. Herzfeld, Theory of Solids, 1936 (Russian translation from German).

[7] T. A. Kontorova, J. Tech. Phys. (USSR) 26, 9, 2021 (1956). [Soviet Physics - Technical Physics, p. 1959].

[8] A. A. Vorob'ev, Dokl. Akad. Nauk SSSR 108, No. 1, 47 (1956). [Soviet Physics - Doklady, p. 242.]

[9] P. Tomka, Magyar. fiz. folyoirat, 2, No. 3, 173 (1954).

[10] L. Z. Gurevich, Elements of Physical Kinetics (in Russian), 1940, p. 231.

Siberian Physicotechnical Institute,
V. V. Kuibyshev Tomsk State University

Received December 17, 1956

CALCULATION OF THE ANISOTROPY OF DIAMAGNETIC SUSCEPTIBILITY OF AROMATIC MOLECULES WITH A METAL MOLECULE MODEL

T. K. Rebane

(Presented by Academician V. A. Fok January 2, 1957)

M. V. Vol'kenshtein and L. A. Borovinskii [1] were the first to use a metal molecule model to calculate the anisotropy of the diamagnetic susceptibility of certain aromatic molecules. In order to apply this model to a broader class of aromatic molecules it is necessary to improve the method of calculating the magnetic properties of molecules using this model. We shall correct an error in the method of calculation employed in [1] and shall propose a new method of calculating the diamagnetic anisotropy of aromatic molecules on a metal model without employing perturbation theory.

In [1] the diamagnetic anisotropy of aromatic molecules was calculated by perturbation theory. The one-dimensional Hamiltonian which describes the behavior of π electrons in a magnetic field was written in the form

$$H = -\frac{1}{2}\frac{d^2}{ds^2} - \frac{i}{c}A_s\frac{d}{ds} + \frac{A_s^2}{2c^2}. \tag{1}$$

The coordinate s is measured along a bond. The units e = m = h = 1 are used.

In [1] the perturbation operator was only the third term in the Hamiltonian. But in the second perturbation approximation it is also necessary to take account of the second term in (1).

However the energy spectrum and the wave functions of π electrons for a metal molecule model in a uniform magnetic field can be obtained exactly without using perturbation theory. From the form of (1) it follows that the one-dimensional wave function for the jth bond is

$$\psi(s_j) = a_j\cos(\sqrt{2E}\ s_j + \delta_j)\,e^{-\frac{i}{c}A_js_j}. \tag{2}$$

(E is the energy of a π electron; A_j is the projection of the vector potential on the jth bond; a_j and δ_j are complex constants).

At each branch point of the conjugated system of bonds (including each break in the molecular contour) the following continuity conditions must be fulfilled:

$$\psi_1 = \psi_2 = \ldots = \psi_p; \tag{3}$$

$$\sum_{l=1}^{p}\left(\psi_l' + \frac{i}{c}A_l\psi_l\right) = 0, \tag{4}$$

where ψ_l and ψ_l' are the values of the one-dimensional wave function and its derivative at the beginning of the lth bond issuing from the branching point. The conditions (4) were first obtained by us and are a generalization of the continuity conditions that are fulfilled in the absence of a magnetic field.

From (2), (3) and (4) we obtain the following secular equation for the determination of the π electron energy spectrum in a magnetic field:

$$\det W(E, \varkappa) = 0, \tag{5}$$

where W is a matrix with the elements

$$W_{lm} = -p_l \delta_{lm} \cos\sqrt{2E}\, a + (1-\delta_{lm})\, \eta_{lm} e^{\frac{i\varkappa S_{lm}}{c}}, \tag{6}$$

in which δ_{lm} is the Kronecker symbol; p_{ll} is the number of C atoms that are neighbors of the lth C atom; a is the length of the C–C aromatic bond; η_{lm} = 1 or 0 depending on whether atoms l and m are linked or not; S_{lm} is the algebraic value of the area of the triangle whose vertices are the l th C atom, the mth C atom and the coordinate origin. The form of (5) is similar to that of the secular equation which determines the energy spectrum of π electrons in a uniform magnetic field by the method of molecular orbits [2].

From (5) and (6) we obtain the following expression for the diamagnetic anisotropy of cyclically linked molecules.

$$\Delta\chi = -\frac{S^2}{c^2 a^2 N}, \tag{7}$$

which agrees with Pauling's semiclassical theory [3]. (S is the area of the cycle and N is the number of C atoms.) For the circular and hexagonal models of benzene molecules Equation (7) gives results which are in accurate agreement with those obtained in [1]. This follows from the high symmetry of these models, which leads to the vanishing of the nondiagonal matrix elements of the second term in (1). But for less symmetrical molecules the method employed in [1] results in serious errors.

Using the implicit dependence of π electron energy on the magnetic field strength which is given by (5) we calculated the diamagnetic anisotropy of some molecules in which the conjugated system of bonds contains branching points. For simplicity the length of all C–C bonds was assumed to be equal to the length of the C–C bond in benzene. The results are given in Table 1 where $\Delta\chi_{\text{theor}}$ is our calculated value of the diamagnetic anisotropy; $\Delta\chi'_{\text{theor}}$ and $\Delta\chi''_{\text{theor}}$ are the values of the diamagnetic anisotropy calculated by the method of molecular orbits [4] with and without taking account of the nonorthogonality integrals; $\Delta\chi_{\text{exp}}$ is the experimental value of the diamagnetic anisotropy given in [4]. The diamagnetic anisotropy of benzene molecules was taken as the unit. In calculating $\Delta\chi_{\text{theor}}$ use was made of the theoretical value of the diamagnetic anisotropy of a benzene molecule which was calculated for the hexagonal metal model of this molecule.

TABLE 1

Molecule	$\Delta\chi_{\text{theor}}$	$\Delta\chi'_{\text{theor}}$	$\Delta\chi''_{\text{theor}}$	$\Delta\chi_{\text{exp}}$
Napthalene	2,011	2,185	2,219	2,06–2,11
Azulene	2,141	2,256	2,269	—
Pentalene	–2,840	–2,778	–2,526	—
Heptalene	–9,495	–8,340	–9,926	—
Anthracene	3,077	3,448	3,530	3,08–3,38

Despite the extreme simplicity of the physical concepts upon which the metal molecule model is based our results agree with experiment just as well as the results obtained by the method of molecular orbits.

The author is profoundly grateful to Professor M. G. Veselov for valuable suggestions and discussions.

LITERATURE CITED

[1] M. V. Vol'kenshtein and L. A. Borovinskii, Dokl. Akad. Nauk SSSR 85, 5, 977 (1952).

[2] F. London, J. Phys. Rad. 8, 10, 397 (1937).

[3] L. Pauling, J. Chem. Phys. 4, 10, 673 (1936).

[4] G. Berthier, M. Mayot and B. Pullman, J. Phys. Rad. 12, 7, 717 (1951).

A. A. Zhdanov Leningrad State University

Received December 26, 1956

THE INFLUENCE OF GRAVITATION ON THE PROPAGATION OF LIGHT*

G. V. Skrotskii

(Presented by Academician V. A. Fok December 12, 1956)

The equation of the electromagnetic field in a vacuum in the presence of finite masses can be written in the form of Maxwell's equations for a moving anisotropic medium. The character of the anisotropy in this instance is determined by the properties of the metric tensor.

Since spatial dimensions in astronomical problems are huge compared with electromagnetic wavelengths even at radio frequencies the coefficients of the equations are functions of the coordinates which vary extremely slowly. Thus in the majority of cases we are able to confine ourselves to the approximation of geometric optics. By using the method which was developed by S. M. Rytov it is possible to determine both the path of light rays and the variation of its polarization along the path.

For example, when a plane electromagnetic wave is propagated in the vicinity of a rotating mass the trajectory of the ray is not generally a plane curve but is twisted in the direction of rotation of the body. The rotation of the plane of polarization is proportional to the angular momentum of the rotating body. It is noteworthy that in the case of rays which issue from the poles of the rotating body and are propagated along the axis of rotation the plane of polarization is also rotated in the direction of rotation.

The propagation of electromagnetic waves in a vacuum in the presence of finite masses is described by the equations

$$\partial_\sigma f^{\rho\sigma} = 0; \quad \partial_\lambda F_{\rho\sigma} + \partial_\rho F_{\sigma\lambda} + \partial_\sigma F_{\lambda\rho} = 0, \tag{1}$$

where

$$\begin{gathered} f^{\rho\sigma} = \varepsilon^{\rho\sigma\alpha\beta} F_{\alpha\beta}, \\ \varepsilon^{\rho\sigma\alpha\beta} = \sqrt{-g}\, g^{\rho\alpha} g^{\sigma\beta}. \end{gathered} \tag{2}$$

(3)

Introducing three-dimensional vectors according to

$$F_{\rho\sigma} \rightarrow (\mathbf{B}, \mathbf{E}); \quad f^{\rho\sigma} \rightarrow (\mathbf{H}, -\mathbf{D})$$

and transforming to a vector notation we obtain a set of equations which are formally identical with Maxwell's equation in a medium:

$$\begin{gathered} \mathbf{E} = -\frac{1}{c}\frac{\partial \mathbf{B}}{\partial t}; \quad \operatorname{div} \mathbf{B} = 0; \\ \mathbf{H} = \frac{1}{c}\frac{\partial \mathbf{D}}{\partial t}; \quad \operatorname{div} \mathbf{D} = 0. \end{gathered} \tag{4}$$

---

*The equations given here for the twisting of a ray and the angle of rotation of the plane of polarization of electromagnetic waves were derived in 1951 by A. R. Ptitsyn under the direction of the author.

The tensor $\varepsilon^{\rho\sigma\alpha\beta}$ which relates the field vectors is analogous to the tensor of electrical and magnetic permeability [1] which is encountered in the relativistic theory of moving anisotropic media. To determine the form of the tensor it is necessary to know the components of the metric tensor $g_{\alpha\beta}$.

Let us for example consider a stationary gravitational field generated by a spherical mass m_0 which is rotating uniformly. The approximate solutions of the gravitational equations which define the gravitational field in the space outside the body can to a high degree of accuracy be represented by [2]

$$g^{00} = -1 - h; \quad g^{11} = g^{22} = g^{33} = 1 - h; \quad g^{0\alpha} = g_{0\alpha} = \frac{2\gamma}{c^3 r^3}[\mathbf{r}, \mathbf{M}]_\alpha, \tag{5}$$

where $h = \frac{2\gamma m_0}{c^2 r}$; γ is the gravitational constant; **M** is the angular momentum of the rotating body.

In accordance with (2) we now obtain

$$\mathbf{D} = \varepsilon\mathbf{E} - [\mathbf{G}, \mathbf{H}]; \quad \mathbf{B} = \mu\mathbf{H} + [\mathbf{G}, \mathbf{E}], \tag{6}$$

where

$$\varepsilon = \sqrt{-g}\,(-g^{00})\,g^{11}; \quad \mu = \frac{1}{\sqrt{-g}\,(g^{11})^2}; \quad \mathbf{G} = \frac{2\gamma}{c^3 r^3}[\mathbf{r}, \mathbf{M}]. \tag{7}$$

In the centrally symmetrical field of a nonrotating mass ($\mathbf{G} = 0$) the relation between the field vectors is very simple.

For processes which occur with the period $\omega = ck$ Equations (4) in the present case become

$$\operatorname{rot}\mathbf{E} = -ik(\mu\mathbf{H} + [\mathbf{G}, \mathbf{E}]); \quad \operatorname{rot}\mathbf{H} = ik(\varepsilon\mathbf{E} - [\mathbf{G}, \mathbf{H}]). \tag{8}$$

Using Rytov's method [3,4] we shall seek a solution of these equations in the form

$$\mathbf{E} = \frac{\vec{\mathscr{E}}}{\sqrt{\varepsilon}}\,e^{ik\Phi}; \quad \mathbf{H} = \frac{\vec{\mathscr{H}}}{\sqrt{\mu}}\,e^{-ik\Phi}. \tag{9}$$

where $\vec{\mathscr{E}}$, $\vec{\mathscr{H}}$ and Φ are functions of the coordinates. Representing $\vec{\mathscr{E}}$ and $\vec{\mathscr{H}}$ as series:

$$\vec{\mathscr{E}} = \vec{\mathscr{E}}_0 + \frac{i}{k}\vec{\mathscr{E}} + \ldots; \quad \vec{\mathscr{H}} = \vec{\mathscr{H}}_0 + \frac{i}{k}\vec{\mathscr{H}}_1 + \ldots, \tag{10}$$

we obtain the following equations for $\vec{\mathscr{E}}_0$ and $\vec{\mathscr{H}}_0$ in zeroth approximation:

$$[\operatorname{grad}\Phi - \mathbf{G}, \vec{\mathscr{H}}_0] + \sqrt{\varepsilon\mu}\,\vec{\mathscr{E}}_0 = 0; \quad -\sqrt{\varepsilon\mu}\,\vec{\mathscr{H}}_0 + [\operatorname{grad}\Phi - \mathbf{G}, \vec{\mathscr{E}}_0] = 0. \tag{11}$$

In first approximation

$$\begin{gathered}[\operatorname{grad}\Phi - \mathbf{G}, \vec{\mathscr{H}}] + \sqrt{\varepsilon\mu}\,\vec{\mathscr{E}} = -\operatorname{rot}\vec{\mathscr{H}}_0 + \frac{1}{2\mu}[\operatorname{grad}\mu, \vec{\mathscr{H}}_0];\\ -\sqrt{\varepsilon\mu}\,\vec{\mathscr{H}} + [\operatorname{grad}\Phi - \mathbf{G}, \vec{\mathscr{E}}_1] = -\operatorname{rot}\vec{\mathscr{E}}_0 + \frac{1}{2\varepsilon}[\operatorname{grad}\varepsilon, \vec{\mathscr{E}}_0].\end{gathered} \tag{12}$$

When the determinant of the homogeneous linear equations (11) is set equal to zero we obtain

$$[(\operatorname{grad}\Phi - \mathbf{G})^2 - \varepsilon\mu]^3 = 0.$$

Thus in zeroth approximation we obtain the generalized eikonal equation

$$\operatorname{grad}\Phi - \mathbf{G} = \sqrt{\varepsilon\mu}\,\mathbf{e}, \tag{13}$$

where $\mathbf{e}$ is a unit vector in the direction of wave propagation at a given point. Directions in the field of the vector $\mathbf{e}$ coincide with the lines of flow of the electromagnetic field energy.

A general solution of the zeroth approximation equations (11), which in this case become

$$[\mathbf{e}, \vec{\mathcal{H}}_0] + \vec{\mathcal{E}}_0 = 0; \quad -\vec{\mathcal{H}}_0 + [\mathbf{e}, \vec{\mathcal{E}}_0] = 0,$$

can be written as

$$\vec{\mathcal{E}}_0 = f_1\mathbf{n} + f_2\mathbf{b}; \quad \vec{\mathcal{H}}_0 = f_1\mathbf{b} - f_2\mathbf{n}, \tag{14}$$

where f_1 and f_2 are arbitrary functions of the coordinates which cannot be determined in the zeroth approximation; $\mathbf{n}$ and $\mathbf{b}$ are unit vectors of the principal normal and binormal to the ray. The vectors $\mathbf{n}, \mathbf{b}, \mathbf{e}$ form an orthogonal set.

The first approximation equations (12) can now be written as follows:

$$\begin{gathered} [\mathbf{e}, \vec{\mathcal{H}}_1] + \vec{\mathcal{E}}_1 = -\frac{1}{\sqrt{\varepsilon\mu}}\left\{\operatorname{rot}\vec{\mathcal{H}}_0 - \frac{1}{2\mu}[\operatorname{grad}\mu, \vec{\mathcal{H}}_0]\right\}, \\ -\vec{\mathcal{H}}_1 + [\mathbf{e}, \vec{\mathcal{E}}_1] = -\frac{1}{\sqrt{\varepsilon\mu}}\left\{\operatorname{rot}\vec{\mathcal{E}}_0 - \frac{1}{2\varepsilon}[\operatorname{grad}\varepsilon, \vec{\mathcal{E}}_0]\right\}. \end{gathered} \tag{15}$$

The requirement for solution of these simultaneous equations is that their right-hand sides be orthogonal to each of the linearly independent solutions of the transposed homogeneous set. Combining the resulting two conditions we obtain the law of variation of intensity along a ray and the important relation

$$\tfrac{1}{2}(\mathbf{n}\operatorname{rot}\mathbf{n} + \mathbf{b}\operatorname{rot}\mathbf{b}) = (\mathbf{e}\operatorname{grad})\Psi, \tag{16}$$

where

$$\Psi = \operatorname{arc\,tan}\frac{f_2}{f_1}, \tag{17}$$

which defines Ψ between the principal normal to the ray and the vector $\vec{\mathcal{E}}_0$. Using the identity

$$\mathbf{n}\operatorname{rot}\mathbf{n} + \mathbf{b}\operatorname{rot}\mathbf{b} = \frac{2}{\rho} + \mathbf{e}\operatorname{rot}\mathbf{e},$$

which is known from differential geometry, where ρ is the radius of torsion of the ray (of the vector $\mathbf{e}$), and considering the $\mathbf{e}$ grad $= d/ds$, where ds is an element of arc length along the curve, we obtain

$$\frac{d\Psi}{ds} = \frac{1}{\rho} + \frac{1}{2}\,\mathbf{e}\operatorname{rot}\mathbf{e}, \tag{18}$$

which is the law of rotation of the plane of polarization of an electromagnetic wave propagating in the gravitational field of a spherically rotating mass.

When the angular velocity of a star is zero we have $\mathbf{e}$ rot $\mathbf{e} = 0$ and $1/\rho = 0$. In this case the trajectory of the ray is planar and the plane of polarization is not rotated.

The right-hand side of (18) is ultimately determined by the geometry of space and is independent of the frequency of the wave. Thus there is no rotational dispersion in a gravitational field.

When a wave is propagated parallel to the axis of rotation of the body the light ray is not only subjected to the Einstein deflection effect but is also turned in the direction of rotation of the body through the angle

$$\varphi = \frac{4\gamma M}{c^3 r^2}, \tag{19}$$

while remaining on the surface of rotation of the Einstein curve. The twisting of the ray is accompanied by turning of the plane of polarization through the angle

$$\Delta\Psi_{\mp\infty} = \frac{8\gamma M}{c^3 r^2}. \tag{20}$$

It is noteworthy that even for rays issuing from the axis of the rotating body and propagated along the axis of rotation the plane of polarization is rotated through the angle

$$\Delta\Psi_0 = 3\,\frac{\gamma M}{c^3 R^2}, \tag{21}$$

where R is the radius of the body. This last fact is further evidence of the absolute character of rotation in the theory of relativity.

For rays which are perpendicular to the axis of rotation z of the body and parallel to the y axis, for example, the rotation of the plane of polarization proceeds in opposite directions on the two sides of the x-z plane so that if the wave goes from $-\infty$ to ∞ the total rotation will vanish. In this case for waves emitted from the surface of the body

$$\Delta\Psi_\perp = \frac{4\gamma M}{c^3 R^2}\, z. \tag{22}$$

We have the factor $\gamma/c^3 \sim 10^{-39}$, so that the effects of the twisting and rotation of the plane of polarization can be appreciable only for very large values of M/R^2. For ordinary stars the rotational effect is very small. Thus for the sun $\Delta\Psi \sim 6 \cdot 10^{-6}$ sec. An appreciable effect is obtained for white dwarfs. Thus for the dwarf L745-46 [5], $\Delta\Psi = 1.65$ sec. For light from an external source the effect is doubled.

LITERATURE CITED

[1] I. Tamm, J. Russ. Phys.-Chem. Soc., Phys. Div. 56, 2-3, 248 (1924) (In Russian).

[2] L. Landau and E. Lifshits, Theory of Fields, 1948.

[3] S. M. Rytov, Dokl. Akad. Nauk SSSR 18, 263 (1938).

[4] S. M. Rytov, Trans. Phys. Inst. Acad. Sci. USSR 2, 1, 49 (1940).

[5] S. M. Petrov, Priroda 1945, 6.

S. M. Kirov Ural Polytechnical Institute Received July 26, 1956

ON THE CAUSES OF ULTRASONIC DISTENSION OF LIQUID SURFACES

L. D. Rozenberg and L. O. Makarov

(Presented by Academician N. N. Andreev January 3, 1957)

The distension of a liquid surface under the influence of ultrasound has been known for a long time and has been extensively used by experimenters for qualitative estimates of the radiation intensity. It is usually assumed that the cause of this phenomenon is radiation pressure. Thus it was shown in the experiments of Hertz and Mende [1] that the direction of the distension at the boundary between two immiscible liquids is independent of the direction of sound energy flow and is determined by the difference of the radiation pressures in the two liquids, which in turn depends on the corresponding velocities of sound propagation.

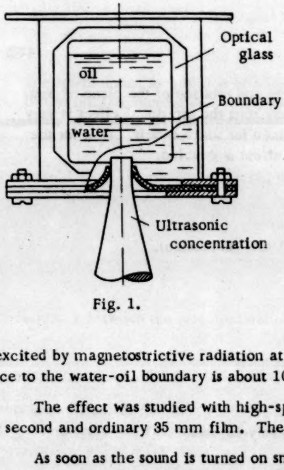

Fig. 1.

In this note we shall show that radiation pressure is not the only cause of the distension. The same effect can be produced by the so-called sonic wind, whose velocity in water can be as high as 0.5 to 1.0 m/sec, as was shown in [2].

The radiation pressure is one of the ponderomotive forces of the sound field and is thus propagated with the velocity of sound; the starting point of all the perturbations induced by this force is thus propagated in space with the same velocity. The sonic wind is a hydrodynamical effect. Therefore for the temporal distinction of these effects it is convenient to investigate the process of establishment of the bulge.

The experimental arrangement is shown in Fig. 1. A flat optical glass container measuring 50 x 50 x 15 mm contains a layer of water and a layer of transformer oil. Through an opening in the rubber bottom of the container the end of an exponential concentrator is introduced; this is excited by magnetostrictive radiation at 24 kc. The end of the concentrator is 8 mm in diameter; the distance to the water-oil boundary is about 10 mm.

The effect was studied with high-speed motion pictures using a Zeiss "Zeit-Lupe" camera at 2000 frames per second and ordinary 35 mm film. The axis of the camera was perpendicular to the plane of Fig. 1.

As soon as the sound is turned on small bubbles are produced vigorously at the end of the vibrator; the sonic wind carries these bubbles upward while new bubbles are produced continuously at the end of the vibrator. The speed of the forward edge of the bubble cloud is determined by the speed of the sonic wind but is apparently not equal to the latter.

Fig. 2a is the picture just before the sound is switched on; a motionless air bubble is located at the boundary and the end of the vibrator coincides with the lower boundary of the frame. In Fig. 2b, $0.8 \cdot 10^{-2}$ sec after switching on of the sound the cloud has moved about half of the distance to the boundary. If the

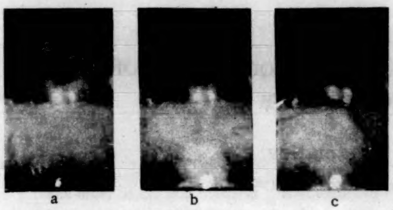
a b c

Fig. 2.

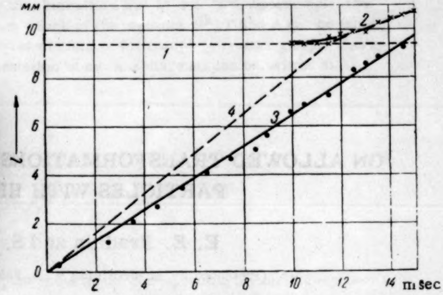

Fig. 3. 1) Oil-water separation; 2) V = 0.42 m/sec; 3) V = 0.64 m/sec; 4) V = 0.89 m/sec.

distension is caused by radiation pressure the effect should be produced in about 10^{-5} sec. But Fig. 2b shows no trace of deformation of the separating boundary. Such traces appear only after $1.2 \cdot 10^{-2}$ sec, when the leading edge of the cloud reaches the boundary. Only after $1.5 \cdot 10^{-2}$ sec is clear distension observed (the dark circular bulge in Fig. 2b).

Fig. 3 shows the dynamics of the effect based on a study of the motion-picture frames. The horizontal axis shows the time that has elapsed after appearance of the first bubbles; the vertical axis gives the path. The horizontal line represents the water-oil separation. Dots indicate the position of the leading edge of the cloud. All points are seen to lie close to the straight line which corresponds to a velocity of propagation of 0.64 m/sec. The deformation of the boundary begins in 11 msec and the corresponding points (indicated by crosses) when the process has already developed also fit a straight line representing 0.42 m/sec velocity of the separating boundary.

As a control we performed the following qualitative experiment: the vibrating end of the concentrator was introduced from above into the oil instead of from below into the water. The direction of the bulge was changed, unlike the experimental result of Hertz and Mende.

It can thus be considered proved that in our experiment we observed a bulging of the boundary between two liquids which was induced by the sonic wind rather than by radiation pressure.

LITERATURE CITED

[1] G. Hertz and H. Mende, Z. Physik 114, 354 (1939).

[2] A. S. Bebchuk, L. Ω Makarov and L. D. Rozenberg, Acoustics Journal (USSR) 2, 2, 113 (1956).*

Acoustics Institute, Academy of Sciences USSR

Received December 21, 1956

---

* [Soviet Physics - Acoustics p. 111.]

ON ALLOWED TRANSFORMATIONS OF THE EQUATIONS FOR PARTICLES WITH HIGHER SPINS

E. E. Fradkin and S. V. Izmailov

(Presented by Academician V. A. Fok December 29, 1956)

1. Particles for all spins are described by equations of the form

$$\left(L^i \frac{\partial}{\partial x_i} + i\varkappa\right) \Psi (x_0,\ x_1,\ x_2,\ x_3) = 0, \tag{1}$$

where $\Psi(x_0, x_1, x_2, x_3) \equiv \Psi(ct, x, y, z)$ is the wave function, which can be transformed by a finite-dimensional representation of the complete Lorentz group; $L^i (i = 0, 1, 2, 3)$ are square matrices; κ is a real nonvanishing constant.

The invariance of (1) under coordinate transformations of the complete Lorentz group is insured by the conditions imposed on the matrices L^i:

$$[L^i I^{jk}] \equiv L^i I^{jk} - I^{jk} L^i = g^{ij} L^k - g^{ik} L^j \quad (i,\ j,\ k = 0,\ 1,\ 2,\ 3); \tag{2}$$

$$[L^i T] = 0, \tag{3}$$

where the I^{jk} are infinitesimal transformations of the corresponding representation of the proper Lorentz group; T is the inversion $x^0 \to x^0$, $x^\alpha \to -x^\alpha$ ($\alpha = 1, 2, 3$). It follows from (2) in particular that

$$L^\mu = [L^0 I^{0\mu}] \quad (\mu = 1,\ 2,\ 3). \tag{4}$$

The general theory of the relativistic invariance of equations such as (1) has been studied in [1].

2. We shall consider the possible linear transformations of the wave function $\Psi(x_0, x_1, x_2, x_3)$, i.e. transformations of the form $\Psi(x_0, x_1, x_2, x_3) = S\Psi(x_0, x_1, x_2, x_3)$ which do not alter the essential characteristics of (1), and we shall determine the form of the matrix S for allowable transformations.

The allowable transformations are, first, those which do not change the form of I^{jk} and T [1], i.e.

$$V^{-1} I^{jk} V = I^{jk}, \quad V^{-1} T V = T \quad (j,\ k = 0,\ 1,\ 2,\ 3). \tag{5}$$

Since our equations (1) can be derived from the corresponding Lagrangian an important part is played by the metric matrix A which is used to define the invariant Hermitian bilinear form $\Psi^* A \Psi$. *

Thus in order to relate the different representations of (1) for a spin 3/2 particle which are given in [1-3] a transformation must be able to change the absolute values of the eigenvalues of the metric matrix A.

---

* An asterisk denotes the Hermitian adjoint function.

While the matrices I^{jk}, T and L^i are subject to similarity transformations like $L^{i\prime} = S^{-1}L^iS$, for example, the metric matrix A is transformed congruently: $A' = S^* AS$.[•] Each of the matrices I^{jk}, T and A can be represented [1] as the direct sum of matrices for irreducible representations of the complete Lorentz group. Therefore the transformation V which satisfies (5) in the representation where A is diagonal can be written as

$$V = \begin{vmatrix} v_1 I_1 & & & \\ & v_2 I_2 & & \\ & & \ddots & \\ & & & v_n I_n \end{vmatrix}, \tag{6}$$

where $v_1, v_2, \ldots, v_n$ are any complex numbers.

The order of the unit matrices I_i is determined by the order of the corresponding irreducible representations of the complete Lorentz group. The eigenvalues of A corresponding to the ith irreducible transformation of the complete Lorentz group are varied in the ratio $|v_i|^2$.

The essential properties of I^{jk}, T, L^i and A are not changed by any unitary transformations. As the metric tensor A is Hermitian, it is always possible by some unitary transformation to obtain a representation in which A is diagonal with the requisite serial order of the eigenvalues. Therefore the general form of the allowable transformations will be[••]

$$S = U_1 V U_2, \tag{7}$$

where U_1 and U_2 are any unitary transformations; V is a transformation like (6).

3. The wave function Ψ contains an arbitrary normalization factor, so that the eigenvalues of A associated with the irreducible representation of the complete Lorentz group with maximum spin can be set equal to ±1 in all equivalent representations. Then in Equation (6) the corresponding $v_k = 1$ and the metric in the subspace with maximum spin is unchanged under allowable transformations. Thus for a spin 1/2 particle the transformation of the wave function contains only one irreducible representation of the complete Lorentz group and the allowable transformations of the Dirac matrices reduce to an arbitrary unitary transformation. The charge density $\Psi^* \Psi$ is an invariant of such transformations.

For particles with higher half-integral spins $s = n + 1/2$ $(n = 1, 2, \ldots, i)$ it is easily shown that only the charge density of a free particle at rest will be an invariant of the allowable transformations (7).

4. Let us consider in greater detail the transformation of (1) for a spin 3/2 particle. References[1-3] contain different representations of the matrices L^i $(i = 0, 1, 2, 3)$ of (1) for a spin 3/2 particle with positive definite charge; Gupta's representation [2] is directly associated with the equations and Lagrangian, that of Pauli and Fierz [4] with auxiliary spinors. On the other hand there is a similar relation of Petras' [3] representation to the spin-tensor equations and corresponding Lagrangian given by Rarita and Schwinger [5] without auxiliary quantities. Consequently, by showing the relationship between the Gel'fand-Iaglom and Petras-Gupta representations we shall be showing the equivalence of the fundamental representations of the equation for spin 3/2 particles according to our definition of allowed transformations (7). The transition from the Gel'fand-Iaglom representation to the Gupta-Petras representations is accomplished through the S_1 and S_2 transformations:

$$S_1 = U_1 V_1 U_2, \quad S_2 = U_1 V_2 U_3. \tag{8}$$

[•] In an S transformation the invariant Hermitian bilinear form $\Psi^* ALP\Psi$, where L is a matrix and P is an operator, is unchanged: $\Psi^* ALP \Psi = \Psi'^* S^* ALPS \Psi' = \Psi'^* A'L'P' \Psi$, where $A' = S^* AS$, $L' = S^{-1}LS$, $P' = S^{-1}PS$.

[••] The transformations (7) can be extended to the Duffin-Kemmer equations for particles with spin 0 and 1. However (7) destroys the Hermitian character of the Kemmer matrices and the usual relation between the metric matrix and the Kemmer matrices.

The Gupta and Petras representations are related by the S_3 transformation:

$$S_3 = U_2^* V_3 U_3. \tag{9}$$

For example $L^{i'} = S_2^{-1} L^i S_2$, where L^i are matrices in the Gel'fand-Iaglom representation with L^0 written as

$$L^0 = \begin{vmatrix} c^{3/2}_{\tau\tau'} & & & & & \\ & c^{3/2}_{\tau\tau'} & & & & \\ & & c^{3/2}_{\tau\tau'} & & & \\ & & & c^{3/2}_{\tau\tau'} & & \\ & & & & c^{1/2}_{\tau\tau'} & \\ & & & & & c^{1/2}_{\tau\tau'} \end{vmatrix}, \tag{10}$$

where $\| c^{3/2}_{\tau\tau'} \|$ and $\| c^{1/2}_{\tau\tau'} \|$ are matrices given in [1] (Equation 7.10), and $L^{i'}$ are explicit matrices in the Petras representation.

The matrices U_i and V_i (i = 1,2,3) in (8) and (9) are*

$$V_i = \begin{vmatrix} I & & & \\ & I & & \\ & & I & \\ & & & k_i I \end{vmatrix}, \quad \text{where } I = \begin{vmatrix} 1 & . & . & . \\ . & 1 & . & . \\ . & . & 1 & . \\ . & . & . & 1 \end{vmatrix};$$

$$i = 1, 2, 3; \quad k_1 = \frac{1}{\sqrt{3}}, \quad k_2 = 2 - \sqrt{3}, \quad k_3 = 2\sqrt{3} - 3; \tag{11}$$

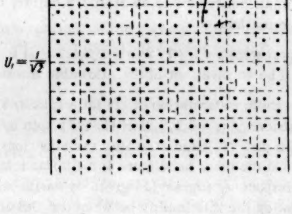

(12)

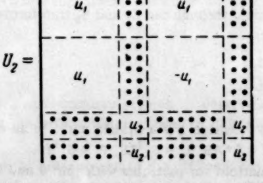

(13)

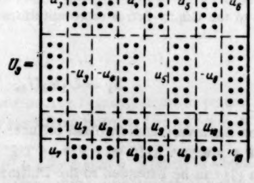

(14)

---

* The unitary matrices U_1, U_2 and U_3 reduce the metric matrices A, A' and A'', respectively, in the representations of Gel'fand and Iaglom, Gupta and Petras to diagonal form, and the matrices V_1, V_2 and V_3 perform the transition from one diagonal metric matrix to another by changing some of the eigenvalues.

where

$$u_1 = \begin{vmatrix} 0 & -\frac{ia}{\sqrt{2}} & ia & ia & -\frac{ia}{\sqrt{2}} & 0 \\ \frac{b}{\sqrt{2}} & b & \frac{b}{\sqrt{2}} & \frac{b}{\sqrt{2}} & b & \frac{b}{\sqrt{2}} \\ 0 & \frac{a}{\sqrt{2}} & a & -a & \frac{a}{\sqrt{2}} & 0 \\ -\frac{ib}{2a} & -\frac{ia}{2} & iab & -iab & \frac{ia}{2} & \frac{ib}{2a} \\ \frac{ib}{\sqrt{2}} & -ib & \frac{ib}{\sqrt{2}} & -\frac{ib}{\sqrt{2}} & ib & -\frac{ib}{\sqrt{2}} \\ -\frac{b}{2a} & \frac{a}{2} & ab & ab & \frac{a}{2} & -\frac{b}{2a} \end{vmatrix}, \quad u_2 = \begin{vmatrix} -\frac{1}{2} & -\frac{1}{2} \\ \frac{i}{2} & -\frac{i}{2} \end{vmatrix},$$

$$u_3 = \begin{vmatrix} \frac{ib}{\sqrt{2}a} & \frac{ib}{\sqrt{2}a} \\ 0 & 0 \\ \frac{b}{\sqrt{2}a} & -\frac{b}{\sqrt{2}a} \\ 0 & 0 \\ 0 & 0 \\ 0 & 0 \end{vmatrix}, \quad u_4 = \begin{vmatrix} -\frac{ia}{2} & -\frac{ia}{2} \\ 0 & 0 \\ \frac{a}{2} & -\frac{a}{2} \\ -i\sqrt{2}a & i\sqrt{2}a \\ 0 & 0 \\ \sqrt{2}a & \sqrt{2}a \end{vmatrix}, \tag{15}$$

$$u_5 = \begin{vmatrix} \frac{a}{2} & -\frac{a}{2} \\ \frac{i}{2} & -\frac{i}{2} \\ \frac{ia}{2} & \frac{ia}{2} \\ -\frac{a}{\sqrt{2}} & -\frac{a}{\sqrt{2}} \\ \frac{1}{2} & \frac{1}{2} \\ -\frac{ia}{\sqrt{2}} & \frac{ia}{\sqrt{2}} \end{vmatrix}, \quad u_6 = \begin{vmatrix} -\frac{ia}{2} & \frac{ia}{2} \\ -\frac{1}{2} & -\frac{1}{2} \\ -\frac{a}{2} & -\frac{a}{2} \\ -\frac{ia}{\sqrt{2}} & -\frac{ia}{\sqrt{2}} \\ -\frac{i}{2} & -\frac{i}{2} \\ -\frac{a}{\sqrt{2}} & \frac{a}{\sqrt{2}} \end{vmatrix},$$

$$u_7 = \begin{vmatrix} -b & b \\ -ib & -ib \end{vmatrix}, \quad u_8 = \begin{vmatrix} b & -b \\ -ib & -ib \end{vmatrix}, \quad u_9 = \begin{vmatrix} ib & ib \\ b & -b \end{vmatrix}, \quad u_{10} = \begin{vmatrix} -b & -b \\ -ib & ib \end{vmatrix},$$

where $a = \frac{1}{\sqrt{6}}, \quad b = \frac{1}{2\sqrt{2}}$.

The essence of these transformations lies in the change of the metric in the "auxiliary" subspace with spin 1/2, which affects the formulation of the auxiliary conditions and the "excess" components of the wave function and equation.

The authors take this opportunity to thank Ia. M. Iaglom for valuable discussions.

LITERATURE CITED

[1] I. M. Gel'fand and Ia. M. Iaglom, J. Exptl. Theoret. Phys. (USSR) 18, 703 (1948).

[2] S. N. Gupta, Phys. Rev. 95, 1334 (1954).

[3] M. Petras, Czechoslov. J. Phys. 5, 160 (1955).

[4] M. Fierz, W. Pauli, Proc. Roy. Soc. London, A 173, 211 (1939).

[5] W. Rarita and J. Schwinger, Phys. Rev. 60, 61 (1941).

A. I. Herzen Leningrad State Pedagogical Institute

Received December 21, 1956

THE EXCITATION OF HYPERSONIC FREQUENCIES IN QUARTZ

K. N. Baranskii

(Presented by the late Academician G. S. Landsberg January 12, 1957)

At the present time the only method of investigating the elastic properties of materials at hypersonic frequencies (10^9-10^{10} cps) is the study of the fine structure of the spectrum of light scattered by thermal waves [1]. For solids this method is complicated by the low intensity of the scattered light. It is therefore natural that an attempt should be made to use ultrasonic methods for the excitation of vibrations in the given range. At present ultrasonic methods are practically limited to frequencies of the order $1\text{-}2 \cdot 10^8$ cps. An ultrasonic frequency of 10^9 cps was attained only by Ringo et al [2] and S. Ia Sokolov [3]. For the purpose of reaching the highest possible ultrasonic frequencies these investigators prepared very thin quartz plates with high fundamental frequencies in order to excite relatively low harmonics at high frequencies.* The ultrasonic technique of exciting piezoquartz is the same at all frequencies from 10^5 to 10^9 cps. Ultra high frequency techniques are not used for this purpose even at 10^9 cps.

We believed that for the purpose of increasing ultrasonic frequencies it is necessary while using modern resonance methods for ultrashort waves to develop a method of applying strong electrical high frequencies to quartz. The solution of this fundamental problem in the generation of ultrasound could also free experimental techniques of the necessity for using thin quartz plates and, as is even more important, permit optical investigation of the processes occurring in massive quartz at ultrasonic frequencies.

As sources of the hf field we used continuous sine-wave generators with coaxial resonators and ceramic tubes (GI-116). These oscillators provided smooth field frequency change from 10^8 to $2 \cdot 10^9$ cps with effective power of 5 to 10 watts (in the work of Ringo et al the oscillator produced 50 to 100 watts). The power of our oscillators was in accordance with the highly resonant character of the systems to which the piezoquartz was connected.

The quartz was mounted in accordance with the preceding considerations. At 10^8 to 10^9 cps the quartz plate was clamped between metal plates connected to the coaxial line, one end of which was connected to the oscillator while the other end was shorted with a plunger. A system of standing electromagnetic waves was created in the system; by moving the plunger it was possible to bring one of the antinodes of the electric field to the point where the metal plates were connected. Above 10^9 cps the quartz plate was placed in a coaxial resonator tuned by a plunger and connected to the oscillator by a 50-ohm cable.

Longitudinal vibrations along the X-axis were excited in rectangular quartz plates whose edges were oriented along the X, Y and Z crystal axes and measured 15, 50 and 20 mm, respectively. Light diffraction by ultrasound was used to observe the quartz vibrations.

The given procedure permitted the excitation of sound vibrations in a thick quartz plate within a broad frequency range up to $2 \cdot 10^9$ cps with the observation of first order diffraction spectra. The fundamental frequency of the plate was 240 kc. Above $3 \cdot 10^8$ cps even and odd harmonics were excited with equal intensity so that the ultrasonic frequencies were separated by 240 kc intervals. Above $6 \cdot 10^8$ cps vibrations were excited in the plate at any oscillator frequency: the intensity of the diffraction spectra was independent of the frequency. This results from the fact that the width of the quartz plate resonance curve at such frequencies is greater than the frequency interval between its harmonics. Running waves are then excited in the quartz.

---

*Thus Ringo et al used a quartz plate 0.038 mm thick and excited the hundredth harmonic of the fundamental frequency.

Thus the use of thick plates of X-cut quartz at hypersonic frequencies enabled one plate to produce any sound frequency; this is very advantageous for the investigation of the frequency dependence of elastic properties of materials.

Measurements of the velocity of longitudinal waves in quartz at 20° by the diffraction method showed that within the limits of accuracy of our measurements (± 1%) the velocity is constant at 5750 m/sec over the entire investigated frequency range. At $1.64 \cdot 10^9$ cps this velocity is obtained from the condition that the angle of diffraction for the mercury line $\lambda = 5780$ A is 9°28' and the length of the sound wave $\Lambda = 3.52 \cdot 10^{-4}$ cm. The Q factor of the quartz plates as measured by the diffraction method at $5 \cdot 10^8$ cps varied from 2500 to 7300.

The first application of the method was the investigation of light diffraction by high ultrasonic frequencies which had been studied theoretically and experimentally by S. M. Rytov in 1935 [4]. He showed that when the ratio $\lambda l / \Lambda^2$ (l is the length of the light path in the ultrasonic field) is greater than unity the spatial character of the ultrasonic grating must affect selectively the (Bragg) reflection of the light. The light intensity for wavelength λ diffracted at angle φ will be a maximum when the angle θ between the direction of the incident light and the plane of the sonic wave front satisfies the condition $\theta = \lambda / 2\Lambda = \varphi / 2$.

Selective reflection actually occurs at $1\text{-}2 \cdot 10^8$ cps and is manifested in the intensity asymmetry of spectra of orders +1 and −1. Above $2 \cdot 10^8$ cps by varying the sign of θ spectra of order +1 and −1 can be observed only alternately. At still higher frequencies the accuracy requirements for the angle θ are increased. For example, at frequencies of the order of 10^9 cps for observation of the yellow or green mercury lines it is necessary to establish different values of θ.

According to Rytov's theory for a given value of θ the intensity of diffracted light differs from zero in the angular range from $\varphi_1 = 2\theta - n\Lambda/l$ to $\varphi_2 = 2\theta + n\Lambda/l$, which corresponds to the interval of light wavelengths $\Delta\lambda = 2n\,\Lambda^2/l$, where n is the refractive index of the medium. At frequencies above $2 \cdot 10^8$ cps when a continuous spectrum lamp is used the diffraction pattern reveals only a narrow portion of the lamp spectrum. By varying the angle θ the diffraction spectrum can successively show different portions of the continuous lamp spectrum, the width of which portions is sharply reduced at higher frequencies. At $1\text{-}2 \cdot 10^9$ cps the diffraction spectrum of an incandescent lamp is a single line whose angular width does not exceed the width of lines in the diffraction spectrum of a high pressure mercury lamp for the same frequencies. Thus the hypersonic grating in quartz acts as a monochromator of light just as a crystal lattice acts as a monochromator of x-rays.

I am indebted to I. A. Iakovlev for suggesting this research and for his continued interest, and to G.P. Motulevich for valuable discussions.

LITERATURE CITED

[1] E. F. Gross, Physik Z. 35, 756 (1934).

[2] G. R. Ringo, I. W. Fitzgerald and B. G. Hurdle, Phys. Rev. 72, 87 (1947).

[3] S. Ia. Sokolov, Dokl. Akad. Nauk SSSR 64, 503 (1949).

[4] S. M. Rytov, J. Exptl. Theoret. Phys. (U.S.S.R.) 5, 843 (1935).

M. V. Lomonosov Moscow State University Received January 9, 1957

THE ABSORPTION OF LIGHT BY CdS CRYSTALS *

V. L. Broude, V. V. Eremenko and E. I. Rashba

(Presented by the late Academician G. S. Landsberg January 7, 1957)

Gross and Iakobson [1] have shown that the absorption spectrum of CdS single crystals at 4.2° K contains a number of narrow bands. These bands are located near the continuous absorption edge and are attributed to excitons [1].

In the study of temperature effects on the absorption spectrum of CdS crystals [2] extreme variation of the bands was observed in different specimens. We have therefore investigated the spectra of CdS hexagonal single crystals at 20.4° K in polarized light. Our specimens were obtained by evaporating Cd and S in an argon atmosphere, by evaporating Cd in a $H_2S + H_2$ atmosphere and by evaporating CdS (recrystallization). **

The specimens had different faces and surface quality. They included perfectly smooth platelets, crystals with fine and coarse striations and twins with oblique extinction relative to the twinning axis. The specimens varied in thickness from 1 to 100 μ. The spectra were studied with the aid of a polarizing microprojector [3] which projected the crystal image magnified 20 × on the plane of the spectrograph slit. By means of an Iceland spar crystal the photographic plate simultaneously received two spectral components corresponding to polarization of the light vector along the hexagonal c̲ axis and perpendicular to it. By shifting the cryostat any part of the crystal could be brought to the slit so that the spectrum was obtained from a portion measuring 0.1×0.0015 mm^2.

Fig. 1a is the absorption spectrum of a CdS crystal in polarized light. The spectrum contains 10 relatively narrow bands between 20,400 and 20,600 cm^{-1} and a few wider bands distributed against the continuous

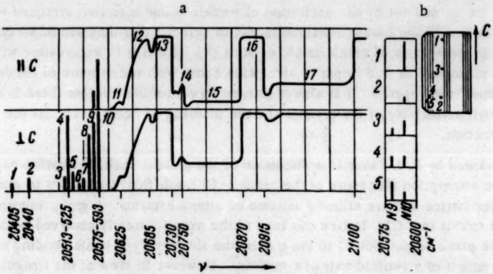

Fig. 1.

---

* Presented at a session of the Scientific Council of the Institute of Physics, Academy of Sciences, U.S.S.R on December 3, 1956.

** All of the investigated specimens were prepared in the laboratory of I. B. Mizetskaia. We take this opportunity of thanking I. B. Mizetskaia and V. D. Fursenko for kindly making them available to us.

background from which they are distinguishable only for the thinnest crystals. In the shorter wave region around 21,100 cm^{-1} there is a beginning of continuous absorption.*

Most noteworthy is the weak polarization of bands 9 and 10, which are clear in both spectral components. Indeed in a crystal with C_{6v}^4 symmetry all of the intrinsic narrow band absorption should be strongly polarized, that is, each line can exist only in the component parallel to c or perpendicular to c; moreover, absorption should be strongly polarized near vacancies and other defects** with a threefold axis of symmetry. Therefore bands 9 and 10 can only be associated with absorption by atoms of the surface layer or with nonsymmetric defects distributed spatially. A second important characteristic is the fact that not only in different specimens but also in different portions of a single specimen the intensity of all bands 1 to 10, their polarization and their spectral position can vary. Therefore Fig. 1a indicates the frequency limits of the most characteristic bands 4 and 10 in different instances; the satellites of these bands are usually shifted correspondingly.

It is especially convenient to observe the variations in bands 8 to 10, which are isolated in the c component; this permits more reliable determination of their variations from the photographs. Fig. 1b shows a typical variation of bands 9 and 10 in the c component of a single specimen; the relative intensities have been estimated visually. A crystal diagram is shown alongside with indication of the points at which the spectra were obtained. Similar variations occur in bands 8 to 10 in the component perpendicular to c as well as in other bands (4, 6 and 7), but the strong background makes it difficult to study these without objective photometry. Bands 1, 2, 3 and 8 are entirely absent from the spectra of some crystals. For example it was possible to project a portion of a crystal in whose spectrum band 2 disappeared and reappeared successively according to the slit width.

Although all bands except 9 and 10 are usually strongly polarized and absent from the c component, in some specimens extremely weak 4 and 8 bands could be observed in the c component; in the spectrum of individual portions of one of the specimens the depolarization of band 8 was extremely marked.

The extreme variation of bands 1 to 10 from crystal to crystal and especially within a single crystal seems to us to prove that they cannot be associated with intrinsic absorption in a perfect lattice (including exciton absorption) and result from the existence of defects.

In order to determine the location of the defects corresponding to bands 9 and 10 various specimens were etched for 2 minutes in a 1:1 solution of HCl. After the etching the intensity of band 10 was strongly increased, and it was very strong even in those portions of the crystal where it had been absent before etching. Therefore absorption in this instance is at least partly localized in the surface layer, which is distorted by etching. We can assume that the defects which give rise to absorption in the remaining strongly polarized bands are spatially distributed.

It is reasonable to assume that the closeness of bands 1-10 to the continuous absorption region results from the fact that they are caused not by the excitation of weakly bound electrons attached to defects but to transitions of electrons in ions of the base material adjacent to defects; thus they are to a certain extent similar to the α and β bands in the spectra of alkali halide crystals [4]. If this is in accordance with reality then in the infrared region we can expect to find impurity absorption bands with which some of bands 1-10 are associated and in whose "shadow" they appear. It is also of interest to determine whether there is any correlation between the photo-electric sensitivity of the crystals and the intensity of bands 1-10. At the present time work is being done in this direction.

As has been remarked by S. I. Pekar in a discussion of the present work, absorption experiments are also not inconsistent with the assumption that some of the bands 1-10 result from transitions to exciton states, which are forbidden in a perfect lattice and are allowed because of internal strains. A group-theoretical study shows that only a few types of strains in a C_{6v}^4 lattice can lead to the experimentally observed polarization of absorption bands 1-7 in the plane perpendicular to the c axis; the simplest type is the bending of the plane perpendicular to c with retention of a twofold axis of symmetry. However in view of the irregular variation of the relative intensities of the separate bands in different crystals and even in a single specimen the entire group of bands 1-10 cannot be attributed to the allowing of ordinarily forbidden transitions.

---

*In the strong absorption after 21,100 cm^{-1} no structure has yet been detected and this absorption appears continuous. But it is possible that the study of still thinner specimens at 4.2°K will permit a more thorough investigation of this region of absorption.

**By defects we understand any imperfections of the crystal structure such as vacancies, impurities, dislocations, etc.

We also investigated the luminescence spectrum of CdS single crystals at 20.4° K.* Both green and blue luminescence was observed [5]. We shall not give a detailed description of the spectrum and its temperature dependence but shall mention one important characteristic. In the spectrum of a very thin crystal, the thinness being required to reduce reabsorption, narrow blue luminescence bands were observed corresponding in frequency to the absorption bands 1,, 2, 4, 8-10; this is in agreement with [6] where it is pointed out that some luminescence bands at 77°K coincide with absorption bands at 4.2°K. In addition the spectrum contains longer wave bands of blue luminescence [7] and a series of broader bands of green luminescence. We believe that the simultaneous presence in the luminescence spectrum of the indicated six bands is evidence that they are not associated with exciton states but rather with electron transitions near defects. At 20.4°K ($kT = 14\ cm^{-1}$) luminescence can occur simultaneously from levels 1-10 in the interval $\sim 200\ cm^{-1}$ only if an equilibrium distribution cannot be established in the excited state, which is extremely unlikely for exciton states. This is possible only if these levels belong to spatially distributed defects.

In conclusion it must be noted that in the broad bands 11-17 which are present in both spectral components no variations were detected; these remained practically unchanged in all specimens and in all portions of a single specimen. We hope that future intensity measurements will completely separate the absorption that results from the presence of defects from the absorption by a perfect lattice and provide an explanation of the structure of the intrinsic absorption edge in CdS crystals.

We take this opportunity of thanking Ukrainian Academician V. E. Lashkarev and Associate Academician A. F. Prikhot'ko for discussions and valuable suggestions.

LITERATURE CITED

[1] E. F. Gross and M. A. Iakobson, Dokl. Akad. Nauk SSSR 102, 485 (1955); E. F. Gross, Izv. Akad. Nauk SSSR, Ser. Fiz. 20, 89 (1956).

[2] V. L. Broude, O. S. Pakhomova and A. F. Prikhot'ko, Optics and Spectroscopy (USSR) 2, No. 3 (1957).

[3] V. L. Broude and V. S. Medvedev, Zavodskaya Lab. 17, 486 (1951).

[4] F. Seitz, Revs. Mod. Phys. 26, 7 (1954).

[5] L. R. Furlong, C. F. Ravilious, Phys. Rev. 98, 954 (1955).

[6] E. F. Gross and M. A. Iakobson, J. Tech. Phys. (USSR) 26, 1369 (1956).**

[7] E. Grillot, J. Phys. Radium 17, 624 (1956).

Physics Institute, Academy of Sciences,
Ukrainian SSR

Received January 7, 1957

---

* Luminescence excited through a black Wood filter passed through the specimen before traversing the spectrograph slit (transillumination).

** [Soviet Physics - Technical Physics, p. 1340.]

CONCENTRATION DEPENDENCE OF THE ABSORPTION SPECTRA OF ORGANIC VAPORS

B. S. Neporent and V. P. Klochkov

(Presented by Academician A. N. Terenin January 14, 1957)

In studies [1,2] of the fluorescence of β-naphthylamine vapor one of the authors established the dependence of the absorption coefficient on the vapor pressure. Later, while investigating the absorption and fluorescence spectra of a family of substituted phthalimides [3-5], we found no important pressure dependence of the absorption spectra of the vapors in a relatively narrow range around 0.1 mm Hg. Also, in collaboration with A. A. Solodovnikov [6] we established that the addition of helium to the vapor of 3-dimethylamino-6-aminophthalimide reduces absorption as a peculiar function of the vapor pressure of the phthalimide vapor similarly to the observations of β-naphthylamine vapor in [2]. This result shows that there is an interaction between the molecules of 3-dimethylamino-6-aminophthalimide at much lower pressures than those which were used in the absorption measurements of [4,5]. It was therefore of interest to investigate the concentration dependence of the absorption spectra of a number of aromatic vapors over a broad range.

The compounds chosen for study belong to different categories in the classification given in [3,7], namely: anthracene (I), 3-acetylaminophthalimide (II), 3-aminophthalimide (III) and 3-dimethylamino-6-aminophthalimide (IV). The molecules of substance I, with a partly resolved spectral structure, are of a simple polyatomic type. Continuous spectra were found for substances II, III and IV [4,5]. These are complex polyatomic molecules. In going from II to III and IV we pass from modulation spectra to attenuation spectra.

The measurements were performed with the apparatus described in [5]; for strong concentrations (vapor pressure 5-0.1 mm Hg) we used vessels 2 and 40 cm long, while for lower concentratons (vapor pressure 10^{-1}-10^{-3} mm Hg) we constructed a cell of long optical path by White's method [7] as improved by Bernstein and Herzberg [8] which permitted measurements with an optical path up to 40 m. The radius of curvature of the mirrors of the cell was 1 m. The temperature dependence of the vapor pressure of phthalimide derivatives was determined by one of the authors [9].

Our principal results are given in Fig. 1., where the vertical axis shows relative values of the absorption coefficient $\epsilon_{rel} = \epsilon/\epsilon_{max}$. The concentrations to which the curves of Fig. 1 refer and the band intensities are given in Table 1.

It follows from the figure that for concentrations varying in a definite range the absorption spectra change; the character of the changes and, in the main, the concentration region in which these changes occur depend on the type of molecule.

Let us consider the nature of these changes for the vapor of 3-aminophthalimide, which was studied in the broadest concentration range ($60 \cdot 10^{15}$-$0.038 \cdot 10^{15}$ molecules/cm^3 or 3.6-$1.9 \cdot 10^{-3}$ mm Hg). Reduction of the concentration from $60 \cdot 10^{15}$ to $2.5 \cdot 10^{15}$ molecules/cm^3 is accompanied by no change of the spectrum. Further reduction to $0.1 \cdot 10^{15}$ molecules/cm^3 is accompanied by slight narrowing of the band and a gradual shift towards higher frequencies followed by the appearance of traces of a vibrational spectral structure (bent curve); when the concentration is further reduced from $0.065 \cdot 10^{15}$ to $0.038 \cdot 10^{15}$ molecules/cm^3 this does not become more pronounced, – the shape of the spectrum ceases to depend on the concentration. Thus the concentration range of 3-aminophthalimide vapor in which the shape of the spectrum changes is approximately $0.1 \cdot 10^{15}$- $1 \cdot 10^{15}$ molecules/cm^3.

TABLE 1

Substance	Vapor temperature in °K	Pressure in mm Hg	Concentration $C \cdot 10^{-15}$ molecules/ / cm³	Length of optical path in cm	Designation in Figure 1
I. Anthracene	493	$1.85 \cdot 10^{-1}$	3.6	42	a
	493	$1.74 \cdot 10^{-1}$	3.4	42	b
	493	$9.3 \cdot 10^{-2}$*	1.8	42	c
	493	$4.8 \cdot 10^{-2}$	0.95	42	d
II. 3-acetylamino-phthalimide	498	$3.25 \cdot 10^{-1}$	6.3	42	a
	498	$8.6 \cdot 10^{-2}$	1.6	42	c
	498	$3.6 \cdot 10^{-2}$	0.7	42	b
	498	$2.6 \cdot 10^{-2}$*	0.5	42	d
	498	$2 \cdot 10^{-2}$	0.39	42	d
III. 3-amino-phthalimide	518	3.58	60	2	a
	493	$1.25 \cdot 10^{-1}$*	2.55	42	a
	493	$6.2 \cdot 10^{-2}$	1.26	42	d
	463	$2.6 \cdot 10^{-2}$	0.47	400	b
	463	$1.2 \cdot 10^{-2}$	0.25	400	
	463	$5.2 \cdot 10^{-3}$	0.105	1600	e
	463	$3.15 \cdot 10^{-3}$*	0.065	2000	c
	463	$1.9 \cdot 10^{-3}$	0.038	3200	c
IV. 3-dimethyl-amino-6-amino-phthalimide	503	$1.17 \cdot 10^{-1}$	2.26	42	b
	450	$5.2 \cdot 10^{-3}$	0.11	1600	c
	450	$3.2 \cdot 10^{-3}$	0.07	1600	c

* Pressure at which spectral change terminates.

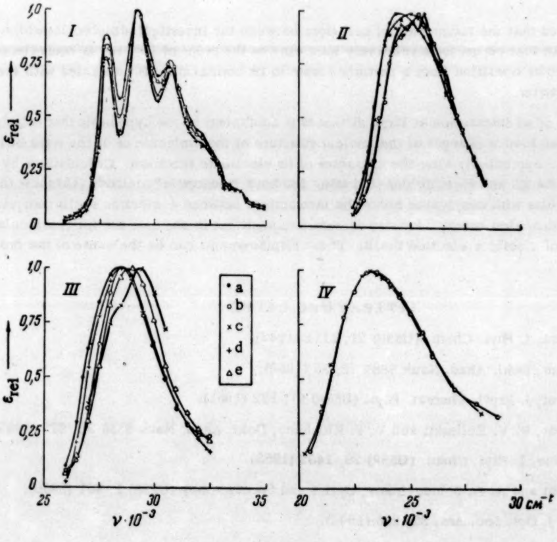

Fig. 1.

Other substances were investigated in a narrower concentration range; nevertheless the data show that for 3-acetylaminophthalimide the spectral changes with pressure reduction cease at $0.5 \cdot 10^{15}$ molecules/cm^3 and for anthracene at $1.8 \cdot 10^{15}$ molecules/cm^3.

Thus in passing from anthracene to 3-aminophthalimide we observe a reduction of the lower concentration boundary at which the change of spectral shape begins, that is, the intermolecular interactions are strengthened with an increased degree of intramolecular interactions [4,5].

The shape of the spectrum of 3-dimethylamino-6-aminophthalimide does not change even when the concentration is reduced to $0.07 \cdot 10^{15}$ molecules/cm^3. Hence it follows that either the spectral changes occur at still lower concentrations than for 3-aminophthalimide or that these interactions do not affect the shape of the spectral band, which is an attenuation spectrum whose forming mechanism is apparently different from the substances I, II and III [10]. The second hypothesis is more probable because the effect of helium on the spectrum of 3-dimethylamino-6-aminophthalimide shows [6] that the interactions in question do occur.

In our investigations [4,5] of the spectra of substituted phthalimides, which were conducted at vapor pressures from 0.1 to 0.4 mm, we concluded on the basis of the fact that the absorption spectra were independent of the vapor pressure, that the continuous character of the spectra resulted from their origin exclusively in intramolecular interactions. The results of the present investigation show that in actuality the spectral shape of the first members of the investigated series of compounds is determined by both intra- and intermolecular interactions. As the degree of intramolecular interaction increases, in accordance with which the substances were serially arranged in [4], the effect of the intermolecular forces is reduced.

A few preliminary remarks must be made regarding the nature of the intermolecular interactions under consideration.

It follows from the data presented that the intermolecular forces which affect the shape of the spectra act either at large distances of the order of hundreds of angstroms or, when the corresponding perturbations of the molecular systems occur in close collisions, the perturbed molecular state lasts 10^{-7}-10^{-5} seconds after the collision. We have no information which would enable us to decide between these two extremely different explanations.

It should be noted that the assumption of collisions between the investigated molecules which result in changes of their structure that persist for a relatively long time of the order of 10^{-5} sec is equivalent to the hypothesis that a molecular transition from a perturbed state to its normal state is associated with the surmounting of some potential barrier.

The assumption of an interaction at large distances is equivalent to the hypothesis that relatively weak intermolecular forces can induce changes of the nuclear structure of the molecule or of the state of its electronic envelope that will appreciably alter the character of its electronic spectrum. Calculations by Coulson and Davies [11] and by Haugh and Hirschfelder [12] using London's "monopole" methods [13] show that in the case of extended molecules with conjugated bonds the interactions between π electron shells comprise by far the greater part of the dispersion energy. We can therefore expect that in our case the intermolecular forces produce displacements of mobile π electron shells. These displacements can be the cause of the broadened spectra.

LITERATURE CITED

[1] B. S. Neporent, J. Phys. Chem. (USSR) 21, 1111 (1947).

[2] B. S. Neporent, Dokl. Akad. Nauk SSSR 72, 35 (1950).

[3] B. S. Neporent, J. Exptl. Theoret. Phys. (USSR) 21, 172 (1951).

[4] B. S. Neporent, V. V. Zelinskii and V. P. Klochkov, Dokl. Akad. Nauk SSSR 92, 927 (1953).

[5] V. P. Klochkov, J. Phys. Chem. (USSR) 29, 1432 (1955).

[6] B. S. Neporent and A. A. Solodovinkov, Optics and Spectroscopy (USSR) 1, 951 (1956).

[7] J. U. White, J. Opt. Soc. Am. 32, 285 (1942).

[8] H. J. Bernstein and C. Herzberg, J. Chem. Phys. 16, 30 (1948).

[9] V. P. Klochkov, J. Phys. Chem. (USSR) 30, 2823 (1956).

[10] B. S. Neporent, J. Phys. Chem. (USSR) 30, 1048 (1956).

[11] C. A. Coulson and P. L. Davies, Trans. Farad. Soc. 48, 777 (1952).

[12] E. F. Haugh and J. O. Hirschfelder, J. Chem. Phys. 23, 1778 (1955).

[13] F. London, J. Phys. Chem. 46, 305 (1942).

Received January 9, 1957

ON THE MULTIPLE EXCITATION OF ATOMS

K. I. Rozgachev and V. A. Fabrikant

(Presented by Academician M. A. Leontovich January 9, 1957)

Only indirect experimental data have been available concerning atomic excitation in stages by collisions with electrons [1].. Theoretical calculations of the probability of multiple excitation are of approximate character [2]. In these processes an excited atom undergoes inelastic collision with an electron which raises the atom to a higher energy level. The excitation potential of the already excited atom can be considerably lower than the direct excitation potential. This last circumstance entails that in multiple excitation to the highest energy levels a very much larger fraction of all the discharge plasma electrons must participate than in the case of direct excitation. Also, the effective cross section of an excited atom must exceed that of a normal atom. Multistage processes thus play an important part in gas discharges.

The present work aimed to provide a direct experimental proof of the existence of multiple electronic excitation and to determine the parameters of such processes. Our experiments are an electronic analog of the well-known experiments of Fuechtbauer and of Wood on multiple optical excitation of atoms [3].

We selected for study the visible mercury triplet 5461-4538-4047 A with the excitation potential 7.73 ev (7^3S_1 level). In this case stepwise excitation from the $6^3P_{0,1,2}$ and 6^1P_1 levels is possible. There must be especially large numbers of atoms on the metastable $6^3P_{0,2}$ levels.

Mercury atoms can be excited to the 6P levels either by electronic collisions or by irradiation with resonance lines. The second method possesses a number of advantages but involves experimental difficulties and will be used by us at a later time.

In the present work the first method was used. The experimental tube with an electron gun producing slow electrons followed the design of Hanley and Schaffernicht [4]. The radiation of the visible triplet was recorded by an ISP-51 spectrograph both photographically and through a 13-stage photomultiplier with antimony-cesium cathode. The photo-currents were amplified by the DuBridge-Brown method using an EM-4 tube. The maximum electron energy was controlled by a retarding field.

For observation of multistage processes it is necessary either to increase the current or raise the mercury vapor pressure in the tube. Our experiments showed that good results are obtained by increasing the pressure to 0.5-1 mm Hg. At these pressures and with collector currents of the order of 5-10 μa excitation in stages was clearly observed.

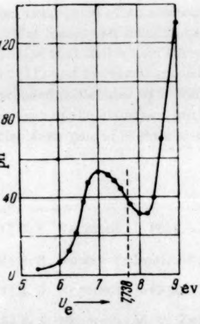

Fig. 1. Photocurrent as a function of electron energy.

Fig. 1 shows one of the experimental curves for the green line 5461 A. The horizontal axis gives electron energies and the vertical axis gives the photocurrent in relative units. Weak emission was observed beginning at 5 ev.

All of the curve to the left of 7.73 ev corresponds purely to excitation in stages. The sharp rise above 8 ev is due to the rapid increase of the cross section for direct excitation.

The peak is somewhat to the right of the peak of the excitation function of 6^3P_1 (6.6 ev). An exact analysis of the curve is difficult because we do not know the exact excitation functions for $6^3P_{0,2}$ and 6^1P_1.

Preliminary measurements showed that the intensity of the visible triplet lines increases in the region of stepwise excitation approximately as the square of the current. This was to be expected for constant lifetime of the atoms in the 6P levels.

LITERATURE CITED

[1] V. Fabrikant, F. Butaeva and I. Tsirg, J. Exptl. Theoret. Phys. (USSR) 8, 35 (1938); V. Fabricant, F. Butaewa, I. Zirg, Sow. Phys. 13, 23 (1938); H. Massey, E. Burhop, Electron and Ionic Impact Phenomena (Oxford, 1952), pp. 68-71.

[2] B. Iavorskii, J. Exptl. Theoret. Phys. (USSR) 17, 315 (1947).

[3] C. Füchtbauer, Physik Z. 21, 635 (1920); R. Wood, Phil. Mag. 50, 775 (1925); 4, 466 (1927).

[4] W. Hanle and W. Schaffernicht, Ann. Phys. 6, 905 (1930).

V. M. Molotov Moscow Power Institute

Received January 7, 1957

THE RELATIVISTIC COLLISION INTEGRAL

N. A. Chernikov

(Presented by Academician V. A. Fok January 14, 1957)

Let a particle α enter a substance which is in general inhomogeneous and of varying density. The particles which compose the substance move with various velocities. We shall assume that only two-particle collisions between the particles α and the particles of the substances are of importance and that external forces which can in general act on the particles do not affect the collisions. We shall assume that all particles are relativistic in Galilean space-time.

It is required to determine the probability $T^{-1}(P_0)\,d\tau$ that particle α, which at some time t_0 leaves the point x_0, y_0, z_0 with momentum $m\mathbf{u}_0$, after the proper time interval $d\tau$ collides with some particle of the substance; m is the rest mass of particle α. The symbol P_0 denotes $\{x_0, y_0, z_0, t_0, \mathbf{u}_0\}$.

It is clear that

$$T^{-1}(P_0) = \sum_{\beta} T^{-1}_{\alpha\beta}(P_0), \tag{1}$$

where $T^{-1}_{\alpha\beta}(P_0)$ is the probability that particle α collides with a definite particle β of the substance. The summation is carried out over all particles of the substance. The subscript α has been omitted in the left-hand side of this equation. Let $A_\beta(P)\,dx\,dy\,dz\,du_1\,du_2\,du_3$ be the probability in some inertial system that at time t particle β is in the volume element dxdydz whose center is at the point x, y, z and that its momentum is between $m_\beta u_k$ and $m_\beta(u_k + du_k)$ where k = 1,2,3 and m_β is the rest mass of particle β. The interaction radius of particles α and β will be denoted by $r_{\alpha\beta}(\widetilde{v})$, where v is the modulus of the relative velocity.

The problem concerning the manner in which $T^{-1}_{\alpha\beta}(P_0)$ is related to the quantities $A_\beta(P)$ and $r_{\alpha\beta}(v)$ is a special case of the probability that the world line of a particle intersects a hypersurface in the space F of particle states. The general problem has been formulated in [1]. The state of a particle refers to the set of values P of its space-time location and its velocity. In the interval between two successive collisions of a particle β with other particles of the substance the motion of β is represented by a curve in space F. This curve will be called the world line of β during this interval. It follows from [1] that the function $A_\beta(P)$ on any hypersurface S in F is the probability density that the world line of β in some interval between collisions with other particles of the substance intersects the hypersurface S.

We shall determine $T^{-1}_{\alpha\beta}(P_0)$ in prerelativistic mechanics. It is obvious that a collision occurs as soon as particle β intersects the hemisphere of radius $r_{\alpha\beta}(\widetilde{v})$ with its center at the position of particle α which is convex in the direction of the vector of relative velocity $\mathbf{v}_0 - \mathbf{v}$ of these particles ($\mathbf{v}_0$ is the velocity of and $\mathbf{v}$ is the velocity of β). The equations of this hemisphere are

$$\begin{aligned}
x &= x_0 + r_{\alpha\beta}(\widetilde{v})\,\{\sin\widetilde{\theta}\cos\widetilde{\varphi}\cos\theta - \cos\widetilde{\theta}\cos\widetilde{\varphi}\sin\theta\cos\varphi + \sin\widetilde{\varphi}\sin\theta\sin\varphi\},\\
y &= y_0 + r_{\alpha\beta}(\widetilde{v})\,\{\sin\widetilde{\theta}\sin\widetilde{\varphi}\cos\theta - \cos\widetilde{\theta}\sin\widetilde{\varphi}\sin\theta\cos\varphi - \cos\widetilde{\varphi}\sin\theta\sin\varphi\},\\
z &= z_0 + r_{\alpha\beta}(\widetilde{v})\,\{\cos\widetilde{\theta}\cos\theta + \sin\widetilde{\theta}\sin\theta\cos\varphi\},
\end{aligned} \tag{2}$$

where $\tilde{v}\sin\tilde{\theta}\cos\tilde{\varphi} = v_{01} - v_1; \quad \tilde{v}\sin\tilde{\theta}\sin\tilde{\varphi} = v_{02} - v_2; \quad \tilde{v}\cos\tilde{\theta} = v_{03} - v_3;$
$0 \leqslant \theta \leqslant \pi/2;\ 0 \leqslant \varphi < 2\pi$. These equations together with $t = t_0$ give a five-dimensional surface $\Gamma(P_0)$ in F. Since we have assumed that external forces do not affect the collisions we must assume that such forces are absent during collisions. We can therefore assume that during the interval $d\tau$ of the proper time of α its state P_0 is displaced in space F by an infinitely small vector distance $\{\mathbf{v}_0, d\tau, d\tau, 0, 0, 0\}$.[*] Every point of the surface $\Gamma(P_0)$ undergoes the same vectorial displacement and this surface sweeps through the six-dimensional strip ΔS. The sought probability $T^{-1}_{\alpha\beta}(P_0)\,d\tau$ is equal to the probability that the world line of β intersects this strip. Hence we obtain

$$T^{-1}_{\alpha\beta}(P_0) = \int\limits_{-\infty}^{+\infty} r^2_{\alpha\beta}(\tilde{v})\,\tilde{v}\,(d\mathbf{v}) \int\limits_0^{\pi/2}\int\limits_0^{2\pi} A_\beta(x, y, z, t_0, \mathbf{v}) \cos\theta \sin\theta \, d\theta \, d\varphi, \tag{3}$$

where x, y, z are defined by (2). If the values of $A_\beta(P)$ on the hemisphere (2) differ little from its value at the center x_0, y_0, z_0 we have for $T^{-1}_{\alpha\beta}(P_0)$ the usual expression

$$T^{-1}_{\alpha\beta}(P_0) = \int\limits_{-\infty}^{+\infty} A_\beta(x_0, y_0, z_0, t_0, \mathbf{v})\,\pi r^2_{\alpha\beta}(\tilde{v})\,\tilde{v}\,(d\mathbf{v}). \tag{4}$$

Under this condition $T^{-1}_{\alpha\beta}(P_0)$ can also be derived in relativistic mechanics by the same method.[**] The hemisphere need only be replaced by a two-dimensional area in space-time perpendicular to the vectors $\{\mathbf{u}, u_4\}$ and $\{\mathbf{u}, u_{04}\}$ with its center at the point x_0, y_0, z_0, t_0 and of area $\sigma_{\alpha\beta}(E_{a_0 a})$ equal to the cross section for the interaction of particles α and β, where $E_{a_0 a} = mc^2\left\{\operatorname{ch}\frac{S_{a_0 a}}{c} - 1\right\}$,[***] $\operatorname{ch}\frac{S_{a_0 a}}{c} = u_4 u_{04} - \frac{\mathbf{u}\mathbf{u}_0}{c^2}$, $u_4 = \sqrt{1 + u^2/c^2}$. When the state P_0 is fixed the set of such areas in space F fills the five-dimensional surface $\gamma(P_0)$. In the interval $d\tau$ of the proper time of α its state P_0 is shifted in space F by the infinitely small vector $\{\mathbf{u}_0 d\tau, u_4 d\tau, 0, 0, 0\}$. Each point of the surface $\gamma(P_0)$ undergoes the same vectorial shift and thus a six-dimensional strip is swept through. The sought probability $T^{-1}_{\alpha\beta}(P_0)\,d\tau$ is, as before, the probability of the intersection of the world line of particle β with this strip. Hence

$$T^{-1}_{\alpha\beta}(P_0) = \int\limits_{-\infty}^{+\infty} A_\beta(x_0, y_0, z_0, t_0, \mathbf{u})\,\sigma_{\alpha\beta}(E_{a_0 a})\,c \operatorname{sh}\frac{S_{a_0 a}}{c}\,da, \tag{5}$$

where $da = \frac{du_1\,du_2\,du_3}{u_4}$. Thus the problem has been solved.

Let us further assume that the particles α and β interact for a short time. Starting from state P^* particle α during proper time interval $d\tau$ can collide with β and then cease to interact with the latter, being in a state which belongs to the elementary region $d \subset F$ with center at point P. Under the above assumptions the probability of such an event is

$$\delta(x - x^*)\,\delta(y - y^*)\,\delta(z - z^*)\,\delta(t - t^*)\,\mathscr{L}_{\alpha\beta}(P; a^*)\,\mu(d)\,d\tau, \tag{6}$$

where $\mu(d) = dx\,dy\,dz\,dt\,da$. Let the differential scattering cross section of particle α with velocity a^* on particle β with velocity a' be

---

[*] Here and hereinafter in relativistic mechanics the coordinates in F will be the Galilean coordinates x, y, z, t of the particle and the coordinates u_1, u_2, u_3 of its velocity given by the ratios of the spatial components of its momentum to its rest mass.

[**] We shall limit ourselves to this condition because for an arbitrary radius of interaction of particles α and β the relativistic treatment will evidently encounter difficulties associated with the kinematics of the particle system.

[***] ["ch" ≡ "cosh;" "sh" ≡ "sinh" – Editor's note.]

$$d\sigma \overset{!}{=} H_{\alpha\beta}(E_{a^*a'}, E_{aa'}, \cos\theta_n)\,da, \tag{7}$$

where

$$\cos\theta_n = \frac{\operatorname{ch}\frac{S_{a^*a'}}{c}\operatorname{ch}\frac{S_{aa'}}{c} - \operatorname{ch}\frac{S_{aa^*}}{c}}{\operatorname{sh}\frac{S_{a^*a'}}{c}\operatorname{sh}\frac{S_{aa'}}{c}}. \tag{8}$$

In the derivation of (5) we replace $\sigma_{\alpha\beta}\,(E_{a_0a})$ by $d\sigma$ and find that the function $\mathscr{L}_{\alpha\beta}$ in (6) is of the form

$$\mathscr{L}_{\alpha\beta}(P; a^*) \overset{!}{=} \int_{-\infty}^{+\infty} A_\beta(x, y, z, t, \mathbf{u}')\, H_{\alpha\beta}(E_{a^*a'}, E_{aa'}, \cos\theta_n)\, c\operatorname{sh}\frac{S_{a^*a'}}{c}\,da'. \tag{9}$$

On the basis of [1] and the results obtained here we can write the relativistic kinematic equation of motion of α in matter. Let T_0^{-1} be the probability of spontaneous decay of α during unit proper time. We denote

$$\mathscr{L}(P; a^*) \overset{!}{=} \sum_\beta \mathscr{L}_{\alpha\beta}(P; a^*), \tag{10}$$

where the summation, as in (1), is taken over all particles in the substance. The equation mentioned is then

$$u_4\frac{\partial A(P)}{\partial t} + \mathbf{u}\nabla A(P) + u_4\frac{\partial}{\partial\mathbf{u}}\left[\frac{\vec{\omega}(P)}{u_4}A(P)\right] + [T^{-1}(P) + T_0^{-1}]\,A(P) = \lambda\int_{-\infty}^{+\infty} A(P^*)\,\mathscr{L}(P: a^*)\,da^* + Q(P). \tag{11}$$

The subscript α has been omitted. Decomposition of $A\,(P;\lambda)$ in powers of λ in this case denotes decomposition according to the number of collisions of α in the substance. (See reference [1] for the rest of the notation).

The quantity

$$\int_{-\infty}^{+\infty} A(P^*)\,\mathscr{L}(P; a^*)\,da^* - A(P)\,T^{-1}(P) \tag{12}$$

is the relativistic Boltzmann collision integral which takes account of collisions between the particle α and particles of the substance.

The author is profoundly grateful to Academician V. A. Fok for discussions.

LITERATURE CITED

[1] N. A. Chernikov, Dokl. Akad. Nauk SSSR 112, 6, 1030 (1957).*

Joint Institute for Nuclear Research

Received January 6, 1957

---

* [Soviet Physics - Doklady. p. 103.]

THE TITANIUM $K\beta$ GROUP IN TITANIUM CARBIDE

E. E. Vainshtein and Iu. N. Vasil'ev

(Presented by Academician A. P. Vinogradov December 25, 1956)

The nature of the chemical forces between metal and nonmetal atoms in the carbides, nitrides and hydrides of the transition elements has interested investigators for many years. However, these forces are still not completely understood.

Several hypotheses have been advanced [1-4] regarding the nature of the chemical bond in these substances as a basis for the experimental work on their magnetic, electrical, crystal, chemical and other properties. Ubbelode [4] examined the problem thoroughly from a thermodynamical point of view. Yet, until recently there has been an almost complete absence of data on the X-ray spectra of the atoms in these compounds and of their variation in solid alloys of different composition. The first comparatively systematic investigation of this type was carried out very recently [5].

Although some of the results of [5] such as those concerning titanium hydride are of a provisional nature and require verification using material of more definitely determined chemical composition, by fluorescence, the results as a whole leave no room for doubt that the energies and fine structure of the X-ray lines of titanium in its oxide, carbide, nitride and hydride reveal significant and accurately measurable variations which through more precise and systematic investigations could throw new light on the nature of the chemical bond and state of the metal atoms in these compounds.

TABLE 1

No. of specimen	C_{tot}, %	C_{free}, %
1	23.7	3.65
2 **	22.1	3.92
3	19.0	0.3
4 *	18.8	0.1
5 **	15.9	0.06
6	14.3	0.1
7 **	12.4	0.04
8	8.8	0.18

Note. Alloy No. 1 consisted of a mixture of carbide No. 3 and carbon black. Alloys No. 6 and No. 8 were mixtures of carbide No. 3 and titanium.

---

* Amount of nitrogen determined at ~0.03%.

** Amount of oxygen determined at ~0.4%

The present paper is the first of a series of investigations of the X-ray spectra of the carbides, nitrides and hydrides of the transition metals; these studies are being carried out by a group at the Institute of Geochemistry and Analytic Chemistry of the Academy of Sciences USSR and the (K. D. Ushinskii) X-Ray Laboratory of the Odessa Pedagogical Institute.

We investigated the $K\beta$ group of titanium X-ray lines in a series of specially* prepared alloys of the Ti−C system with nonmetal content varying from 9 to 24 %. The designations and compositions of the alloys are given in Table 1.

Most of the alloys were prepared by the usual method from a mixture of TiO_2 and carbon black heated in a hydrogen atmosphere at 1800-2000°. Three alloys were made with specimen No. 3 which could very nearly be represented by the formula TiC. After chemical analysis the alloys were subjected to an X-ray structural analysis. The lattice constants of the alloys were compared with the literature [6] and showed good agreement.

In the single-phase region there was a linear increase of the lattice constant of the carbides (from 4.28 to 4.32 A) as the carbon content was increased to 20%, and a constant value for alloys with larger nonmetal content. No metallic titanium was detected in the alloys.

A RSD-2 vacuum focusing spectrograph [7] was used with a bent quartz crystal analyzer. The crystal had a 1 m radius of curvature. The reflection planes were $(10\bar{1}0)$. A 10 × 50 mm crystal polished by the Johanson method [8] was bent in a special four-point crystal holder [9].

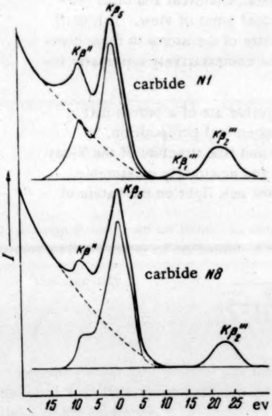

Fig. 1. Titanium $K\beta$ lines in carbide No. 1 with maximum C content and in carbide No. 8 with minimum C content.

The titanium spectra were photographed in the second order of reflection on film placed at right angles to the X-ray beam. The linear dispersion of the spectrograph in the investigated region was 5.7 XU/mm. To fix the position of the $K\beta_1$ and $K\beta_5$ lines of titanium the $K\alpha_{1,2}$ lines of vanadium were used as reference lines. The positions of the $K\beta''$, $K\beta_1'''$ and $K\beta_2'''$ lines were measured with reference to $K\beta_5$. The specimen was placed on the copper anode of a powerful sectional X-ray tube which was operated at 12 kv and 55 ma. Each of the spectrograms was analyzed with a MF-2 microphotometer at three points and the results were averaged. Not fewer than three identical spectra were obtained with each alloy and showed good reproducibility.

Figure 1 shows two spectra containing the $K\beta_5$, $K\beta''$, $K\beta_1'''$, and $K\beta_2'''$ lines of titanium in the alloys with maximum (carbide No. 1) and minimum (carbide No. 8 [8]) carbon content. The positions of the $K\beta_1$, $K\beta_5$, $K\beta''$, $K\beta_1'''$ and $K\beta_2'''$ lines in the titanium spectra shown in Fig. 1 and in alloys with intermediate carbon content are identical within the limits of error of the measurements (± 0.2 ev). Only the relative intensities of the lines vary, especially the ratio of the $K\beta''$ peak to the $K\beta_5$ peak. An idea of the variation of the ratio $IK\beta''/IK\beta_5$ with the carbon content is given by Curve 1 of Fig. 2. Curve 2 shows the variation of the integral intensity of the combined $K\beta''$-$K\beta_5$ band compared with the $K\beta_2'''$ line, which was arbitrarily selected as an internal intensity standard [5] in each of the spectrograms. The $K\beta_5$ half-width remains constant for alloys with large carbon content and tends to increase in the titanium spectra of low-carbon carbides. On the average the $K\beta_2'''$ line is about 25% as intense as the $K\beta_5$ line. $K\beta_1'''$ is on the average 5 (± 0.8) times less intense than $K\beta_2'''$ and tends to become weaker as the carbon content of the alloy is diminished. In the titanium spectrum of some alloys $K\beta_1'''$ can hardly be distinguished from the background.

---

* The authors take this opportunity to thank E. A. Shchetlina for assistance in preparing the alloys.

Certain generalization can be drawn from the experimental data.

1. The positions of $K\beta_1$ and $K\beta_5$ is unchanged in the titanium spectrum of carbides with the carbon content varying from 9 to 20%. This also applies to the short-wave $K\beta_5$ boundary.

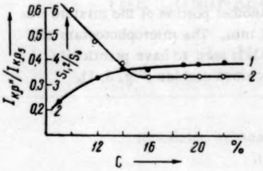

Fig. 2. $IK\beta''/IK\beta_5$ (1) and the relative intensity of the $K\beta''-K\beta_5$ X-Ray emission band (2) from titanium in carbides as a function of the carbon content of the alloys.

2. The separation of the $K\beta''$ and $K\beta_5$ peaks in the X-ray spectra of carbides of different composition is 7.9 ev. These two lines form essentially a single emission band with two clearly distinguishable peaks. In this respect this spectrum is distinguished qualitatively from the titanium spectrum in its dioxide, in which the $K\beta''$ band is separated from the titanium $K\beta_5$ line by a considerably greater distance [5] and is evidently an independent line.

3. As the carbon content of the carbides increases the relative intensity of the $K\beta''$ line or of the long-wave peak of the total $K\beta''-K\beta_5$ absorption band in the alloy increases. The speed of increase considerably exceeds that of the relative intensity of the $K\beta''$ line, as would be expected from the increased relative carbon content of the alloys and the assumption of unchanged probability of the corresponding radiative transition in carbides of varying composition. A regular change of the probability of this radiative transition in carbides of varying carbon content, with which we are concerned here, may have two causes; a difference of interatomic spacing in alloys of different composition and a change in the degree of overlapping of the atomic wave functions in these compounds. This could also explain the dependence of the integral intensity of the titanium $K\beta''-K\beta_5$ emission band in carbides on the carbon content.

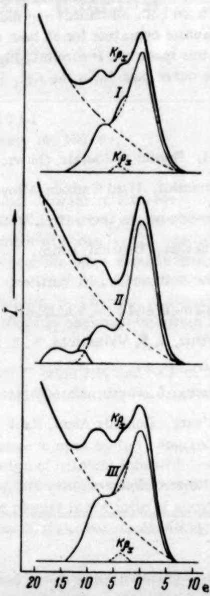

Fig. 3. The origin of the $K\beta_x$ line in the titanium X-ray spectrum of low-carbon carbides.

As a check of the conclusions concerning the character of the bonds in the alloys which may be drawn from the experimental data we are now investigating the X-ray absorption spectra of the same carbides.

In the fine structure of titanium emission spectra from some of the low-carbon carbides (Nos. 7 and 8) we observed two additional weak lines. One of these is easily identified as the $K\beta''$ line of titanium in its oxide which was present as an impurity in the specimen. The origin of the other line ($K\beta_x$ in Curve I of Fig. 3) could not be determined. It cannot be attributed to the presence of impurities * but must be associated

---

* Including nitrides, whose $K\beta_5$ line is in the longer wave portion of the spectrum.

with some processes which occur in the carbide at high temperatures (~ 1800°) and is greatly weakened at lower temperatures (~ 500°). This conclusion is supported by the results of the following experiment. Powdered TiO_2 and TiC whose spectra did not contain the $K\beta_X$ line were mixed in the ratio 1 : 3. A portion of the mixture was immediately placed on the anode of the X-ray tube and the X-ray spectrum was photographed; the temperature here could not exceed 500°. The spectrum obtained in this way (Fig. 3, II) was the combined titanium spectrum from both substances and did not contain the $K\beta_X$ line. Another portion of the mixture was first heated in a graphite container for an hour at 1850° and a pressure of 0.1 mm. The microphotogram of the spectrum from this specimen is shown in Fig. 3, III. The evidence of TiO_2 is seen to have practically disappeared and the curve that shows the $K\beta_X$ line resembles that for a low-carbon carbide (Fig. 3, I).

LITERATURE CITED

[1] D. Bernal, Physics of Metals (Moscow, 1933) (Russian translation).

[2] Ia. S. Umanskii, Hard Carbide Alloys (1947).

[3] S. A. Nemnonov, J. Tech. Phys. USSR 18, 246 (1948).

[4] A. P. Ubbelode, Uspekhi Khim. 7, 1692 (1933).

[5] E. E. Vainshtein and Iu. N. Vasil'ev, Doklady Akad. Nauk (SSSR) 114, 1, 53 (1957).•

[6] Ia. S. Umanskii and S. S. Khidekel', J. Phys. Chem. (USSR) 15, 9 (1941).

[7] K. I. Narbutt, E. E. Vainshtein, A. B. Gil'varg, and L. M. Bel'aev, Izv. Akad. Nauk SSSR, Ser. Fiz. 20, 152 (1956).

[8] T̄. Johanson, Z. Physik 82, 507 (1933).

[9] A. B. Gil'varg, Doklady Akad. Nauk SSSR 72, 489 (1950).

V. I. Vernadskii Institute of Geochemistry and
Analytic Chemistry,
Academy of Sciences, USSR

Received November 27, 1956.

• [Soviet Physics - Doklady, p. 207.]

THE LUMINESCENCE OF TRIVALENT URANIUM

L. N. Galkin and P. P. Feofilov

(Presented by Academician A. N. Terenin January 14, 1957)

Until recently it has been supposed that only hexavalent compounds of uranium are able to luminesce, especially those compounds which contain uranium in the uranyl ion UO_2^{++}. The bright green luminescence from this source has been much studied and has been discussed in a number of books [1-4]. Special emphasis has been laid on the absence of luminescence in compounds where the uranium has a valence different from 6 [4]. However, since the electronic configuration of the actinides is similar to that of the lanthanides (see [5], for example) for which the luminescence of trivalent ions is well known, it is natural to expect to observe luminescence from trivalent ions of the actinides. Luminescence has recently been reported from Am^{+++} [6] and Pu^{+++} [7] in $LaCl_3$ crystals.

In our study of artificial single crystals of fluorite CaF_2, strontium fluoride SrF_2 and barium fluoride BaF_2 containing about 0.1 to 0.3 % of uranium and grown under strongly reducing conditions we detected intense luminescence in the infrared region around 2.0-2.5 μ.

The single crystals were vacuum grown by the method which was developed by I. V. Stepanov [8]. In order to create the strongly reducing conditions required for the formation of uranium ions with lower valences, the original batch of pulverized and specially purified crystals of natural fluorite or specially synthesized fine-crystalline strontium and barium fluorides * contained a graphite powder in the ratio of about 10^{-3} g/g. The crystals which were thus grown were deeply colored as follows: red (CaF_2), red-orange (SrF_2) and orange (BaF_2) because of strong absorption bands in the visible region.

The absorption spectrum of a CaF_2 crystal containing uranium and grown under reducing conditions is shown in Fig. 1. Up to 1.3 μ the spectrum was measured with a SF-4 spectrophotometer, from 0.9 to 1.9 μ with the infrared spectrophotometer of N. G. Iaroslavskii [9]; in the long-wave region with an IKS-11 spectrophotometer.**

The absorption spectrum is seen to consist of a number of bands in the ultraviolet, visible and infrared regions. The peaks of the principal bands at room temperature are around $\underline{2.22}$, $\underline{2.15}$, 1.84, 1.34, $\underline{1.23}$, 1.045, 1.025, 0.99, 0.95, $\underline{0.89}$, $\underline{0.84}$, 0.71, 0.69, 0.64, $\underline{0.55}$, $\underline{0.51}$, $\underline{0.45}$, 0.34, $\underline{0.28}$ (the underlined values indicate the most intense bands). Similar absorption spectra were observed in crystals of SrF_2 and BaF_2 containing uranium ions. In these crystals, however, the group of strong bands in the blue-green region has been shifted, while unchanged in number and shape of the bands, toward longer waves by ~25 mμ for SrF_2 and ~ 50 mμ for BaF_2, which determines the difference in crystal coloration.

At the temperature of liquid air the spectra reveal a large number of very narrow lines, some of which have a width of the order of 1-3 A.

---

* Synthesized by I. A. Siniukova and E. G. Chernevskaia.

** The authors are indebted to N. G. Iaroslavskii, E. M. Makhov, and A. N. Aleksandrov for measurements of the infrared absorption spectra. K. P. Vasilevskii and A. V. Shablia also assisted in the initial stages of our work.

The luminescence spectrum was investigated with apparatus which consisted of a mirror monochromator and diffraction grating (300 lines/mm) a cooled lead sulfide photoconductive cell as receiver, an ac amplifier and EPP-09 recording instrument. The exciting source was a SVD-250 mercury lamp whose light passed through water and heat-absorbing glass which removed the infrared radiation. The exciting light was modulated by a perforated disk.

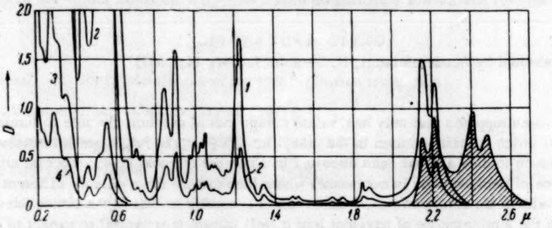

Fig. 1. Absorption and luminescence (shaded) spectra of a single crystal of CaF_2 with 0.25% U. Thickness of samples: 1) 30 mm; 2) 10 mm; 3) 1.5 mm; 4) 0.5 mm. Room temperature.

The luminescence of CaF_2-U crystals is very intense even at room temperature and consists of a number of bands in the interval 2.1-2.5 μ (Fig. 1).* At room temperature four bands are observed with peaks at about 2.15; 2.21; 2.42; and 2.49 μ. The two luminescence bands of shortest wavelength coincide within the limits of accuracy of the measurements with the longest-wave absorption bands; therefore resonance transitions are taking place.

The luminescence spectra of SrF_2-U and BaF_2-U crystals are in the same region but differ in details of the structure. Thus, the narrow bands in the spectrum of cooled BaF_2 crystals are observed around 2.18; 2.20; 2.29; 2.40; and 2.46 μ. The slight dependence of the luminescence spectrum on the material containing the uranium ions shows the weak interaction with the surrounding medium of the levels responsible for the long-wave absorption and emission. On the other hand the higher levels, which correspond to the shorter-wave (visible) absorption, are strongly shifted with a variation of the parameters of the crystal lattice containing the ions.

There is some basis for supposing that the luminescence which we detected can be ascribed to trivalent U^{+++} ions: 1) intense absorption and the characteristic banded spectrum of compounds containing trivalent uranium [10-14]; 2) the uniform distribution of the coloration of the crystal, which apparently results from the similarity of the ionic radius of U^{+++} and the radii of TR^{+++} ions, which are known to easily form mixed crystals with CaF_2 that exhibit isomorphic substitution [15]; 3) the recent discovery of U^{+++} ions in artificial CaF_2-U and SrF_2-U crystals by the use of paramagnetic resonance [16]. The conditions under which the crystals were grown in the last work mentioned were not described by the authors, but they could hardly have been more strongly reductive than the conditions for our own crystals.

U^{+++} ions have the electronic configuration $[R_n]5f^3$. The absorption and luminescence spectra which we observed must be associated with forbidden transitions within the 5f shell in the same way as the spectra of the rare earths are determined by transitions within the 4f shell. The transitions which give the long-wave absorption and luminescence must be between the levels ${}^4I_{9/2}$ (the ground state) and ${}^4I_{11/2}$. According to Jorgensen's calculations [14] the separation of these levels is 41008 cm^{-1} (2.44 μ). The next two strong absorption bands (1.23 and 0.89μ) result most likely from transitions to the ${}^4I_{13/2}$ and ${}^4I_{15/2}$ levels. The relatively high probability of the transitions which give the strong coloration of the crystals (while crystals which contain neodymium, the analog of uranium, are colorless with the same concentration of the activator) are characteristic for ions of the actinides [5].

---

* The luminescence spectrum in Fig. 1 was plotted from the recorded data without taking account of the spectral sensitivity of the instrument and the intensity distribution curves are only qualitative.

It is known that compounds of trivalent uranium are extremely unstable; this makes the study of their optical properties very difficult. The U^{+++} ions formed in the MeF_2 lattice are very stable; this apparently results from the forced valence stabilization of these ions by isomorphic substitution of Me^{++} ions.* The highly stable optical properties of single crystals of the alkali fluorides activated by trivalent uranium permit a thorough investigation of their luminescence spectra.

We are profoundly grateful to I. V. Stepanov and M. A. Vasil'eva, who grew the single crystals which were studied. O. V. Sokolova rendered great assistance in our study of the absorption spectra.

LITERATURE CITED

[1] E. Nichols and H. Howes, Fluorescence of the Uranyl Salts (Washington, 1919).

[2] P. Pringsheim, Fluorescence and Phosphorescence (Interscience Publishers, New York, 1949), Russian translation, 1951, Foreign Lit. Press.

[3] V. L. Levshin, Photoluminescence of Liquids and Solids (1951).

[4] G. H. Dieke and A. B. F. Duncan, Spectroscopic Properties of Uranium Compounds (New York, 1949).

[5] M. A. El'iashevich, The Spectra of the Rare Earths (Moscow, 1953) in Russian).

[6] D. M. Gruen, J. G. Conway, R. D. McLaughlin, and B. B. Cunningham, J. Chem. Phys. 24, 115 (1956).

[7] B. B. Cunningham, D. M. Gruen, J. G. Conway, and R. D. McLaughlin, J. Chem. Phys. 24, 1275 (1956).

[8] I. V. Stepanov and P. P. Feofilov, Report at the First Conference on Crystal Growth (Moscow, 1956).

[9] N. Ia. Iaroslavskii, Vestnik Leningrad Univ. 1950, No. 3, 55.

[10] The Transuranium Elements, Nat. Nuclear Energy Ser. (New York, 1949).

[11] R. Rohmer, R. Freymann, A. Chevet, and P. Hamon, Bull. Soc. Chim. France, 1952, No. 5-6, 603.

[12] F. Ephraim and M. Mezener, Helv. Chim. Acta 16, 1257 (1953).

[13] S. Freed and K. M. Sancier, J. Chem. Phys. 22, 928 (1954).

[14] Chr. K. Jørgensen, Dan. Mat. Fys. Medd. 29, 11 (1955).

[15] I. V. Stepanov and P. P. Feofilov, Doklady Akad. Nauk SSSR 108, 615 (1956).**

[16] B. Bleaney, P. M. Llewellyn, and D. A. Jones, Proc. Phys. Soc. B 69, 858 (1956).

Received January 8, 1957.

---

* The excess positive charge which results from such substitution can be neutralized in several ways [15].

** [Soviet Physics - Doklady, p. 350.]

AN EXPERIMENTAL STUDY OF THE RELATION BETWEEN THE SPEED OF HIGHLY ELASTIC RUPTURE AND THE STRAIN RATE

V. E. Gul' and G. P. Krutetskaia

(Presented by Academician V. A. Kargin December 22, 1956)

During the deformation of a polymer in a highly elastic state energy is expended to produce the strain and the simultaneous rupture process. The latter can in turn be subdivided into the formation of elementary rupture centers and the process of their growth.

In the present investigation we have endeavored to study the laws of the growth of ruptures as related to various factors: the magnitude of the defect, the strain rate, the deforming stress and the specific cohesive energy of vulcanized rubber. For this purpose we used samples of unfilled vulcanized SKN-18, SKN-26 and SKN-40 nitrile rubber with different degrees of cross linking. The specimens were rectangular, 50 mm wide and bore notches 5, 2.5 and 1.0 mm long at right angles to the direction of strain. We also used unnotched specimens. We used a RMM-60 tensile-testing machine at strain rates of 100, 200, 500, and 1000 mm/min. The relationship between the speed of rupture growth and other factors was studied with the aid of high-speed motion pictures at 800 and 4000 frames per second.* When such films were projected at 16 frames/sec the process under investigation was slowed down from 10 to 500 times. A special reading device was used to perform various measurements on the image of a rupturing specimen. For determination of the time at which various changes occur on the film a MN-7 neon lamp was used which furnished 100 flashes per second at 50 cycles. The light from this lamp was focused on the edge of the film through an optical system at equal time intervals. Figure 1 shows frames of the initial and final stages of rupture. In the initial stage of deformation the specimen was measured at intervals of 20-50 frames. Beginning with the instant of notch (l) enlargement (the beginning of rupture growth) the measurements were made every 2-5 frames and when the speed of rupture increased nonuniformly measurements were made on successive frames. A total of 300 high-speed films were obtained, so that some relationships could be clearly determined.

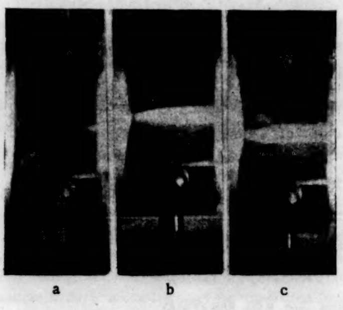

Fig. 1. Separate frames taken during the rupture of vulcanized rubber at 40°: a) beginning of rupture; b and c) final stages of the rupture.

All of the experimental data which will be presented hereinafter were obtained at +40°. It was found experimentally that the kinetics of rupture growth is very strongly affected by temperature.

The relation between the speed of rupture growth $(\Delta l/\Delta t) = v'$ and time t showed that the area bounded by the $\Delta l/\Delta t - t$ curve for all of the specimens is constant and independent of the strain rate. To some degree this provides a test of the accuracy of the experiment because $\int_0^{\tau} v' \cdot dt = l$, where τ is the time from the beginning of the straining to the rupture of the specimen. Figure 2 shows typical results obtained by the above-described method of reading the films.

---

* The authors are indebted to I. V. Kurskii for taking the high-speed motion pictures. V. Kovriga also assisted with the experimental work.

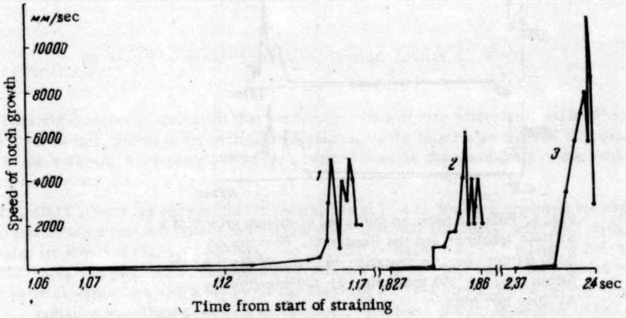

Fig. 2. Relation between speed of rupture increase and notch size for vulcanized SKN-26 specimens. Strain rate 1000 mm/min. 1) Initial notch on sample 5 mm; 2) 2.5 mm; 3) 1 mm.

The speed of rupture increase at a given strain rate remains extremely small during almost the entire experiment before it increases quickly and abruptly. When a line is drawn from the apex of a notch in the direction of the rupture it is easily observed that in unfilled vulcanized nitrile rubber during the initial stage of the deformation additional stretching occurs at the apex and consequently a secondary orientation of the material. This secondary orientation, which is detected from the thickening of transverse line at the notch apex, is reduced as the strain rate is increased and as the rupture increases. The size of the notch strongly affects the kinetics of rupture growth. As the relative notch length l/L increases (where L is the width of the specimen) there is a reduction of the time τ from the beginning of the straining of the specimen to the instant of complete rupture, as is clearly shown by the data represented in Fig. 2.

Figure 3 shows some results obtained concerning the kinetics of rupture growth at different strain rates. In all instances we observed a reduction of the time τ with increased strain rate. It is also easy to observe a general tendency toward increase of the maximum value of v' with increased strain rate v_1 (Fig. 3). During the process of rupture growth the speed of rupture varies continuously. But in principle it would be possible to find a strain rate at which the rupturing process would proceed at constant speed through the same distance l in the same time τ. It is therefore convenient to introduce as a quantitative characteristic the concept of a mean integral (or mean) rupture speed $\underline{v}$. Increased strain rate with other conditions remaining unchanged is accompanied by an increase of the mean rupture speed $v = \int_0^{\tau} v' dt/\tau = S/\tau$. (Fig. 3), where S is the area bounded by the curve $v' = f(t)$ and the $\underline{t}$ axis. In logarithmic coordinates a linear dependence is obtained (Fig. 4).

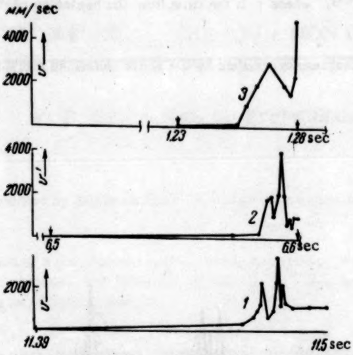

Fig. 3. Relation between the speed of rupture growth of a SKN-40 specimen and the strain rate. Photography at 1000 frames/sec. Temperature 40°. Notch depth 5 mm. Strain rate: 1) 100 mm/min; 2) 200 mm/min; 3) 1000 mm/min.

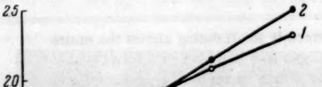

Fig. 4. Logarithm of the mean integral speed of rupture growth $\bar{v}$ as a function of strain rate v_1: 1) vulcanized SKN-40; 2) SKN-18.

Thus, within the limits of the speeds which were investigated the values of $\bar{v}$ and v_1 are related by

$$v = Av_1^n, \qquad (1)$$

where A and n are constants.

A more general relation would of course allow for the speed of rupture when $v_1 = 0$, i.e.,

$$v = Av_1^n + f(\sigma), \qquad (2)$$

where σ is the stress.

However, our experimental results show that the second term does not appreciably affect the value of $\bar{v}$. A comparison of the results obtained from vulcanized specimens which differ only in the polarity of the rubbers leads us to the conclusion that increasing polarity with other conditions unchanged is accompanied by a reduction of the mean rupture speed.

(M. V. Lomonosov) Moscow Institute for
Precision Chemical Engineering.

Received December 22, 1956.

THE LUMINESCENCE OF ZINC OXIDE-BORIC OXIDE PHOSPHORS

Iu. S. Leonov

(Presented by Academician A. N. Terenin January 12, 1957)

The literature contains an indication that the luminescence of zinc oxide-boric oxide phosphors activated by manganese varies from yellow to green in color depending on the relative amounts of zinc oxide and boric oxide [1]. In our work with these phosphors we have noticed that the change of color of the luminescence also depends on other factors.

The $ZnO-B_2O_3$ system has been studied in several papers [2-4]. We have improved the experimental data and have established that this system can contain the compounds $ZnO \cdot B_2O_3$ and $3ZnO \cdot B_2O_3$. The Debye powder patterns are shown in Fig. 1.* $ZnO \cdot B_2O_3$ was prepared by heating a 1:1 mixture of ZnO and B_2O_3 at 850° (a); $3ZnO \cdot B_2O_3$ was prepared by heating a 3:1 mixture at 1000° (b). The heating period was 15 min. The powder patterns were taken with a RPK-57.4 camera using a BSV-4 electron tube (with a copper anticathode). K_β radiation was filtered out by a nickel filter. The boric anhydride because of its lack of crystal structure does not give a diffraction pattern. We therefore compared the powder patterns with the pattern of zinc oxide alone. Pattern a in addition to the distinct lines which are characteristic of $ZnO \cdot B_2O_3$ shows a few lines of zinc oxide and of $3ZnO \cdot B_2O_3$, while pattern b, which is principally that of $3ZnO \cdot B_2O_3$, contains a few lines of zinc oxide and of $ZnO \cdot B_2O_3$. This results from incompleteness of the solid phase reaction.

The most characteristic lines are as follows: for $ZnO \cdot B_2O_3$, 2.98 (vs), 2.30 (m), 1.84 (m), 1.73 (s), 1.30 (m), 1.26 (m), 1.14 (m), 1.01 (m), 0.977 (m), 0.915 (m), 0.865 (m), 0.786 (m); for $3ZnO \cdot B_2O_3$, 3.96 (m), 3.26 (s), 3.11 (s), 2.72 (m), 2.46 (m), 2.12 (m), 1.62 (m), 1.52 (m), 1.48 (m), 1.42 (m).

Our results from the compounds formed with 1:1 and 3:1 ratios are in agreement with [4].

These two compounds were used for the preparation of phosphors. Figure 2 shows the green spectrum of $ZnO \cdot B_2O_3$ (Mn) (a) and the orange emission of $3ZnO \cdot B_2O_3$ (Mn) (b). The first phosphor was prepared by heating a 1:1 batch of ZnO and B_2O_3 with 5% by weight of manganese sulfate at 850° for 15 min; the second phosphor resulting from heating of a 3:1 batch of ZnO and B_2O_3 with 1% by weight of manganese sulfate at 1000° for 1 hr. The luminescence spectra were recorded by a FEU-19 photomultiplier. The phosphors were excited by the 2537 A line filtered out of the spectrum of a low-pressure mercury lamp; the filter system consisted of an UG-5 filter which passes the near ultraviolet and a filter (bromine vapor) which passes the 2537 A line and absorbs the other mercury lines.

Reference [5] contains a description of a $3ZnO \cdot 2B_2O_3$ (Mn) luminophor. Since the $ZnO-B_2O_3$ system can result in the formation of only two compounds with 1:1 and 3:1 ratios of the oxides it was naturally assumed that a 3:2 ratio of zinc oxide and boric anhydride yields a mixture of these two phosphors. We prepared phosphors with this ratio of the constituents and recorded the spectrum (Fig. 2, b). Our hypothesis was confirmed; the spectrum consists of two bands representing emission from the two phosphors with 3:1 and 1:1 ratios of ZnO and B_2O_3.

Zinc-borate phosphors are characterized by their ability to store light sums. It was of interest to verify our conclusion regarding the existence of the two different phosphors by a comparison in this respect. We obtained the thermal emission curves of $ZnO \cdot B_2O_3$ (Mn) (Fig. 3, a) and $3ZnO \cdot B_2O_3$ (Mn) (Fig. 3, b). The first phosphor was prepared by heating a 1 : 1 mixture of ZnO and B_2O_3 with 0.01% Mn; the second resulted from heating of a 3 : 1 mixture with 0.05% Mn. We were able to work with a broad temperature range covering the interval from the temperature of liquid nitrogen to 500° K. The heating rate was varied in this temperature range: from the liquid nitrogen temperature to 213° K the phosphor was heated in air at the rate of 18 deg/min; from 213° to the end of luminescence the phosphor was heated (in a furnace) at the rate of 5 deg/min. At the liquid nitrogen temperature excitation was provided by a PRK-4 mercury lamp without a

---

* There is no Figure 1 in the original Russian – [Editor's note.]

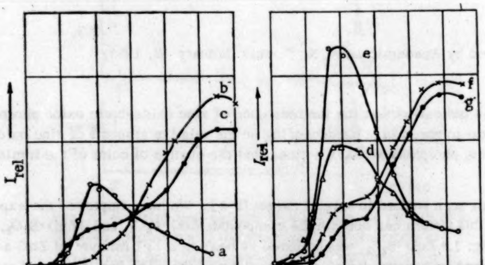

Fig. 2. Luminescence spectra of the phosphors.
a) $ZnO \cdot B_2O_3$ (Mn); b) $3ZnO \cdot B_2O_3$ (Mn); c) a phosphor obtained by heating a 3 : 2 mixture of ZnO and B_2O_3 with 1% of manganese; d, e, f, g) phosphors obtained by heating a 1 : 1 mixture of ZnO and B_2O_3 at 840° for 15 min with different manganese contents: d) 1%; e) 3%; f) 5%; g) 7% Mn (the manganese was in the form of a chloride).

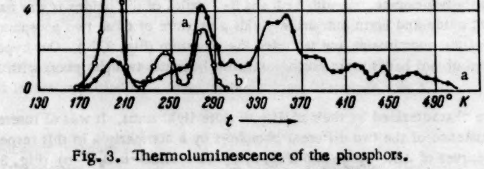

Fig. 3. Thermoluminescence of the phosphors.
a) $ZnO \cdot B_2O_3$ (Mn); b) $3ZnO \cdot B_2O_3$ (Mn).

light filter, in a thick layer, up to saturation. The operating regime of the mercury lamp was maintained constant. Brightness of emission was measured by a photometer (with a Lummer cube and an Alentsev diaphragm). Figure 3 shows that the two phosphors have a few common trapping levels as well as different levels with are characteristic of each phosphor individually.* The set of shallow traps (with a peak at 203° K) belong to the $3ZnO \cdot B_2O_3$ (Mn) phosphor; the luminescence color at 203° K is orange. The traps above 300° K belong to $ZnO \cdot B_2O_3$ (Mn) and the emission above 300° K is green. The trapping levels corresponding to the peaks at 240° and 280° K are common to the two phosphors; luminescence from these levels can be both green and orange.

Thus, all data from an X-ray analysis of these phosphors, their luminescence spectra and their thermal luminescence curves show clearly that two distinct phosphors $ZnO \cdot B_2O_3$ (Mn) and $3ZnO \cdot B_2O_3$ (Mn) exist. But it was not clear why with the same initial mixture the color of luminescence depends on the conditions of synthesis. We therefore made a careful study of the solid phase reactions in a mixture of zinc oxide and boric acid, using X-ray and thermal analyses. At the same time we observed some luminescent properties (color of emission, thermoluminescence). The differential heating curves were recorded with a Kurnakov pyrometer.

Figure 4 shows one of our heating curves, that for a 1:1 mixture of ZnO and B_2O_3. On this curve the low-temperature effect at 95-140° results from removal of water from the boracic acid; the rest, with the exception of the last (920-980°) reflect the interaction of the components. The initiation of the interaction of boric anhydride with zinc oxide (the exothermal effect at 515-600°) is associated with the softening of the boric anhydride and its transition into a liquid phase (500-600°). This is to be expected if we consider the role of the liquid phase in the interaction of components during solid-phase reactions [6]. The effect at 920-980° results from melting of the resultant product.

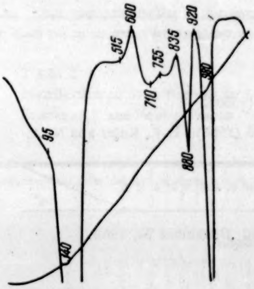

Fig. 4. Heating curve of a mixture of zinc oxide and boracic acid ($ZnO \cdot B_2O_3 = 1:1$).

From the thermograms, powder patterns and luminescent properties of the phosphors we derived the following picture of the reaction mechanism. Independently of the composition of the initial mixture heating to 780° for 15-20 min results first in the formation of a small quantity of $3ZnO \cdot B_2O_3$ and therefore when the activator is present we have the phosphor $3ZnO \cdot B_2O_3$ (Mn) with orange emission. When the temperature is raised $ZnO \cdot B_2O_3$ is formed and thus the phosphor $ZnO \cdot B_2O_3$ (Mn) with green emission. However, if the boric anhydride was entirely used up but some zinc oxide remained further temperature increase produced a larger quantity of $3ZnO \cdot B_2O_3$ (Mn) with orange emission. Thus, gradual raising of the firing temperature produces a change of the luminescent color because as a result of the solid-phase reactions there is a variation in the ratio of $3ZnO \cdot B_2O_3$ (Mn) and $ZnO \cdot B_2O_3$ (Mn). These findings are in agreement with the hypothesis that the predominance of formation of one of the two compounds is determined by the thermodynamic conditions rather than the ratio of the constituents [7].

An understanding of the causes of the change of luminescent properties is assisted considerably by phase diagrams of the system from which the base material is formed, because we are then able to determine exactly what phases can be formed in the system and the conditions for their existence. But it must be remembered that deductions based on a phase diagram are valid only for the equilibrium state. Phases which are formed during solid-phase reactions often do not reach a state of equilibrium; therefore the laws which are expressed through a phase diagram are satisfied only in part [8]. At higher firing temperatures as equilibrium is approached the phase diagram expresses with increasing completeness the processes that are taking place in the system. This is especially marked in the system under consideration here.

---

* The same characteristic difference of the thermal luminescence curves was observed in the two phosphors when the manganese content was identical.

It is worth noting that the ratio of the two phosphors (3:1 and 1:1) differs with various concentrations of the manganese chloride activator (Fig. 2, d, e, f, g) and also depending upon whether the activator is in the original mixture or is put into a mixture which had been heated previously. The luminophors which are formed in these two instances differ in luminescent color and in afterglow as well as in stored light sums.

The author is very grateful to Professor M. A. Konstantinova-Shlezinger for directing this work, to Z. A. Trapeznikova and M. V. Fok for a discussion of individual problems and to L. T. Kantardzhian for providing the apparatus used in obtaining the luminescence spectra.

LITERATURE CITED

[1] N. D. Zhirov, Luminophors 1940.

[2] E. Ingerson, G. W. Morey, and O. F. Tuttle, Am. J. Sci. 246, 31 (1948).

[3] D. S. Beliankin, V. V. Lapin, and N. A. Toropov, Physico-Chemical Systems in Silicate Technology (1954).

[4] H. P. Roocksby and A. H. McKeag, G.E.C. Journal 17, 89 (1950); Cited in Problems of Modern Physics, Luminescence (USSR) 2, 47 (1951).

[5] M. Curie, Fluorescence et Phosphorescence (1946), p. 161.

[6] A. M. Ginstling, J. Phys. Chem. (USSR) 25, 3, 277 (1952).

[7] O. P. Mchedlov-Petrosian, J. Phys. Chem. (USSR) 24, 11, 1299 (1950).

[8] Ia. A. Ugai and Iu. A. Baslyk, J. Gen. Chem. (USSR) 25, 9, 1645 (1955); E. K. Keler and N. A. Godina, Doklady Akad. Nauk SSSR 103, 2, 247 (1955).

P. N. Lebedev Physical Institute,
Academy of Sciences, USSR.

Received December 24, 1956.

THE RELATION BETWEEN THE NUMBER OF SHOWER PARTICLES AND THE ATOMIC NUMBER OF A DISINTEGRATING NUCLEUS

Zh. S. Takibaev

(Presented by Academician D. V. Skobel'tsyn January 16, 1957)

The method of embedded filaments [1] makes it possible to study the number of shower particles as a function of the atomic number of a nucleus undergoing disintegration through the action of cosmic rays in the stratosphere. Nuclear emulsions between which aluminum and tungsten filaments had been inserted were raised into the stratosphere by balloons. The stacks of emulsions and filaments were exposed at 28 km for a few hours. Table 1 gives the star distribution according to the number of light tracks ($7 > n_s \geq 1$) of secondary shower particles as a function of the total number N_h of heavy tracks. The table shows that many more shower particles are observed in stars formed in tungsten than in aluminum. A single collision of a particle with a tungsten nucleus produces 1.13 ± 0.12 shower particles; in the case of aluminum the result is 0.48 ± 0.08 particles. Thus, the probability of the production of shower particles as a result of collisions with cosmic rays is more than twice as great for tungsten as for aluminum.

TABLE 1

Distribution of Stars Formed in Tungsten and Aluminum According to the Number of Light Tracks (n_s) and Heavy Tracks ($N_h = N_g + N_b$) in the Stratosphere.

	Tungsten																								Aluminum										
n_s \ N_h	2	3	4	5	6	7	8	9	10	11	12	13	14	15	17	18	20	21	23	24	25	28	34	37	2	3	4	5	6	7	8	9	10	11	12
0	1	1	4	8	11	7	7	1	1	1	1	1											1		1	6	9	17	7	8	2	2	1	0	0
1						1	1		1	2			1														1	1	2	2	1	2	1	1	1
2								1	1	1	1	1																	1	1	1		1		
3								1			1				1	1																			
4									1			1			1			1		1														1	
5														1		1					1	1									1				
6																	1							1											1
Total	1	1	4	8	11	8	8	3	4	4	3	3	1	1	2	2	1	1		1	1	1	1	1	1	6	10	18	10	11	5	4	3	2	1
	Total 71 stars																								Total 71 stars										

It is usually assumed [2] that the number of shower particles equals the number of pions generated. Therefore, many more pions are produced per collision in tungsten than in aluminum. This denotes that pions are produced not only in a single collision of the primary particle with a nucleon of the nucleus but also in succeeding collisions.

In [3] it was shown that the probability of production of slow pions (stopped in the emulsion) in lead nuclei is approximately 5-7 times greater than the probability for their production in carbon nuclei. A comparison of the results in [3] with our present results leads to the conclusion that fast pions are also produced in tungsten nuclei with greater probability than in aluminum, although the probabilities for the last two elements differ by a factor of only about 2. It thus follows that the probability of slow pion production is much more strongly dependent on atomic number than the probability of shower particle production.

These data show that the mechanism for the production of slow pions as well as of pions distinguished as shower particles in stars with $n_s < 6$ must be explained by a multiple-plural production theory.

When we estimate the energy of the shower-producing particles from the number of light and gray tracks in accordance with the empirical results of [4] we obtain $F_{min} \approx 10$ Bev when $n_s = 6$. Hence, we conclude that at least up to 10 Bev the probability of pion production is greater in tungsten than in aluminum.

According to cosmotron and betatron data in the 1-6 Bev range the average multiplicity is almost independent of the atomic number of the target nucleus. It is possible that as the primary particle energy increases an ever-increasing number of nucleons of the target nucleus will participate in the production of mesons, which would result in some, but apparently not very great, dependence of the number of ejected mesons on atomic number. However, it is not yet known in what energy range Fermi's statistical theory [5] can be applied to the collision of a nucleon with a group of nucleons.

At high energies all nucleons which are in the path of the incident particle participate in meson production and only in this case can we apply the concept [6] of collision with a cylinder of nucleons of the target nucleus. These considerations show that it is not now possible to compare the data with the theory of multiple meson production.

If it is assumed that the number of shower particles is proportional to the average number of collisions between the primary particle and nucleons along its path through the nucleus we obtain $\bar{n}_W/\bar{n}_{Al} = (A_W/A_{Al})^{1/3} = 1.9$, which is quite close to the experimental value. If delta nucleons also participate in the production of the shower particles this ratio must be of the order $2^{(A_W^{1/3} - A_{Al}^{1/3})/1.5} = 3{,}4$. [7]. The experimental result cited above is thus between $(A_W/A_{Al})^{1/3}$ and $2^{(A_W^{1/3} - A_{Al}^{1/3})/2}$. In other words

$$(A_W/A_{Al})^{1/3} \leqslant (n_W/n_{Al})_{exp} < 2^{(A_W^{1/3} - A_{Al}^{1/3})/1.5},$$

which means that delta nucleons can also take part to a small degree in shower particle production in stars with $n_s < 6$.

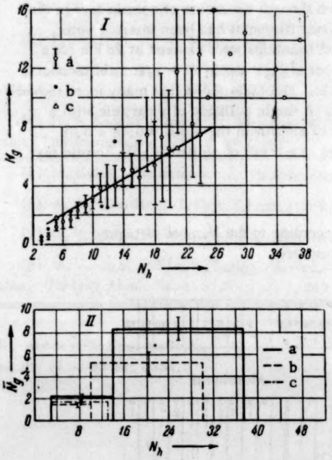

Fig. 1. I) Average number of gray tracks (protons with E = 30-500 Mev) per star $\bar{N}_g$ as a function of the number N_h of heavy tracks: a) for tungsten; b) for aluminum; c) in an emulsion. II) average number of gray tracks $\bar{N}_g$ per star corresponding to various ranges of the number N_h of heavy tracks. For simplicity the stars are divided into groups according to N_h: 3-10; 3-13; 10-30; 14-37; a) for tungsten in the stratosphere; b) for tungsten at a mountain altitude; c) for aluminum in the stratosphere.

We hope that the continuing study in our laboratory of the interaction between cosmic particles and heavy (W) and light (Al) nuclei will furnish important information concerning the mechanism of fast pion (shower particle) production as a function of atomic number. We have used the method of embedded filaments, whose advantages are obvious especially for the study of nuclear disintegrations with a small number of shower particles. This method is superior to the pellicle stack method for the study of extensive showers because with the latter the majority of shower particle tracks are not observed during scanning. This results from the fact that in a pellicle stack the showers consist of jets of light tracks, and the tracks of particles which form large angles with the jet axis can be determined only with great difficulty. Many details of the nuclear disintegration also remain uncertain (the numbers of black and gray tracks, their composition, etc.).

In addition to the relation between the number of shower particles and atomic number we have investigated other important problems which provide important information regarding the mechanism of nuclear disintegration by cosmic rays.

For example, study has shown that the energy spectrum of recoil nucleons ejected during the disintegration of tungsten nuclei is quite different from the energy spectrum of corresponding nucleons from aluminum.

In the first case low-energy recoil protons predominate (below 100 Mev); in the second case there are more high-energy protons (above 100 Mev), and this result holds true when large amounts of energy are released. A better and more reasonable explanation of this effect can be obtained by assuming individual independent interactions between the primary nucleon and the nucleons of the target nucleus.

By comparing experimental results (the numbers of stars produced in wires of different elements) obtained on mountains (near Alma-Ata) and in stratospheric flights at the latitude of Moscow we find that the "transparency" (regarding the production of stars with $N_h \geq 3$) of aluminum and copper atoms compared with tungsten atoms is reduced as the average energy of the star-producing particles increases from 600 to 3000 Mev (the average energies at mountain and stratospheric altitudes, respectively), and that around 3000 Mev these nuclei are "opaque." This is not in disagreement with laboratory data obtained [8] by irradiating different elements with protons accelerated up to 1400 Mev.

An analysis of the prong distribution of stars formed in different elements at 4000-4400 m as well as in the stratosphere shows that the number of ejected fast protons with 30 to 500 Mev increases with increasing atomic number as well as increasing energy of the star-producing particle. In other words, the number of gray tracks per star rises with incident particle energy more rapidly in stars produced in tungsten than in aluminum (Fig. 1). This experimental result agrees best with the hypothesis of cascade nucleon collisions within the nucleus.

We note in conclusion that the results of the present work cannot be compared directly with data from other experiments because our method was not used previously to study the relation between shower particle yield and atomic number.

The author is indebted to Associate Academician S. N. Vernov (of the Academy of Sciences of the USSR) and to N. L. Grigorov for several remarks and for discussions.

LITERATURE CITED

[1] Zh. S. Takibaev, J. Exptl.-Theoret. Phys. (USSR) 24, 233 (1953); Bull. Acad. Sci. USSR, Phys. Ser. 19, 541 (1955).

[2] U. Camerini, W. Lock, and D. Perkins, Progress in Cosmic Ray Physics (Amsterdam, 1952).

[3] D. Kaipov and Zh. S. Takibaev, J. Exptl.-Theoret. Phys. (USSR) 30, 3, 471 (1956).

[4] U. Camerini and I. Davies, et al., Phil. Mag. 42, 1241 (1951).

[5] E. Fermi, Progr. Theor. Phys. 5, 570 (1950).

[6] S. Z. Belen'kii and L. D. Landau, Uspekhi Fiz. Nauk 57, 309 (1955).

[7] I. L. Rozental' and D. S. Cherniavskii, Uspekhi Fiz. Nauk 52, 185 (1954).

[8] V. A. Nedzel, Phys. Rev. 94, 174 (1954).

[9] V. P. Dzhelepov, V. I. Satarov, and B. M. Golovin, Doklady Akad. Nauk SSSR 104, 717 (1955).

[10] T. Coor, and D. A. Hill, et al., Phys. Rev. 98, 1369 (1955).

Physico-Technical Institute,
Academy of Sciences, Kazakh SSR

Received June 4, 1956.

ON THE PULSATIONS OF A PLASMA FILAMENT

A. G. Kulikovskii

(Presented by Academician L. I. Sedov January 22, 1957)

The problem of plasma filament pulsations has arisen in connection with experimental investigations of large-current sparks in gases [1]. An approximate solution has been given by M. A. Leontovich and S. M. Osovets [2]. Here we present a certain class of exact solutions of the equations of magnetohydrodynamics and including periodic solutions in particular.

We shall consider the one-dimensional axially symmetrical motions of an infinite gas of infinite conductivity. Certain solutions of magnetohydrodynamics in Lagrangian coordinates can be written as follows:

$$\frac{\partial^2 r}{\partial t^2} = -\frac{1}{\rho}\left(\frac{\partial p}{\partial r} + \frac{1}{8\pi}\frac{\partial H^2}{\partial r} + \frac{1}{4\pi}\frac{H^2}{r}\right);$$

$$\rho = \rho_0 \frac{r_0}{r}\frac{\partial r_0}{\partial r}; \quad p = p_0 \frac{\rho^\gamma}{\rho_0^\gamma}; \quad H = H_0 \frac{\partial r_0}{\partial r}. \tag{1}$$

Here r is the coordinate of a particle; r_0, ρ_0, p_0, H_0 are, respectively, the coordinate, density, pressure and magnetic field strength for the particle at $t = 0$ with the magnetic lines of force assumed to be closed concentric circles.

The first equation expresses the acceleration of the particle, the second, third and fourth equations represent the laws of conservation of mass, entropy and magnetic flux. All solutions were obtained with homogeneous deformation, that is, such that

$$\frac{r}{r_0} = \mu(t), \tag{2}$$

where μ is independent of r_0. Then

$$v = \frac{\partial r}{\partial t} = r_0\mu'(t) = r\frac{\mu'(t)}{\mu(t)}, \tag{3}$$

that is, the velocity is linearly dependent on the radius. These solutions are similar to that obtained by L. I. Sedov [3, 4] in the absence of magnetic forces, which, like the proposed solution, contains a single arbitrary function.

The solution is given by

$$\rho = \rho_0\mu^{-2}; \tag{4}$$

$$p = p_0\mu^{-2\gamma}; \tag{5}$$

$$H^2 = H_0^2 \mu^{-2}, \tag{6}$$

where ρ_0 is an arbitrary function of r_0:

$$p_0 = A \int_0^{r_0} \rho_0 r_0 dr_0 + N; \tag{7}$$

$$H_0^2 = \frac{8\pi B}{r_0^2} \int_0^{r_0} \rho_0 r_0^3 dr_0 + \frac{M}{r_0^2}. \tag{8}$$

Here A, B, N and M are arbitrary constants. Assuming $r_0 = 0$ we find that $N \geq 0$ and $M \geq 0$. The sign of A is the same as that of dp_0/dr_0. The sign of B agrees with the same of the first term of (8). From the Maxwell equation

$$\frac{4\pi}{c} j = \operatorname{rot} H \tag{9}$$

we find that when $t = 0$ the concentrated current $i_0 = \pm \frac{c}{2} \sqrt{M}$ flows along the axis of the symmetry and that in addition at all other points of space there is a distributed current of the density

$$j_0 = \pm \frac{c}{8\pi} \frac{B\varphi'(r_0)}{\sqrt{M + B\varphi(r_0)}}, \quad \text{where} \quad \varphi(r_0) = 8\pi \int_0^{r_0} \rho_0 r_0^3 dr_0.$$

Thus, when $B > 0$ the distributed current agrees in direction with the concentrated current along the axis of symmetry; when $B < 0$ these currents are opposite. When $M = 0$, that is, there is no concentrated current, B must be positive.

For $\mu(t)$ we obtain the differential equation

$$\left(\frac{d\mu}{dt}\right)^2 = \frac{A}{\gamma - 1} \mu^{2-2\gamma} - 2B \ln \mu + C = f(\mu) \tag{10}$$

(C is an arbitrary constant), whence

$$t = \pm \int \frac{d\mu}{\sqrt{f(\mu)}}.$$

The following cases are possible:

1) $A > 0$, $B > 0$. When $d\mu/dt < 0$ at $t = 0$, μ becomes zero for a finite time and the gas contracts to a point. When $d\mu/dt > 0$, μ first reaches its maximum value, followed by the same contraction. We assume that at the instant of contraction the velocity changes discontinuously and expansion is renewed.

2) $A < 0$, $B < 0$. When $d\mu/dt > 0$ at $t = 0$ dispersal occurs: μ increases toward infinity as $t \to \infty$. We then have for the velocity $d\mu/dt \to \infty$. When $d\mu/dt < 0$ at $t = 0$ at first μ reaches its minimum value followed by dispersal.

3) $A > 0$, $B < 0$. There are three possible cases:

a) $f(\mu)$ has no roots. Then, when $d\mu/dt > 0$ at $t = 0$, scattering occurs and when $d\mu/dt < 0$ at $t = 0$ contraction takes place.

b) $f(\mu)$ has one double root μ_0. Then the limited velocity $\mu \rightarrow \mu_0$ is possible at $t \rightarrow \infty$. In the opposite case we have scattering or contraction depending on the sign of $\mu_0 - 1$. When $\mu_0 = 1$ this represents unstable equilibrium.

c) $f(\mu)$ has two roots between which the value 1 cannot lie. When $1 \leq \mu_1 < \mu_2$, the motion is qualitatively the same as in case 1. When $\mu_1 < \mu_2 \leq 1$, the motion is similar to case 2.

4) $A < 0$, $B > 0$. We then have either two roots with $\mu_1 < 1 < \mu_2$ or one double root $\mu_1 = \mu_2 = 1$. Stable equilibrium occurs in the case of the double root $\mu = 1$. When $\mu_1 < 1 < \mu_2$ oscillations occur with a period which depends on the constants A, B, and C.

5) $A = 0$; the pressure is constant. When $B > 0$ the motion is similar to case 1. When $B < 0$ the motion is similar to case 2.

6) $B = 0$; the magnetic forces are in equilibrium. Let $A > 0$. When $f(\mu)$ has a root the motion is similar to case 1. When no root exists and $d\mu/dt > 0$ scattering occurs with the velocity $d\mu/dt \rightarrow \sqrt{C}$, and when $d\mu/dt < 0$ contraction occurs. When $A < 0$ the motion is similar to case 2, but $d\mu/dt \rightarrow \sqrt{C}$ as $t \rightarrow \infty$.

We shall now consider a cylinder of finite length and finite radius $r_0 = R$. In order that events within the cylinder be described by the solution it is sufficient to place conducting walls at the ends of the cylinder and on its lateral surface apply a pressure equal to the total pressure from within

$$p^*(R, t) = p_0(R)\mu^{-2\gamma} + \frac{1}{8\pi} H_0^2(R)\mu^{-2}.$$

This pressure can be produced by a piston and also by an external electromagnetic field. The pressure of the electromagnetic field on the cylinder surface can be represented by $\frac{1}{8\pi} H_{ex}^2$ (H_{ex} is the external field strength). By Equation (9) the total current along the cylinder must be

$$I(t) = \frac{c}{2} R\mu H_{ex} = \frac{c}{2} R\sqrt{8\pi p_0(R)\mu^{2-2\gamma} + H_0^2(R)}.$$

In particular, when $p_0(R) = 0$ the total current is constant in time.

Therefore, in order that the solution describe events within the cylinder the pressure applied to the ends of the cylinder must be such that the total current will be $I(t)$. Such pressure can always be applied and can easily be calculated. The current flowing inside the cylinder is independent of the pressure applied and is obtained from the equations of magnetohydrodynamics. The applied pressure affects only the magnitude of the surface current.

Let us now consider the energy balance. The work performed by external forces

$$2\pi R^2 p^*(\mu)\mu\, d\mu = 2\pi R^2\Big(\mu^{1-2\gamma} A\int_0^R \rho_0 r_0\, dr_0 + \mu^{1-2\gamma} N + \mu^{-1}\frac{B}{R^2}\int_0^R \rho_0 r_0^3\, dr_0 + \mu^{-1}\frac{8\pi M}{R^2}\Big) d\mu \tag{11}$$

is expended in increasing the internal energy and in creating kinetic energy. The last term in this equation is independent of R, that is, there is a transfer of energy toward the axis of symmetry where for $M \neq 0$ the energy is infinite. The first three terms approach zero as $R \rightarrow 0$ so that the energy which corresponds to these terms and flows through the boundary is distributed over the entire fluid mass. It can be seen from (6) that the magnetic energy of a particle remains constant. It can therefore be assumed that the entire third term represents increase of the kinetic energy, the entire second term represents increase of the internal energy and the first term represents the increase partly of the kinetic energy and partly of the internal energy. In contraction the external forces do an infinite amount of work on the cylinder and each term in (11) is infinite. During scattering the magnetic forces (of the last two terms) also do an infinite amount of work at the expense of the infinite energy at the center. In the oscillatory case the work performed by the cylinder surface is finite.

The solution which has been obtained here is easily extended to the case of helical magnetic lines of force. In this case the right-hand side of Equation (1) contains the additional term $-\frac{1}{8\pi\rho}\frac{\partial H_z^2}{\partial r}$, where H_z is the magnetic field component parallel to the axis of symmetry. In this equation H will denote the magnetic field component perpendicular to the axis of symmetry. Then to Equations (5), (6), (7), and (8) we add

$$H_z^2 = H_{z0}^2\mu^{-4}, \tag{6'}$$

$$H_{z0} = 8\pi D\int_0^{r_0} \rho_0 r_0\, dr_0 + L \tag{8'}$$

(D and L are arbitrary constants) and instead of (10) we obtain

$$\left(\frac{\partial\mu}{\partial t}\right)^2 = \frac{A}{\gamma-1}\mu^{2-2\gamma} - 2\mathrm{B}\ln\mu - D\mu^{-2} + C. \tag{10'}$$

LITERATURE CITED

[1] L. A. Artsimovich, A. M. Andrianov, O. A. Bazilevskaia, Iu. G. Prokhorov, and N. V. Filipov, Atomic Energy (USSR), 1956, No. 3.

[2] M. A. Leontovich and S. M. Osovets, Atomic Energy (USSR) 1956, No. 3.

[3] L. I. Sedov, Doklady Akad. Nauk SSSR 90, 5, 735 (1953).

[4] L. I. Sedov, Dimensional and Similarity Methods in Mechanics (Moscow, 1954), p. 237.*

M. V. Lomonosov Moscow State University

Received January 16, 1957.

---

* In Russian

OSCILLATIONS OF AN INFINITE CYLINDER OF GAS ACTED ON BY ITS OWN GRAVITY AND A MAGNETIC FIELD

I. M. Iavorskaia

(Presented by Academician L. I. Sedov April 1, 1957)

We shall consider one-dimensional nonstationary motions of a gas which can be related to the motion of cosmic masses acted on by magnetic fields. Our fundamental assumption is that the electrical conductivity of the gas is so large that the magnetic lines of force are practically "frozen" in the medium. We shall also consider radial motions of a gas with cylindrical symmetry acted on by Newtonian gravitation and an internal magnetic field. We shall also consider gaseous motion in which the velocity depends linearly on distance from the axis of symmetry. Such motion has previously been studied by L. I. Sedov [1, 2], M. S. Lidov [3] and A. G. Kulikovskii [4].

1. Let us assume that the internal magnetic field is directed along the axis of symmetry. A similar linear problem concerning radial oscillations of small amplitude has been studied by Chandrasekhar and Fermi [5] in connection with problems of gravitational stability.

In this case the equations of motion in cylindrical coordinates are [4]

$$\frac{\partial^2 r}{\partial t^2} = -\frac{1}{\rho}\frac{\partial p}{\partial r} - \frac{2Gm}{r} - \frac{1}{8\pi}\frac{1}{\rho}\frac{\partial H^2}{\partial r};$$

$$\rho = \rho_0(r_0)\frac{r_0}{r}\frac{\partial r_0}{\partial r}; \quad p = p_0(r_0)\frac{\rho^{\gamma}}{\rho_0^{\gamma}}; \tag{1}$$

$$m = m_0 = 2\pi\int_0^{r_0}\rho_0(r_0)\,r_0\,dr_0; \quad H = H_0(r_0)\frac{r_0}{r}\frac{\partial r_0}{\partial r},$$

where t is the time and r_0 is the Lagrangian coordinate; the remaining notation is clear from the equations.

We shall study the exact particular solution of (1):

$$r = r_0\mu(t); \quad v = r_0\mu'(t) = r\frac{\mu'(t)}{\mu(t)};$$

$$\rho = \rho_0\mu^{-2}(t); \quad p = p_0(r_0)\,\mu^{-2\gamma}(t); \quad H^2 = H_0^2(r_0)\,\mu^{-4}(t),$$

in which $\mu(t)$ satisfies the equation

$$t = \pm\int\frac{d\mu}{\sqrt{f(\mu)}},$$

where

$$f(\mu) = \frac{A}{\gamma-1}\frac{1}{\mu^{2(\gamma-1)}} + \frac{B}{\mu^2} - 2C\ln\mu + D;$$

$$A = \frac{1}{\rho_0 r_0}\frac{\partial p_0}{\partial r_0}; \quad B = \frac{1}{8\pi}\frac{1}{\rho_0 r_0}\frac{\partial H_0^2}{\partial r_0}; \quad C = \frac{2Gm_0}{r_0^2},$$

whence it follows immediately that

$$\rho_0 = \text{const}; \quad p_0 = \frac{A\rho_0 r_0^2}{2} + \overline{p}; \quad H_0^2 = 4\pi B\rho_0 r_0^2 + \overline{H}^2. \tag{*}$$

It is evident that C > 0 always. When gravitational forces are neglected, C = 0. The motion of the gas will differ, depending on the values of A, B, C and D.

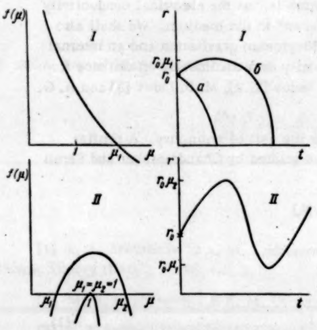

Fig. 1. The form of the function f(μ) and the law of motion of a gas particle in cases I and II.

We note all possible cases:

I. The gradients of the pressure and magnetic field strength at the initial instant are positive (A > 0; B > 0).

The function f(μ) has the root $\mu_1 > 1$; f'(μ) < 0.

a) When $(dr/dt)_{t=0} < 0$ the gas contracts to a point after a finite time interval.

b) When $(dr/dt)_{t=0} > 0$ the gas expands to a certain maximum volume, its velocity becomes zero and under the action of the forces the gas begins to return to the center (Fig. 1, I). We can imagine that in time the gas begins to expand again and that the process is repeated, so that periodic pulsations of the gas occur.

II. The gradient of the magnetic field is negative (A ≠ 0; B < 0; $\gamma < 2$). When $\gamma > 2$ the sign of A is the determining factor.

f(μ) has the roots $\mu_1 < 1$ and $\mu_2 > 1$. The motion of the gas has the form of periodic oscillations. The oscillatory period depends on the values of A, B, C, and D. In a special case f(μ) can have the double root $\mu_1 = \mu_2 = 1$. This means that at the initial instant no forces act on the gas (A + B + C = 0) and the initial velocity is zero $\left(\frac{A}{\gamma - 1} + B + D = 0\right)$. Figure 1, II shows that this represents stable equilibrium.

III. The pressure gradient is negative (A < 0) and the magnetic field gradient is positive (B > 0).

When f(μ) has a root $\mu < 1$ the motion is analogous to case II; otherwise it is analogous to case I.

IV. The magnetic field is constant (B = 0).

Then when A > 0 $(dp_0/dr_0 > 0)$ the motion is analogous to case I; when A < 0 $(dp_0/dr_0 < 0)$ it is analogous to case II.

V. The gas pressure at the initial instant is constant.

This is completely analogous to the preceding case with A replaced by B.

VI. The magnetic field is constant and the gravitational forces are absent.

This coincides with the absence of inertial forces in [1].

VII. Gravitational forces are absent (C = 0).

In this case one of the boundary conditions $\rho_0 = \text{const}$ is dropped, and the solution is in more general form depending on the arbitrary function $\rho_0(r_0)$.

a) When $A \neq 0$; $B > 0$; $D > 0$, depending on the sign of $\left|\frac{dr}{dt}\right|_{t=0}$ and the roots of $f(\mu)$ the ga either contracts to a point or is dispersed.

b) When $A \neq 0$, $B > 0$; $D < 0$ the gas contracts in a finite time interval.

c) When $A < 0$; $B < 0$; $D > 0$ the gas expands to infinity with finite velocity.

d) When $A > 0$; $B < 0$; $D < 0$ there is periodic oscillatory motion.

e) When $A > 0$; $B < 0$; $D > 0$ total scattering occurs.

VIII. The pressure and magnetic field strength are constant ($A = 0$; $B = 0$).

The motion of the gas is analogous to case I.

We see from the foregoing investigation that in the presence of gravitational forces and a magnetic field along the axis of symmetry and with initial distributions given by (•), dispersal of the gaseous configuration is impossible.

2. We shall now discuss the case in which the magnetic lines of force are closed concentric circles.

The equations of motion in this case differ from those of Kulikovskii [4] only by the addition of a term that takes account of gravitational forces. But the solution will have the more special form

$$r = r_0\mu(t); \quad \rho = \rho_0\mu^{-2}(t);$$
$$p = p_0(r_0)\mu^{-2\gamma}(t); \quad H^2 = H_0^2(r_0)\mu^{-2}(t),$$

where

$$\rho_0 = \text{const}; \quad p_0 = \frac{A\rho_0 r_0^2}{r} + \bar{p}; \quad H_0^2 = 2\pi B\rho_0 r_0^2 + \frac{\overline{H}^2}{r_0^2};$$

$$t = \pm\int\frac{d\mu}{\sqrt{f(\mu)}}; \quad C = 2\pi G\rho_0;$$

$$f(\mu) = \frac{A}{\gamma - 1}\frac{1}{\mu^{2(\gamma-1)}} - 2B\ln\mu - 2C\ln\mu + D, \qquad (\bullet\bullet)$$

i.e., the solution is independent of the arbitrary function. The second and third terms in (••) can be combined through the replacement of B by $B' = B + C$.

Thus, for motions of the type under consideration the effect of the gravitational forces is equivalent to a change of the gradient of the magnetic field. All of the results obtained in [4] remain valid with B replaced by B'. In this case when $B' < 0$ and in the presence of gravitational forces total dispersal of the gaseous configuration is possible.

LITERATURE CITED

[1] L. I. Sedov, Similarity and Dimensional Methods in Mechanics (Moscow, 1954).

[2] L. I. Sedov, Doklady Akad. Nauk SSSR 90, 5 (1953).

[3] M. L. Lidov, Doklady Akad. Nauk SSSR 97, 3 (1954).

[4] A. G. Kulikovskii, Doklady Akad. Nauk SSSR 114, 5, 984 (1957).*

[5] S. Chandrasekhar and E. Fermi, Problems of Modern Physics (USSR) No. 2, 108, 1954 .

M. V. Lomonosov Moscow State University

Received March 27, 1957.

---

*[Soviet Physics - Doklady, p. 269.]

ON THE STATISTICAL THEORY OF CRYSTALLIZATION

E. A. Arinshtein

(Presented by Academician N. N. Bogoliubov February 12, 1957)

In an earlier paper [1] we used N. N. Bogoliubov's method to construct a statistical theory of the crystallization of one-component systems. The method can be extended to multi-component systems with short-range forces. The distribution functions are then determined by the generating functional

$$\mathscr{L}(u_\alpha) = \int D\,\Pi\,(1 + v_\alpha u_\alpha(i))\,dq_i,$$

which contains n auxiliary functions u_α, $\alpha = 1, \ldots, n$, where n is the number of components [2]. The functional equation for this functional is

$$\frac{\delta\mathscr{L}(u_\alpha)}{\delta u_\alpha(1)} = (z_\alpha v_\alpha)\,\mathscr{L}\Big(u_\beta(i)\,(1 + f_{1i}^{\alpha\beta}) + \frac{1}{v_\alpha} f_{1i}^{\alpha\beta}\Big). \tag{1}$$

The equation for the generating functional of the correlation functions, $W = \ln\mathscr{L}$, is obtained by taking the logarithmic functional derivative of Equation (1):

$$\frac{\delta^2 W(u)}{\delta u_{\alpha_1}(1)\,\delta u_{\alpha_2}(2)} = \frac{\delta W(u)}{\delta u_{\alpha_1}(1)}\left\{\frac{\delta W u_\beta(i)\,(1 + f_{1i}^{\alpha_1\beta}) + \frac{1}{v_{\alpha_1}} f_{1i}^{\alpha_1\beta}}{\delta u_{\alpha_1}(2)} - \frac{\delta W(u)}{\delta u_{\alpha_2}(2)}\right\}. \tag{2}$$

As in [1], by means of further functional differentiation and successive substitutions it is possible to express all distribution functions in terms of unary functions $F_\alpha(i)$ and to obtain for the unary functions the equations

$$\ln\frac{F_{\alpha_1}(1)}{z_{\alpha_1} v_{\alpha_1}} = \sum_{\Sigma s=1}^{\infty} \frac{1}{s_1!\ldots s_n!\, v_1^{s_1}\ldots v_n^{s_n}} \times$$
$$\times \int K_{\alpha_1\ldots\alpha_{\Sigma+1}}(1, \ldots, \Sigma s + 1)\, F_{\alpha_2}(2)\ldots F_{\alpha_{\Sigma+1}}(\Sigma + 1)\, dq_2\ldots dq_{\Sigma+1}. \tag{3}$$

The numbers $s_1, \ldots, s_n$ indicate how many times the corresponding subscript is found among the subscripts $\alpha_1, \ldots, \alpha_{\Sigma+1}$. Equation (3) is equivalent to the problem of determining the extremum of the functional

$$A(F_\alpha) = \vartheta\left\{\sum_\alpha \frac{v}{v_\alpha}\langle F_\alpha(1)\ln F_\alpha(1)\rangle_{\text{av}} - \right.$$
$$- \sum_{\Sigma s=2}^{\infty} \frac{v}{s_1!\ldots s_n!\, v_1^{s_1}\ldots v_n^{s_n}}\,\frac{1}{V}\int K_{\alpha_1\ldots\alpha_\Sigma}(1, \ldots \Sigma)\, F_{\alpha_1}(1)\ldots, F_{\alpha_\Sigma}(\Sigma)\, dq_1\ldots dq_\Sigma -$$
$$\left. - \sum_\alpha \frac{v}{v_\alpha}\ln\frac{(2\pi m_\alpha \vartheta)^{3/2} v_\alpha}{h^3}\right\} \tag{4}$$

subject to the supplementary conditions $\langle F_\alpha(1)\rangle_{\mathrm{av}} = 1$. Here $1 + (z_\alpha v_\alpha)$ are Lagrangian multipliers, $1/v = \sum_\alpha 1/v_\alpha$; the functions with a single subscript are unary distribution functions for the corresponding components.

As in [1] the functional $A(F_\alpha)$ is the specific free energy. The thermodynamical identities $p = -\partial A/\partial v$ and $E = -\vartheta^2 \partial (A/\vartheta)/\partial\vartheta$ are verified just as in [1] with the single difference that some binary functions $F_{\alpha_1\alpha_2}(i, j)$ are introduced.

Equation (4) for the free energy enables us to solve the problem of the crystallization of multi-component systems. We shall consider a two-component system as an example.

The appearance of solid solutions of one component in another reduces to the determination of a periodic solution for F_1 with $F_2 \equiv 1$ (or vice versa), which is identical with the problem studied in [1]. Since the thermodynamical functions depend on the concentration of the components the liquidus and solidus curves can be distinguished (see [3] for example).

Let us consider the formation of a binary crystal of definite composition and structure such as a β-brass crystal, which is a simple cubic lattice of one kind of atom that becomes body-centered with atoms of the other kind. The distribution functions are taken as sums of Gaussian distributions [1]:

$$\begin{aligned}
F_1 = {} & \frac{v}{(2\pi)^{3/2}}\left\{\frac{1+\xi}{r_1^3(\xi)}\sum_l \exp\left[-\frac{(\mathbf{r}-\mathbf{r}_l)^2}{2r_1^2(\xi)}\right] + \frac{1-\xi}{r_1^3(-\xi)}\sum_l \exp\left[-\frac{(\mathbf{r}-\mathbf{r}_l-\mathbf{r}')^2}{2r_1^2(-\xi)}\right]\right\} = \\
& = \sum_l \exp\left[i(\mathbf{k}_l\mathbf{r})\right]\left\{\left[\frac{1+\xi}{2}\exp\left(-\frac{1}{2}k_l^2 r_1^2(\xi)\right) + \right.\right. \\
& \left. + \frac{1-\xi}{2}\exp\left(-\frac{1}{2}k_l^2 r_1^2(-\xi)\right)\right]\cos\frac{(\mathbf{k}_l\mathbf{r}')}{2} - \\
& \left. - i\left[\frac{1+\xi}{2}\exp\left(-\frac{1}{2}k_l^2 r_1^2(\xi)\right) - \frac{1-\xi}{2}\exp\left(-\frac{1}{2}k_l^2 r_1^2(-\xi)\right)\right]\sin\frac{(\mathbf{k}_l\mathbf{r}')}{2}\right\}
\end{aligned} \tag{5}$$

$$\begin{aligned}
F_2 = {} & \frac{v}{(2\pi)^{3/2}}\left\{\frac{1-\xi}{r_2^3(-\xi)}\sum_l \exp\left[-\frac{(\mathbf{r}-\mathbf{r}_l)^2}{2r_2^2(-\xi)}\right] + \frac{1+\xi}{r_2^3(\xi)}\sum_l \exp\left[-\frac{(\mathbf{r}-\mathbf{r}_l-\mathbf{r}')^2}{2r_2^2(\xi)}\right]\right\} = \\
& = \sum_l \exp\left[i(\mathbf{k}_l\mathbf{r})\right]\left\{\left[\frac{1+\xi}{2}\exp\left(-\frac{1}{2}k_l^2 r_2^2(\xi)\right) + \right.\right. \\
& \left. + \frac{1-\xi}{2}\exp\left(-\frac{1}{2}k_l^2 r_2^2(-\xi)\right)\right]\cos\frac{(\mathbf{k}_l\mathbf{r}')}{2} + \\
& \left. + i\left[\frac{1+\xi}{2}\exp\left(-\frac{1}{2}k_l^2 r_2^2(\xi)\right) - \frac{1-\xi}{2}\exp\left(-\frac{1}{2}k_l^2 r_2^2(-\xi)\right)\right]\sin\frac{(\mathbf{k}_l\mathbf{r}')}{2}\right\}.
\end{aligned} \tag{6}$$

Here $\mathbf{r}'$ is the displacement vector of the two simple Bravais lattices; ξ is the degree of order [3]. When we substitute (5) and (6) into (4) and sum over the reciprocal lattice all products of an odd number of the functions $\sin\frac{(\mathbf{k}_l\mathbf{r}')}{2}$ (for identical and different $\mathbf{k}_l$) drop out, and when $\mathbf{r}_1$ and $\mathbf{r}_2$ are expanded in powers of ϵ we obtain for the free energy

$$\begin{aligned}
A_{\mathrm{sol}} = A_{\mathrm{liq}} - \upsilon\vartheta \{ & [(\sigma_{11}(k) - 1)(1+\alpha)^2 x^2 - 2\sigma_{12}(k)(1+\alpha)(1+\beta)xy + \\
& + (\sigma_{22}(k) - 1)(1+\beta)^2 y^2]\,\varepsilon^2 + 2\,[(\sigma_{11}(k\sqrt{2}) - 1)(1 - \xi^2 + (1+\alpha)^2\xi^2)^2 x^4 + \\
& + 2\sigma_{12}(k\sqrt{2})(1 - \xi^2 + (1+\alpha)^2\xi^2)(1 - \xi^2 + (1+\beta)^2\xi^2)\,x^2y^2 + \\
& + (\sigma_{22}(k\sqrt{2}) - 1)(1 - \xi^2 + (1+\beta)^2\xi^2)^2 y^4] + \ldots\}.
\end{aligned} \tag{7}$$

The quantities x, y, α, β, ξ, where $\exp\left(-\frac{k^2 r_1^2(\xi)}{2}\right) = x(1+\alpha\xi)$, $\exp\left(-\frac{k^2 r_2^2(\xi)}{2}\right) = y(1+\beta\xi)$, are variational parameters in the expansion of the functional A (F). The integrals

$$\sigma_{ij} = \frac{4\pi}{v}\int_0^\infty K_{ij}(r)\,\frac{\sin kr}{kr}\,r^2\,dr$$

differ from those in [1] in that the kernels depend on the component subscripts.

Even without solving the entire set of equations which determine crystal equilibrium and the values of the variational parameters it is possible to determine the conditions under which continuous crystallization is possible. In the vicinity of points of continuous crystallization x and y are small; in the vicinity of points of continuous order ξ will be small. Crystallization occurs when $A_{\text{solid}} \leq A_{\text{liquid}}$.

The degree of order ξ is zero if the quadratic form $(\sigma_{11}(k)-1)\,u^2 - 2\sigma_{12}(k)\,uv + (\sigma_{22}(k)-1)\,v^2$ is negative-definite, for which the following conditions must be satisfied

$$\sigma_{11}(k) < 1;\quad (\sigma_{11}(k)-1)(\sigma_{22}(k)-1) > \sigma_{12}^2(k). \tag{8}$$

It follows from (8) that we at the same time have $\sigma_{22}(k) < 1$. If $(\sigma_{11}(k\sqrt{2})-1)\,w^2 + 2\sigma_{12}(k\sqrt{2})\,wt + (\sigma_{22}(k\sqrt{2})-1)\,t^2$ is then also negative in the region of positive values of w and t, there is no crystalline structure. Then, in addition to (8) the following conditions must be satisfied:

$$\sigma_{11}(k\sqrt{2}) < 1;\quad (\sigma_{11}(k\sqrt{2})-1)(\sigma_{22}(k\sqrt{2})-1) > \sigma_{12}^2(k\sqrt{2}), \tag{9}$$

or, if the second condition of (9) is violated,

$$\sigma_{11}(k\sqrt{2}) < 1;\quad \sigma_{22}(k\sqrt{2}) < 1;\quad \sigma_{12}(k\sqrt{2}) < 0. \tag{10}$$

The violation of the conditions in (8) while satisfying those in (9) or (10) results in continuous crystallization in an ordered structure. The transition points are determined by

$$(\sigma_{11}(k)-1)(\sigma_{22}(k)-1) - \sigma_{12}^2(k) = 0. \tag{11}$$

When, on the other hand, (9) and (10) are violated while (8) is satisfied, if the next term of the expansion (7) which does not contain ξ is positive, continuous crystallization in a disordered structure occurs at points which obey the equation

$$(\sigma_{11}(k\sqrt{2})-1)(\sigma_{22}(k\sqrt{2})-1) - \sigma_{12}^2(k\sqrt{2}) = 0. \tag{12}$$

Equations (11) and (12) define two curves in the v, T plane. Curve (12) terminates at their point of intersection, while (11) becomes the transition curve from the disordered to the ordered state. The Expansion (7) contains only even degrees of the order parameter ϵ; this leads to results that are familiar from the thermodynamic theory of second order phase transitions which was developed by Landau and Lifshits [3].

LITERATURE CITED

[1] E. A. Arinshtein, Doklady Akad. Nauk SSSR 112, 4, 615 (1957).*

[2] N. N. Bogoliubov, Problems of Dynamical Theory and Statistical Physics, 1946 (in Russian).

[3] L. D. Landau and E. M. Lifshits, Statistical Physics, 1951 (in Russian).

Tomsk Structural Engineering Institute

Received February 12, 1957.

---

* [Soviet Physics - Doklady, p. 54.]

THE Lβ_3 AND Lβ_4 LINES OF GERMANIUM

G. P. Borovikova and M. I. Korsunskii

(Presented by Academician G. V. Kurdiumov February 6, 1957)

The L series of germanium was studied by several investigators from 1921 to 1937 [1-3]. These studies used high-vacuum x-ray spectrographs with Bragg focussing. A flat mica crystal was used to analyze the x radiation. A metal x-ray tube with primary excitation was employed. Gwinner used an ion tube with hydrogen cooling. The following diagram and nondiagram lines of the L series were observed: L$\alpha_{1,2}$, Lβ_1, L$_l$, L$_\eta$ and Lα', Lα'', Lα''', Lβ', Lβ''. This list shows that the study of the germanium L series was incomplete. In particular, the lines Lβ_3 and Lβ_4 were not observed. It is known that Lβ_3 corresponds to the transition $L_I \rightarrow M_{III}$ and Lβ_4 to the transition $L_I \rightarrow M_{II}$. The normal electron configuration of the germanium atom is as follows:

$$\underset{K}{(1s)^2}\ \underset{L_I}{(2s)^2}\ \underset{L_{II-III}}{(2p)^6}\ \underset{M_I}{(3s)^2}\ \underset{M_{II-III}}{(3p)^6}\ \underset{M_{IV-V}}{(3d)^{10}}\ \underset{N_I}{(4s)^2}\ \underset{N_{II-III}}{(4p)^2}$$

The M_{II-III} level of germanium is thus interior and completely filled. The K$\beta_{1,3}$ line, which corresponds to the $K \rightarrow M_{II-III}$ transition, has been observed and its wavelength has been measured quite accurately. It is not clear why the L spectrum does not contain lines corresponding to the transitions $L_I \rightarrow M_{III}$ and $L_I \rightarrow M_{II}$. The present work was undertaken for the purpose of detecting lines corresponding to these transitions (Lβ_3 and Lβ_4) and to measure their wavelengths and intensities.

Apparatus and experimental method. The L spectrum of germanium was obtained from a tube of the Krasnikov type [4] used in fluorescent analysis. But it cannot be asserted that the spectrum is purely fluorescent because a small number of electrons still struck the secondary anode. The direct current was 1/20 of the total current through the tube and was measured at 0.5 ma. Such a small current with a broad focus and with strong cooling by running water could not appreciably heat the secondary anode on which the investigated substance was placed. The temperature of the specimen was measured by a thermocouple in direct contact with the anode. In our experiments the temperature of the germanium did not exceed 50°. The primary anode of the tube was covered with an aluminum plate. The principal exciting radiation consisted of the Al Kα_1 and Kα_2 lines with the wavelengths 8321.37 and 8323.82 XU. Since the secondary anode was close to the crystal within the focal circle the entire focal spot participated in the production of the spectrum. The tube was operated at 5-3.5 kv and 10 ma with exposures from 9 to 12 hours. The x-ray spectrum was resolved by a high-vacuum high-luminosity spectrograph with a 10 × 40 mm

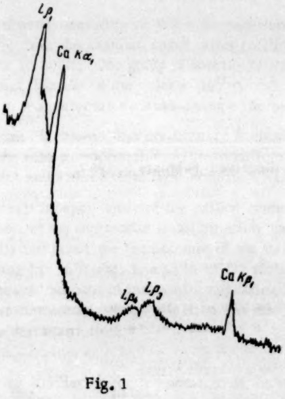

Fig. 1

mica crystal of 990 mm bending radius. The spectrograph shared the vacuum of the x-ray tube at $5\text{-}6 \cdot 10^{-6}$ mm Hg. Agfa Isopan F film was used to photograph the spectrum. The film was shielded from light by an aluminum foil of about 2μ thickness. A recording MF-4 microphotometer was used.

Experimental results. The possible $L\beta_3$ wavelength was determined by interpolation to be 9570 XU through plotting of $\lambda = f(z)$. A pure germanium single crystal was placed on the secondary anode of the x-ray tube. For the purpose of photographing the $L\beta_{3,4}$ lines the spectrograph was focused at 9570 XU. In all photographs of this spectral region, obtained under different conditions of excitation, two close lines were observed (Fig. 1). The corresponding wavelengths were 9561 and 9620 XU, as calculated from the microphotograms. The linear dispersion in the given range of angles of reflection was 35.4 XU/mm. The $K\alpha_1$ and $K\beta_1$ third-order calcium lines were used for comparison. The calcium was contained in $CaCO_3$. In calculating the wavelengths a correction was introduced for deviation from the Bragg law. The temperature correction was under 0.1 XU and was therefore neglected. Errors in determining the wavelengths were about 2 XU.

A comparison of the measured wavelengths with the values for the known wavelengths from all elements in all possible orders showed that the observed lines belong to germanium. This is also supported by the fact that the germanium single crystal specimens were of high purity. The microphotograms in Fig. 1 show that the shorter wavelength is more intense. It is known from the literature that in the $L\beta_{3,4}$ doublet the shorter wavelength $L\beta_3$, which corresponds to the $L_I \rightarrow M_{III}$ transition, is stronger by a factor of about 1.5 than $L\beta_4$, which corresponds to $L_I \rightarrow M_{II}$. The shorter wavelength is closer to the wavelength of $L\beta_3$ as determined by interpolation. On this basis the stronger line at 9561 XU was taken to be the $L\beta_3$ germanium line and 9620 XU as $L\beta_4$. It should be noted that this procedure makes the doublet separation for germanium somewhat too large. For the elements above germanium, beginning with $_{37}$Rb, the $L\beta_{3,4}$ doublet separation is 35 XU. We have obtained 59 XU. But it must be kept in mind that germanium is close to the group of elements in which the M shell is built up; therefore in this group the separation of the M_{II} and M_{III} levels may be somewhat greater than the usual value in heavier elements.

It is difficult to establish the intensity ratio of $L\beta_1$ and $L\beta_{3,4}$ because there was considerable difference in the densities of the lines. When $L\beta_3$ and $L\beta_4$ are dense enough for photometric study $L\beta_1$ is overexposed. Therefore, the intensity ratios of $L\beta_3$, $L\beta_4$, and $L\beta_1$ could only be estimated by converting the $L\beta_1$ intensity in accordance with the exposure times of the photograph containing $L\beta_3$, $L\beta_4$, and $L\beta_1$ and the photograph on which the density of $L\beta_1$ was 0.44. The ratio $IL\beta_3 : IL\beta_1$ obtained in this way was 0.127. We obtained very low intensities for $L\beta_3$ and $L\beta_4$. This low intensity and the large background which accompanies the primary method evidently prevented earlier investigators from observing these lines.

LITERATURE CITED

[1] E. Hjalmar, Z. Physik 7, 341 (1921).

[2] R. Thoraeus, Phil. Mag. 7, 2, 1007 (1926).

[3] E. Gwinner, Z. Physik 108, H. 7-8, 523 (1938).

[4] A. I. Krasnikov, Factory Lab. (USSR) 4-5 (1939).

V. I. Lenin Kharkov Polytechnic Institute

Received February 5, 1957.

THE EFFECT OF NEUTRON IRRADIATION ON THE MARTENSITE TRANSFORMATION

A. I. Zakharov and O. P. Maksimova

(Presented by Academician G. V. Kurdiumov February 11, 1957)

Neutron irradiation as a new and effective means of influencing the state of matter [1-4] is of interest not only as a method of modifying structure and thus producing certain changes in the properties of metals and alloys [5-8], but also and equally well as a method of studying the nature of phase transformations by first altering the state of the initial phase to cause some change in its stability and in the kinetics of subsequent phase transformations. We believe that this method is promising for the study of martensite transformations. The strictly regular directed shift of atoms in a martensite transformation [9] makes it extremely sensitive to any disturbance of the lattice structure in the original austenite phase. The occurrence of the transformation at relatively low temperatures should permit us to study the kinetics at temperatures that will permit a large retention of the radiation-induced imperfections.

The complete picture of the radiation-induced imperfections that result in metal and alloy lattices from elastic collisions between fast neutrons and atomic nuclei is very complicated. Irradiation can give rise to different types of defects with varying stability. It is assumed that the defects of relatively low stability are numerous and equal in quantity to the concentration of interstitial atoms and vacancies. Structural changes of relatively high stability are associated with the formation of more macroscopic and complex defects due to local melting and recrystallization of large individual zones [3, 10-11].

We are here making a first attempt to employ neutron irradiation for the investigation of martensite transformations. We have studied steels and alloys for which a thorough study had previously been made of the effect of previous plastic deformation on martensite transformation [13, 14]: 50G8 medium-carbon manganese steel (0.48% C; 7.7% Mn; 2.2% Cu; $T_m = -10°$); 140G4 high-carbon manganese steel (1.40% C; 4.0% Mn; $T_m = -94°$); 50N21 medium-carbon nickel steel (0.50% C; 21.0% Ni; $T_m = -28°$) and iron-nickel-manganese alloys N23G3 (0.025% C; 22.7% Ni; 2.88% Mn; $T_m = -20°$) and N22G3 (0.020% C; 22.4% Ni; 3.48% Mn; $T_m = -39°$).

Specimens measuring 2 × 3 × 24 mm were irradiated in the core of an ordinary heavy-water physical reactor [15] near the uranium rods * after preliminary thermal treatment consisting of vacuum annealing at 1100° for 10 hours. One group of specimens was irradiated for 100 hours and another for 200 hours. The total neutron flux was of the order of 10^{17} n/cm^2. The change of stability of the austenite was estimated from the shape of magnetometer curves during extreme cooling and heating.

Our results showed that preliminary neutron irradiation strongly affects austenite stability with respect to the martensite transformation. This modification of stability, which is manifested by a shift of the martensite point and altered final transformation, varies in different materials.

In steels independently of the carbon content and character of the alloyage irradiation increases the intensiveness of the martensite transformation that occurs with subsequent deep cooling. Thus in 50G8 steel irradiation raises the temperature of the start of the transformation by 15° and increases the effect of deep cooling by 10% (Fig. 1, a). In 50N21 nickel steel the irradiation activation of austenite is also manifested by an increased amount of martensite appearing in the initial "explosion." In 50G8 manganese steel, which has the highest martensite point, indication was also found of a possible direct radiation-induced austenite → martensite transformation.

---

* During irradiation the temperature of the specimens did not increase more than 40°.

The effect of radiation is entirely different in noncarbon alloys of iron, nickel and manganese (N23G3 and N22G3). In these alloys irradiation for either 100 or 200 hours always has a stabilizing effect on the γ-phase; the martensite point is lowered and the intensiveness of the transformation is reduced (Fig. 1, b).

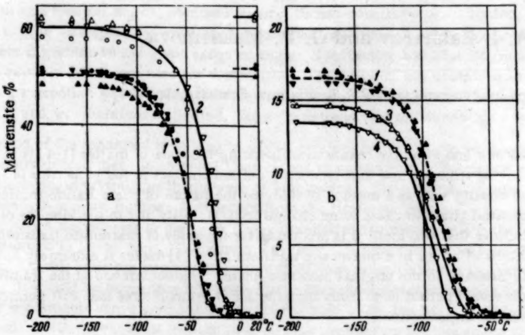

Fig. 1. Varying influence of neutron irradiation on martensite transformation.
a) activating effect (50G8 steel), b) inhibiting effect (N22G3 alloy):
1) unirradiated, 2) 100 hour irradiation, 3) 200 hour irradiation, 4) 200 hour irradiation and 5 hour annealing at 100°.

A comparison of our data with the results obtained in investigation of plastic deformation [13, 14] shows that the effects of the two different factors have much in common; the unique behavior which a material exhibits after preliminary plastic deformation is generally the same as its behavior after irradiation (the stability is altered in the same direction).

Do steels exhibit inhibition under relatively strong irradiation as in the case of plastic deformation, or does irradiation unlike plastic deformation always induce in steels only the activation of austenite? In answer to this question the data supports the first alternative; in 50G8 steel an activation maximum was observed depending on the period of irradiation (an increase of irradiation period from 100 to 200 hours reduced the activating effect by a factor of more than two).

Prolonged aging of irradiated specimens at room temperature leads to increased austenite stability. This inhibiting effect of long aging is manifested in steels by a gradual elimination of the activating effect of the radiation (Fig. 2) and in iron-nickel-manganese alloys by further increased austenite stability (Fig. 3). A similar but even stronger effect results from annealing at 100° (Fig. 2). Thus, the effect of low annealing in irradiated steels resembles what is observed after relatively small activating deformations [16]; in both instances the activating effect gradually disappears.

A study of all the data, comparison with the picture of the change of austenite stability under plastic deformation [13, 14, 16] and the existing ideas concerning the nature of radiation defects [1-8, 10-12] leads us to the following conclusions. It would hardly be correct to assume that the activation produced by radiation exists only in steels fundamentally, and inhibition only in alloys. It is evident that during irradiation of metals and alloys there is a simultaneous development of structural changes which affect austenite stability in opposite directions. The net effect, that is, the observation of an activating or inhibiting result, depends on the total neutron flux (which determines the degree of radiation damage) and on the properties of the material (the elastico-plastic properties of austenite etc.). In the earlier stages of irradiation there is evident predominance of damage which favors transformation; in later stages there are structural changes which have the opposite effect. This hypothesis is supported by the appearance of an activation maximum in steel.

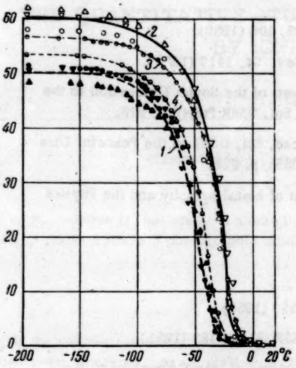

Fig. 2. Reduction of activating effect by aging and low annealing of 50G8 steel.
1) No irradiation; 2) 100 hour irradiation and 90 day aging; 3) 100 hour irradiation and 330 day aging; 4) 125 hour irradiation and 162 day aging with 10 hour annealing at 100°.

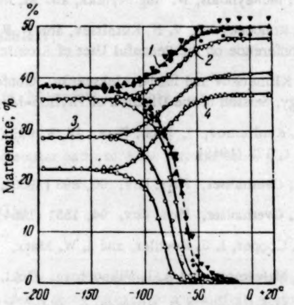

Fig. 3. Further increase of γ-phase stability during aging of irradiated N23G3 alloy.
1) No irradiation; 2) 100 hour irradiation and 130 day aging; 3) 100 hour irradiation and 334 day aging; 4) 200 hour irradiation and 234 day aging.

The low temperature stability of the activating effect (its disappearance during aging and annealing at 100°) shows that it results from the formation of interstitial-vacancy pairs, which we know to be capable of recombination at very low temperatures (beginning at 50° K) [12]. The favorable influence of these defects on martensite transformation must be associated with the appearance of elastic deformations of the lattice around points with increased concentrations of interstial atoms and vacancies [5, 10, 12], because it is known that strains in general have a stimulating effect on martensite transformation through reduction of the potential barriers which must be overcome by atoms during the phase transition. The probability of development of large local strains must increase with the elastic properties of the original austenite phase. This is the evident reason for the pronounced activation in steels.

The stabilizing effect of irradiation is evidently caused by the production of more complex defects [3] which we know to possess high intrinsic temperature stability [8, 10]. According to current notions such defects result under irradiation from the development of breakdown and reorientation of crystals and comprise groups of small differently oriented crystals that are formed in zones of local melting and recrystallization. The disordered state of such portions and the small size of each crystal in the group must limit the possibilities for the creation and growth of martensite crystals. The elimination of these defects and the corresponding elimination of the stabilizing effect of the radiation are possible only at temperatures which insure recrystallization.

LITERATURE CITED

[1] F. Seitz, Collection of translations, "The Influence of Radiation on Semiconductors and Insulators," 1951.

[2] G. I. Dienes, Ann. Rev. Nuclear Science 2, 187 (1953).

[3] I. A. Brinkman, J. Appl. Phys. 25, 961 (1954).

[4] A. I. Zakharov, Progr. Phys. Sci. 57, 4, 525 (1956).

[5] I. W. Marx, H. G. Cooper, and I. W. Henderson, Phys. Rev. 88, 106 (1952).

[6] A. W. McReynolds, W. Augustyniak, and M. McKeow Phys. Rev. 94, 1417 (1954).

[7] S. T. Konobeevskii, V. N. Kutaitsev, and N. F. Pravdiuk, Reports of the Soviet Delegation to the International Conference on the Peaceful Uses of Atomic Energy (Acad. Sci. USSR Press), p. 276.

[8] V. I. Klimenkov and Iu. N. Alekseenko, Conference of the Acad. Sci. USSR on the Peaceful Uses of Atomic Energy, Session of the Division of Physico-Math. Sciences (1955), p. 322.

[9] G. V. Kurdiumov, J. Tech. Phys. 18, 8, 999 (1948); Problems of Metallography and the Physics of Metals, No. 1, 132 (1949).

[10] A. W. Overhauser, Phys. Rev. 90, 393 (1953).

[11] A. W. Overhauser, Phys. Rev. 94, 1551 (1954).

[12] H. G. Cooper, I. S. Kochler, and I. W. Marx, Phys. Rev. 97, 599 (1955).

[13] O. P. Maksimova and A. I. Nikonorova, Dokl. Akad. Nauk SSSR 81, 2, 183 (1951).

[14] O. P. Maksimova, A. I. Nikonorova, and G. K. Pogorelov, Problems of Metallography and the Physics of Metals, No. 4, 144 (1955).

[15] A. I. Alikhanov, V. V. Vladimirskii, S. Ia. Nikitin, A. D. Galanin, S. A. Gavrilova, and M. A. Burgov, The Construction and Theory of Reactors, (Acad. Sci. USSR Press, Moscow, 1955).

[16] G. V. Kurdiumov, O. P. Maksimova, and A. I. Nikonorova, Doklady Akad. Nauk SSSR 114, No. 4 (1957).

Central Research Institute of
Ferrous Metallurgy

Received November 21, 1956.

THE QUANTITATIVE STUDY OF LATENT IMAGE FORMATION BY IONIZING PARTICLES

A. L. Kartuzhanskii

(Presented by Academician A. F. Ioffe November 22, 1956)

A. P. Zhdanov [1] has used the analogy of mean free molecular paths to show that the density ν of an ionizing particle track in a photographic emulsion is given by

$$\nu = \frac{C_{\text{vol}}}{\pi d^3/6}\frac{\pi d^2}{4} = \frac{3C_{\text{vol}}}{2d} \tag{1}$$

(C_{vol} is the volume concentration of AgHal in the emulsion; d is the diameter of an emulsion crystal assumed to be spherical). As we shall show, this formula provides a new approach to a quantitative study of latent image formation by ionizing particles passing through photographic emulsion crystals. But it must be kept in mind that Zhdanov's formula in the above form assumes that each crystal touched by a particle is developable. If only a portion of the crystals are developable the right-hand side of (1) must be multiplied by the factor P which denotes the probability of developability.

For the purpose of determining P we assume that the passage of a particle through a crystal produces in the latter a sufficient number of conduction electrons for the subsequent formation of a developable center only when the path of the particle in the crystal exceeds a certain minimum length l or, equivalently, moves within a sphere of diameter $\delta = \sqrt{d^2 - l^2}$, the tangent to which has the length l within the crystal. Replacement of the complete sphere (of diameter d) by the "effective sphere" (of diameter δ) in the calculation of ν leads only to the replacement of $\frac{\pi d^2}{4}$ by $\frac{\pi \delta^2}{4}$, as follows:

$$\nu = \frac{C_{\text{vol}}}{\pi d^3/6}\frac{\pi \delta^2}{4} = \frac{3C_{\text{vol}}}{2d}\left(\frac{\delta}{d}\right)^2, \tag{2}$$

whence

$$P = \left(\frac{\delta}{d}\right)^2 = 1 - \left(\frac{l}{d}\right)^2.$$

Recently K. S. Bogomolov et al. [2] by assuming that the mean free path of a conduction electron is small compared with the size of a crystal showed experimentally that the particle is effective only while passing through a certain surface region ("crust") of the crystal, and that for any value of d the thickness b of the crust is only 0.03 μ (from previous data of other authors [3] it followed that b was considerably larger, ~ 0.2 μ). The minimum path l in a crystal is in this connection not a unique function of the distance δ from the center (Fig. 1). Therefore, instead of δ [see Equation (2)] we now have δ_1 and δ_2, the diameters of two spheres the tangents to which have the length l within the crystal crust. It can be shown that in this case

$$\nu = \frac{C_{\text{vol}}}{\pi d^3/6}\frac{\pi\delta_2^2 - \pi\delta_1^2}{4} = \frac{3C_{\text{vol}}}{2d}\frac{\delta_2^2 - \delta_1^2}{d^2}, \tag{3}$$

whence

$$P = \frac{\delta_2^2 - \delta_1^2}{d^2}.$$

In any event Equation (2), or correspondingly (3), enables us from the known values of C_{vol} and $\underline{d}$ for a given emulsion and the experimental value of ν to obtain P and then the minimum path l that provides a photographically effective passage of a given particle through a crystal of the emulsion.

Using (2) we have

$$l = d\sqrt{1 - P} = d\sqrt{1 - \frac{2\nu d}{3C_{vol}}}. \qquad (4)$$

Applying (3) we obtain l from the solution of a set of three equations: (3) and the two relations

$$l = \sqrt{d^2 - \delta_2^2} \qquad \text{when } \delta > d - 2b;$$
$$l = \sqrt{d^2 - \delta_1^2} - \sqrt{(d - 2b)^2 - \delta_1^2} \qquad \text{when } \delta \leqslant d - 2b,$$

connecting δ_1, δ_2, and l, as can be seen from Fig. 1. For l we obtain the biquadratic equation

$$l^4 + \frac{8}{3}\left[\frac{\nu d^3}{8C_{vol}} - b(d - b)\right] l^2 - \frac{16}{3} b^2 (d - b)^2 = 0, \qquad (5)$$

which has one positive real root. We note that (4) and (5) do not give identical numerical values of l and that the difference increases as b/d is reduced; however for the majority of numerical emulsions, where d ~ 0.2-0.3 μ, the crust occupies a large portion of the crystal volume so that the difference is small.

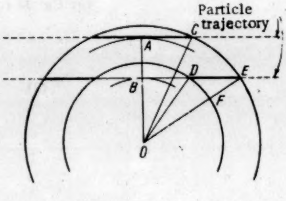

Fig. 1. OE = d/2; OF = d/2 − b; AC = DE = = l /2; OB = δ_1/2; OA = δ_2 /2.

Having obtained l we can determine the minimum number $\underline{n}$ of conduction electrons required to permit development of the emulsion crystals. If the stopping power of AgHal is ~ 3000 [4] the energy loss dE/dx is about 700 ev per 1 μ of path in the AgHal for a particle with minimum ionizing power. Since the liberation of a single electron by the particle requires ~5.8 ev [5] the energy expended by the particle frees n =(700 / 5.8)l conduction electrons in a single crystal. For a particle with a different value of dE/dx we have

$$n \cong 120 \frac{dE/dx}{(dE/dx)_{min}} l. \qquad (6)$$

As we have shown [6] the value of $\underline{n}$ which corresponds to the development threshold is related to the number N of sensitive crystal centers and the minimum number n_0 of Ag atoms in the developable center by

$$n = N(n_0 - 1) + 1, \qquad (7)$$

where n_0 and sometimes N can be determined independently. Then the use of (4) or (5), (6) and (7) to analyze the tracks of particles with threshold energy which are barely recorded by a given emulsion enables us to determine the loss of conduction electrons when the substitution of known values of N, n_0 and n in (7) leads to an inequality, and to determine N when it is unknown.

The present short note is not an attempt to provide an exhaustive quantitative study of the formation of latent images by ionizing particles. Therefore we shall give only two examples of the application of this method to an analysis of particle tracks.

In one of our experiments two emulsions of different particle sensitivity, which were obtained from the same original emulsion ($C_{vol} = 0.5$ and $d = 0.7\ \mu$) by varying the conditions of second ripening, were exposed to electrons of moderate energy from the beta emitter C^{14} and to relativistic energies in cosmic rays. For both emulsions we knew N and n_0; from noninterchangeability data n_0 with full development was 8 ± 1 for the more sensitive emulsion (which will be denoted by I) and 12 ± 1 for the lesser sensitive (II); from an electron-microscopic study N was 5 in both instances, that is, the sensitivity centers in the crystals of these emulsions differed in efficiency (depth) but not in number. Tracks of relativistic electrons were detected only in emulsion I, with $\nu = 0.3\ \mu^{-1}$; therefore for emulsion II we can assume $\nu \leq 0.15\text{-}0.18\ \mu^{-1}$ (below the difference threshold). Since in these emulsions $d \gg b$ we may use Equation (5). Calculation gives for emulsion I, $l = 0.3\ \mu$, $n = 36$ and for II, $l \geq 0.38\ \mu$, $n \geq 46$. Substitution for n in (7) leads for I to an approximate equality, that is, the electron losses are very small if at all existent, which is in good agreement with [7]. For II, as was to be expected, $n - 1 < N(n_0 - 1)$, which signifies undevelopability.

The tracks of the entire beta spectrum of C^{14} were detected in both emulsions; for the initial portions of the tracks of longest range particles we obtained $\nu \cong 0.6\ \mu^{-1}$ in I and $\nu \cong 0.2\ \mu^{-1}$ in II. Taking $\left(\frac{dE}{dx}\right)_{E_{max}C^{14}} = 1.7 \left(\frac{dE}{dx}\right)_{min}$, we obtain $l = 0.21\ \mu$ and $n = 43$ for I and $l = 0.35\ \mu$ and $n = 71$ for II. This gives conduction electron losses of 20-25 % for both emulsions, which is considerably greater than the result in [7] for a finer-grained Ilford G5 emulsion (< 10%) with the same ionizing power. It is possible that these losses are associated not so much with recombination as with the formation of deep latent images. A calculation using (4), which in this instance is unjustified, gives much larger losses than those indicated above, in complete disagreement with [7].

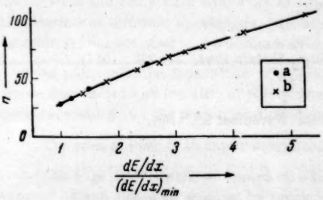

Fig. 2. a) pions; b) beta particles.

Interesting results are obtained from an analysis by the foregoing method of the data on track density in Ilford G5 emulsions ($d = 0.3\ \mu$) for pions of 24 to 224 Mev [8] and beta particles of 30 to 250 kev [9].

Using Equation (5) instead of (4) together with data on dE/dx for particles of different energies [4, 10] we can obtain the dependence of n on dE/dx which is represented in Fig. 2. We see that the minimum number of conduction electrons required for development of a crystal increases with the ionizing power, that is, we observe a kind of decrease of the "quantum yield." Since for this emulsion the recombination losses of electrons for minimum ionizing power are negligibly small [7], and n_0 from our data is 7-8, from $(dE/dx)_{min}$ it is easy to obtain $N = \frac{n - 1}{n_0 - 1}$; the value of 4 is found. Then from data on recombination losses [7] N can be obtained for other values of dE/dx since n_0 remains unchanged; in the range under consideration N increases continuously to 14-15. This means that with an increase of the instantaneous concentration of conduction electrons in a crystal the number of centers that participate in the concentration of photolytic Ag increases at the expense of the centers that are not designed for this role under optimal conditions. Such additional centers, which may be deep-seated or which may require for their conversion into developable centers a larger number of Ag atoms than the principal centers, compete with the principal centers and thus assist the continuously increasing recombination effect in reducing the effective use of conduction electrons. The calculation of n and N in this manner from (4) gives very similar qualitative results; somewhat higher values of $\underline{n}$ and N which are thus obtained are possibly caused by processes in the entire crystal as well as in the crust. Then the difference between the values of $\underline{n}$ and N calculated from (4) and (5) might serve for an estimate of the losses associated with the formation of deep latent images.

The author is deeply grateful to B. L. Birbrair for valuable suggestions in connection with this work.

LITERATURE CITED

[1] A. P. Jdanov, J. Phys. Radium 6, 233 (1935).

[2] K. S. Bogomolov et al., J. Scientific and Appl. Photog. (USSR) 1, 84, 121 (1956).

[3] H. Hoerlin and F. A. Hamm, J. Appl. Phys. 24, 1514 (1953).

[4] J. H. Webb, Uspekhi Fiz. Nauk 38, 77 (1949).

[5] K. A. Yamakawa, Phys. Rev. 82, 522 (1951).

[6] A. L. Kartyzhanskii, Doklady Akad. Nauk SSSR 109, 285 (1956).*

[7] M. Della Corte, M. Ramat, and L. Ronchi, Nuovo Cimento 1, 958 (1953).

[8] B. Zajac and M. A. S. Ross, Nature 164, 311 (1949).

[9] J. R. Fleming and J. J. Lord Phys. Rev. 92, 511 (1953).

[10] A. Beiser, Uspekhi Fiz. Nauk 52, 377 (1954) (Translation of Revs. Modern Phys. 24, 273, 1952).

Leningrad Agricultural Institute

Received November 21, 1956.

---

*[Soviet Physics - Doklady, p. 421.]

THE SPECTRAL RESPONSE CURVES FOR PHOTOCONDUCTIVITY IN CdS SINGLE CRYSTALS

Academician V. E. Lashkarev (Ukrainian Academy of Sciences),
E. A. Sal'kov, G. A. Fedorus and M. K. Sheinkman

The subject of this paper has been treated by several authors [3-7]. However the methods used and the dissimilar results obtained leave unclear the cause of the falling off of photoconductivity in the short-wave portion of the fundamental absorption band. Thus, in [4-6] an attempt was made to explain the decline of photoconductivity by a decrease of the lifetime τ of photocarriers (free electrons) due to surface recombination. The method used by Lambe [5] (measurement of the photocurrent at 100 kc) seems to us to require justification and comparison with more familiar procedures, and the method of Bube [6] (equalization of the photocurrent at different wavelengths) will be shown below to lead to equivocal results. Fassbender and Seraphin [7] did not observe the decrease of $\tau(\lambda)$.

In addition to the dependence $\tau(\lambda)$ the causes of reduced photocurrent in the fundamental absorption region may be reduced mobility of photocarriers, a higher light reflection coefficient and the decrease of the quantum yield β (or the proportional photocurrent yield $\underline{a}$ [1]) in this region.

The present work is an experimental check of these hypotheses.

The experiments were performed on CdS single crystals produced by synthesis of cadmium and sulfur vapors.* Electrodes were prepared by vacuum deposition of indium. The light source was an UM-2 monochromator combined with a special 340 watt incandescent lamp. The light intensity was variable within a wide range.

The spectral response curve of the photocurrent was obtained under stationary illumination of the specimen; the intensity of the light of different wavelengths L_p was maintained constant at $36 \cdot 10^{12}$ quanta /cm$^2 \cdot$ sec. The spectral dependence of the photocarrier lifetime was conducted as follows.

We measured the instantaneous decay time of the photocurrent (τ^0) when the light was switched off by determining the time for a drop of 5-10 % from its stationary value (Δt_5, Δt_{10}) during the initial linear decay. The light intensity at each wavelength was the same as during the study of the spectral dependence of the photocurrent (L_p).

The time τ^0 was determined as $10\Delta t_{10}$ or $20\Delta t_5$. A similar procedure (measurement of the time of photocurrent decay by 5 or 16%) was used by Lambe [5] and Bube [6] with the important difference that in our case we equated the number of incident quanta of the different wavelengths while Bube equated the photocurrents [6].

The photocurrent yield a_0 was measured from the amplitude of the initial portion of the oscillogram of photocurrent rise during illumination by light pulses that were many times shorter than the relaxation time of the photoconduction (0.5 millisecond) and separated by 3-minute dark periods [1]. During the dark periods there was complete decay of photostimulation of the specimen due to the light pulses [2]. We also measured the differential yield a_d by this method under additional constant illumination of the specimen by light of the same spectral composition as the pulses but of much greater intensity. The intensity of this illumination at each wavelength was such that the photocurrent due to this cause was in accordance with the spectral response curve.

---

* The authors are indebted to I. B. Mizetskkaia for preparation of the crystals.

The mobility of photocarriers was determined by measurements of the conductivity and Hall effect.* The experiment showed that the conductivity does not depend on the wavelength from 4500 to 5500 A, with 10% accuracy.

Measurements of the light reflection coefficient showed that during the transition to strongly absorbed light the reflection coefficient remains practically unchanged and that its magnitude in the fundamental absorption region does not exceed 20%.

Figure 1 shows that the curve of $\tau^0(\lambda)$ has a minimum at the photocurrent maximum; the spectral curves $a_0(\lambda)$ and $a_d(\lambda)$ are similar to $I_{ph}(\lambda)$ with a sharper maximum for $a_d(\lambda)$.

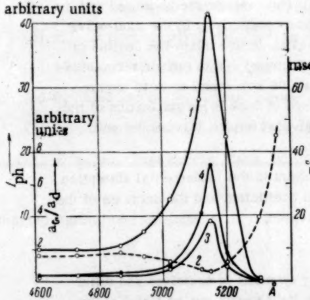

Fig. 1. Spectral curves: 1) photocurrent I_{ph}; 2) instantaneous decay time τ^0; 3) photocurrent yield a_0; 4) yield a_d. Curves 3 and 4 are reduced to the same scale at λ = 4610 A.

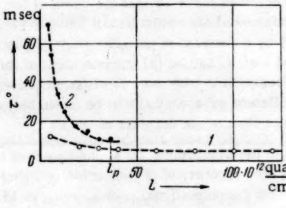

Fig. 2. Dependence of the instantaneous decay time τ^0 on the intensity of incident light L: 1) illumination at 5120 A; 2) 4610 A.

The curve $a_0(\lambda)$ $[a_d(\lambda)]$ can be explained by the exciton mechanism of photoconduction in CdS single crystals which has been proposed by one of the authors [2]. We can imagine that excitons created at the surface of the semiconductor in a layer $\sim 10^{-5}$ cm thick during absorption of light in the fundamental absorption region of the lattice cannot diffuse into the interior and are largely annihilated without photostimulation at local levels associated with the surface structure. At the transition to weakly absorbed light excitons appear throughout the semiconductor and suffer photodissociation, thus stimulating the specimen and increasing the number of photocurrent carriers.

The curve $\tau^0(\lambda)$ (Fig. 1, 2) can be explained by the dependence of τ^0 on the photocarrier concentration, which is shown by curves 1 and 2 of Fig. 2.

Indeed, it follows from Fig. 2 that with decreased illumination, with a corresponding reduction of photocarrier concentration, $\tau^0(L)$ begins to increase. It is of interest that under strong illumination $\tau^0(L)$ remains practically constant.

A stronger dependence of $\tau^0(L)$ and larger absolute values of τ^0 for 4610 A can be explained by the following reasoning: during illumination with strongly absorbed light (4610 A) the photocarrier concentration is smaller than during illumination with weakly absorbed light (5120 A) although the thickness of the layer in which the carriers are concentrated is much smaller in the first instance than in the second. This ceases to seem strange if we remember the sharp reduction of photocurrent yield a with the transition to the short-wave region (Fig. 1, 3 and 4).

---

* These measurements were made by A. P. Trofimenko, to whom the authors hereby express their thanks.

Figure 3 shows the unsuitability of Bube's method [6] of measuring $\tau^0(\lambda)$ by equalizing the photocurrents at different wavelengths and his attempt to use the resulting curve of $\tau^0(\lambda)$ to explain the spectral dependence of the photocurrent. It is clear that this method can give different curves for $\tau^0(\lambda)$ depending on the magnitude of the photocurrent which is used as the experimental parameter. The rise of $\tau^0(\lambda)$ is here associated with a reduced carrier concentration that results from increased thickness of the photoconductive layer upon transition to weakly absorbed light.

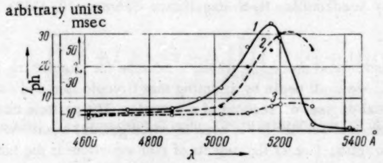

Fig. 3. Spectral response curves: 1) photocurrent; 2 and 3) instantaneous decay time τ^0 obtained by equalizing photocurrents at different wavelengths; 2) with 3 μa photocurrent; 3) with 40 μa.

We have thus shown that the cause of the reduced photocurrent in the fundamental absorption region of CdS single crystals is the reduced photocurrent yield and not a smaller carrier lifetime.

In conclusion we wish to point out that many authors assume unity as the value of the photocurrent quantum yield β over the entire spectrum and use this as a basis for calculating the photocurrent lifetime τ [8, 9] or assume ohmic contacts [10]. But our experiments have shown that the assumption $\beta = 1$ is inconsistent with our observations of the wavelength dependence of the yield.

LITERATURE CITED

[1] V. E. Lashkarev, J. Exptl.-Theoret. Phys. (USSR) 19, 876 (1949).

[2] V. E. Lashkarev and G. A. Fedorus, Izv. Akad. Nauk SSSR, Ser. Phys. 16, 1, 81 (1952).

[3] R. H. Bube, Phys. Rev. 98, 431 (1955).

[4] R. H. Bube, J. Chem. Phys. 21, 1409 (1953).

[5] J. Lambe, Phys. Rev. 98, 985 (1955).

[6] R. H. Bube, Phys. Rev. 101, 1669 (1956).

[7] J. Fassbender and B. Seraphin, Ann. Physik 10, Nos. 6-7, 374 (1952).

[8] A. Rose, Proc. Institute of Radio Engineers 43, 1837 (1955).

[9] R. H. Bube, J. Chem. Phys. 23, 18 (1955).

[10] R. W. Smith, Phys. Rev. 97, 1525 (1955).

Physics Institute,
Academy of Sciences, Ukrainian SSR

Received February 21, 1957.

ON THE RELATIONSHIP BETWEEN ORDINARY SPACE AND ISOTOPIC SPIN SPACE

G. A. Sokolik

(Presented by Academician N. N. Bogoliubov February 13, 1957)

1. We shall develop a mathematical procedure which is suitable for establishing the relationship between ordinary space and isotopic space. We shall begin by assuming that isotopic spin and other invariants related to charge can be interpreted as internal degrees of freedom of a particle. The particle can then be described by the equations of Pais [1] or Ivanenko and Sokolik [2] or even by more general equations [3] which describe particles of all spatial and isotopic spins. One of the defects of such equations is the fact that they separate into independent parts for the spatial and charge variables. It is reasonable to develop a theory which generalizes the equations of [1-3] in the form

$$\left(\Gamma_i \frac{\partial}{\partial x_i} + x\right)\psi = 0 \quad (i = 1, 2, \ldots, n) \tag{1}$$

x_1 is the imaginary variable of time. x_1, x_2, x_3, and x_4 are coordinates in Minkowski space. The remaining $n - 4$ coordinates represent isotopic space.

2. We shall solve the general problem of obtaining all equations (1) which are invariant under rotations and reflections in n-dimensional space. The invariance conditions are

$$\begin{gathered}[\Gamma_i I_{jk}] = g^{ij}\Gamma_k - g^{ik}\Gamma_j, \\ g^{nn} = -g^{11} = \cdots = g^{n-1,\,n-1} = 1, \quad g_{ik} = 0, \quad i \neq k,\end{gathered} \tag{2}$$

where the I_{ij} are infinitesimal operators representing the n-dimensional orthogonal group obtained in [4]. Our problem of classifying the equations according to representations of the continuous (here orthogonal) group reduces [5] to finding the irreducible representations of the group that are obtained from reduction of the direct product of any representation by the identical representation (the n-dimensional vector) $\partial \psi_i / \partial x_j$, where ψ_i is transformed in accordance with the arbitrary representation and the gradient $\partial / \partial x_j$ according to the identical representation.

3. According to [4] the basis vector of the representation is provided by the numerical tables obtained from the inequalities

$$\begin{gathered}m_{2p+1,\,i+1} \leqslant m_{2p,\,i} \leqslant m_{2p+1,\,i} \quad -m_{2p,\,p} \leqslant m_{2p-1,\,p} \leqslant m_{2p,\,p}, \\ m_{2p,\,i+1} \leqslant m_{2p-1,\,i} \leqslant m_{2p,\,i} \quad (i = 1, 2, \ldots, p).\end{gathered} \tag{3}$$

We shall derive the dimensions of the representations herefrom.

For the (2k + 2)-dimensional group we have

$$\begin{gathered}S_{2k+2} = \prod_{1 < j + i \leqslant k+1} \frac{(p_i + p_j)(p_i - p_j)}{\alpha_k}, \\ p_i = m_{2k+1,\,i} + k - i + 1 \quad (k = 1, 2, \ldots);\end{gathered} \tag{4}$$

for the (2k + 1) - dimensional group

$$S_{2k+1} = \prod_{1<j+i<k} (p_i - p_j)(p_i + p_j + 1) \prod_{i=1}^{k} \frac{2p_l + 1}{\beta_k} \quad (p_l = m_{2k,\,l} + k - i), \quad (4')$$

where α_k and β are of the form

$$\alpha_k = \prod_{l=0}^{k-1} (k + l + 1)(k - l + 1) \prod_{j=1}^{k-1} \prod_{i=0}^{j-1} \frac{(j+i)(j-i)}{2k+2},$$

$$\beta_k = \prod_{i=0}^{k-2} (2i + 1) \prod_{l=0}^{k-2} (k + l + 1)(k - l) \prod_{j=1}^{k-2} \prod_{l=0}^{j-1} (j + i + 1)(j - i). \quad (5)$$

Using the fact that for the (2k + 2) - dimensional group the maximum vector of the representation

$$\xi \begin{bmatrix} m_{2k+1,\,1} \cdots m_{2k+1,\,k} \\ \cdots\cdots\cdots\cdots \\ m_{41} \quad m_{42} \\ m_{31} \quad m_{32} \\ m_{21} \\ m_{11} \end{bmatrix}.$$

is the eigenvector of the commuting representation operators $I_{2k+2,\,2k+1} \ldots I_{21}$, with the weights given by

$$I_{2k+2,\,2k+2}\,\xi(\alpha) = m_{2k+1,\,k+1}\,\xi(\alpha) \ldots I_{21}\,\xi(\alpha) = m_{2k+1,\,1}\,\xi(\alpha), \quad (6)$$

we obtain the resolution of the direct product of two representations of the (2k + 2) - dimensional group into irreducible representations. In the special case when one of these is the identical representation τ_0 we have

$$[(m_{2k+1,\,1} \ldots m_{2k+1,\,k+1}) \times \tau_0] = (m_{2k+1,\,1} \pm 1 \ldots m_{2k+1,\,k+1}) \dot{+} \ldots \quad (7)$$
$$\ldots \dot{+} (m_{2k,\,1} \ldots m_{2k,\,k} \pm 1); \quad \tau_0 = (1, 0 \ldots 0).$$

For the (2k + 1) - dimensional case we have similarly

$$[(m_{2k,\,1} \ldots m_{2k,\,k}) \times \tau_0] = (m_{2k,\,1} \pm 1 \ldots m_{2k,\,k}) \dot{+} \ldots$$
$$\ldots \dot{+} (m_{2k,\,1} \ldots m_{2k,\,k} \pm 1) + \Delta_{m_{2k,\,k}} (m_{2k,\,1} \ldots m_{2k,\,k});$$

$$\Delta_{m_{2k,\,k}} = \begin{cases} 1, & m_{2k,\,k} \neq 0; \\ 0, & m_{2k,\,k} = 0. \end{cases}$$

We shall say that the representations τ and τ' are coupled if τ' is one of the irreducible representations into which the product $[\tau \times (1, 0 \ldots 0)]$ is reduced. We thus obtain the general rule: for the (2k + 2) - dimentional group a representation cannot be coupled with itself, but for the (2k + 1) - dimensional group this can occur if all $m_{2k,\,i}$ are different from zero.

4. In order to determine the matrices Γ_i in the (2k + 2) - dimensional case it is sufficient to obtain the matrix Γ_{2k+2}. The remaining matrices are expressed in terms of this matrix by means of formulas derived from (2):

$$[\Gamma_{2k+2}, I_{2k+2,\, k+1}] = \Gamma_{2k+1} \ldots [\Gamma_{2k+2}, I_{2k+1,\, 1}] = \Gamma_1.$$

The matrix Γ_{2k+2} is

$$\Gamma_{2k+2}\xi(\alpha)_\tau = \sum_{\tau'\alpha'} C_{\alpha\alpha'}^{\tau\tau'} \xi(\alpha')_{\tau'} \tag{8}$$

and satisfies the invariance condition that follows from (2):

$$[[\Gamma_{2k+2}, I_{2k+2,\, 2k+1}]\, I_{2k+2,\, 2k+1}] = \Gamma_{2k+2}. \tag{9}$$

Using the relations $0 = [\Gamma_{2k+2}, I_{2k+1,2k}] = \ldots = [\Gamma_{2k+2}, I_{21}]$, which also follow from (2), we now write (8) according to Schur's lemma in the form

$$\Gamma_{2k+2}\xi(\alpha)_\tau = \sum_{\tau'} C_{\tau\tau'}^{m_{2k,1} \ldots m_{2k,k}} \xi(\alpha)\tau' \tag{10}$$

Substituting into (9) Formula (10) and the matrix elements of the infinitesimal representation from [4] we obtain a set of homogeneous equations in $C_{\tau\tau'}^{m_{2k,1} \ldots m_{2k,k}}$. This set consists of $k!/(k-2)!\,2!$ subsets, each of which corresponds to a pair of numbers $m_{2k,i}\ m_{2k,j}$, and is formed with respect to different $C_{\tau\tau'}^{m_{2k,i} \pm 1, m_{2k,j}}$, $C_{\tau\tau'}^{m_{2k,i} m_{2k,j} \pm 1}$ $C_{\tau\tau'}^{m_{2k,i} \pm 1, m_{2k,j} \pm 1}$, $C_{\tau\tau'}^{m_{2k,i} m_{2k,j}}$. As was shown above the solution of this set of equations can differ from zero only when τ and τ' are coupled representations, because when the irreducible representation τ is contained in the representation by which ψ is transformed τ' must be in the representation by which $\partial\psi/\partial x_j$ is transformed.

Substituting the coupling conditions (7) we have for (2k + 2) - dimensional space the general formula

$$C_{\tau\tau'}^{m_{2k,1} \ldots m_{2k,k}} = C_{\tau\tau'} \times$$
$$\times \prod_{1 < j < h} \sqrt{(m_{2k,j} + m_{2k+1,j} + 2k - i - j + 2)(m_{2k,j} - m_{2k+1,i} + i - j - 1)}, \tag{11}$$
$$m'_{2k+1,i} = m_{2k+1,i} + 1; \quad m'_{2k+1,j} = m_{2k+1,j} \quad (i \neq j),$$

where $C_{\tau\tau'}$ are arbitrary complex constants.

For the (2k + 1) - dimensional group we can analogously obtain a general formula for the matrix coefficients Γ_{2k+1}:

$$C_{vv'}^{m_{2k-1,1} \ldots m_{2k-1,k}} = C_{vv'} \times$$
$$\prod_{1 < j < h} \times \sqrt{(m_{2k,i} + m_{1k-1,i} + 2k - j - i + 1)(m_{2k,i} - m_{2k-1,j} - j + i - 1)}, \tag{12}$$

when

$$m'_{2k,\,i} = m_{2k,\,i} + 1; \quad m'_{2k,\,j} = m_{2k,\,j}, \quad i \neq j;$$

$$C_{\nu\nu'}^{m_{2k-1,\,1}\cdots m_{2k-1,\,k}} = C_{\nu\nu'} \prod_{1<j<k} m_{2k-1}, \tag{12'}$$

when

$$m_{2k,\,i} = m_{2k,\,i}\,,$$

where the ν are irreducible representations of the (2k + 1) - dimensional group. *

5. In conclusion we obtain the invariance conditions of (1) with respect to the inversions $x' = -x$, $x'_n = x_n$ or $x' = x$, $x'_n = -x_n$, where x are the remaining n − 1 coordinates. For 2k + 2 = n the operators T satisfy the relations

$$[TI_{2k+2,\,2k+1}]_+ = 0; \quad [TI_{2k+1,\,2k}] = \cdots = [TI_{2,1}] = 0. \tag{13}$$

It can be shown that for the (2k + 2) - dimensional group $\tau = (m_{2k+1,\,1} \ldots m_{2k+1,\,k+1})$ upon inversion becomes $\tau = (m_{2k+1,\,1} \ldots - m_{2k+1,\,k+1})$. If $m_{2k+1,\,k+1} = 0$, τ and $\dot{\tau}$ coincide. In the first case T is of the form

$$T \begin{pmatrix} 0 & (-1)^{\Sigma\lambda_i} \\ (-1)^{\Sigma\lambda_i} & 0 \end{pmatrix}, \quad \lambda_i = m_{2k,\,i} + \begin{cases} 1 \\ 0 \end{cases} \quad (i = 1, 2, \ldots, k). \tag{14}$$

The matrix operates on the vector $\begin{pmatrix} \xi(\alpha)\,\tau \\ \xi(\alpha)\,\dot{\tau} \end{pmatrix}$.

In the second case we have $T = (-1)^{\Sigma\lambda_i}$. By discovering the invariance condition with respect to the inversions $[T\Gamma_{2k+2}] = 0$ we obtain the conditions for the $C_{\tau\dot{\tau}}$, which coincide with the invariance conditions for n = 4 that are given in [6]. For the (2k + 1) - dimensional group, τ and $\dot{\tau}$ coincide, with $T = (-1)^{\Sigma\lambda_i}$.**

6. Thus, the matrices Γ_{2k+2} and Γ_{2k+1} consist of blocks numbered according to the irreducible representations of the (2k + 2) - and (2k + 1) - dimensional groups given by the numbers $m_{2k+1,\,1} \ldots \ldots m_{2k+1,\,k+1}$ and $m_{2k,\,1} \ldots m_{2k,\,k}$, as follows:

$$\| C_{\tau\tau'}^{m_{2k,\,1}\cdots m_{2k,\,k}} \| \times I_{2k+1}; \qquad \| C_{\nu\nu'}^{m_{2k-1,\,1}\cdots m_{2k-1,\,k}} \| \times I_{2k}. \tag{15}$$

I_{2k+1} and I_{2k} are unit matrices of the dimensions S_{2k+1} and S_{2k} (4), (4'). When Γ_i can be reduced to diagonal form with eigenvalues different from zero and, as can easily be seen from (15), each eigenvalue has the multiplicity S_{2k+1} or S_{2k}, we can interpret $m_{2k,\,1} \ldots m_{2k,\,k}$ or $m_{2k-1,\,1} \ldots m_{2k-1,\,k}$ as a generalization of ordinary spatial spin. The numbers can be identified with the values of the spin, isotopic spin and other invariants of the isotopic group of dimension greater than three. For the 8-dimensional group the $C_{\tau\tau'}^{m_{61} m_{62} m_{63}}$ will be given by three numbers which can be associated with spin, isotopic spin and Gell-Mann strangeness (the isotopic space in this case is 4-dimensional). As an example of the application of the unified description of ordinary and isotopic space we can point to the possibility of interpreting the now familiar paradox regarding the nonconservation of parity for K mesons [8]. Using (14) and changing the value of λ_2 by unity (for $n = 8$) it is possible to compensate the parity change in Minkowski space by a parity change in isotopic spin space. Thus, from this point of view the paradox is explained by the fact that the parity of K mesons holds for inversion in a space which unites Minkowski space and isotopic spin space.

---

* The derived formulas give the Clebsch-Gordan coefficients which describe the reduction of the product of an arbitrary representation of the n-dimensional orthogonal group by an n-dimensional vector and which agree with the Γ_i.

** The ordinary parity operator T_0, which represents inversion in space-time, commutes with $I_{2k+2,\,2k+1}$.

In conclusion I wish to thank Academician N. N. Bogoliubov, Professor D. D. Ivanenko and M. L. Tsetlin for their interest and for fruitful discussions.

LITERATURE CITED

[1] A. Pais, Physica 19, 8, 69 (1953).

[2] D. Ivanenko and G. Sokolik, Doklady Akad. Nauk SSSR 97, 4 (1954).

[3] I. E. Tamm and V. L. Ginzburg, J. Exptl.-Theoret. Phys. (USSR) 17, 227 (1947).

[4] I. M. Gel'fand and M. L. Tsetlin, Doklady Akad. Nauk SSSR 71, 6 (1950).

[5] E. Cartan, Theory of Spinors (Foreign Lit. Press, 1947), Russian translation from French.

[6] B. L. Van der Waerden, Die gruppentheoretische Methode in der Quantenmechanik (Berlin, 1932).

[7] I. M. Gel'fand and A. M. Iaglom, J. Exptl.-Theoret. Phys. (USSR) 18, 703 (1948).

[8] T. D. Lee, and C. N. Yang, Phys. Rev. 102, 1, 290 (1956).

M. V. Lomonosov Moscow State University

Received February 12, 1957.

DISTRIBUTION FUNCTIONS FOR A CLASSICAL ELECTRON GAS

S. V. Tiablikov and V. V. Tolmachev

(Presented by Academician N. N. Bogoliubov December 27, 1957)

For gases in statistical equilibrium it is important to calculate the binary distribution function or, as it is sometimes called, the radial distribution function. Effective methods of constructing such functions have been proposed by N. N. Bogoliubov [1] and are well known.

For a Coulomb interaction between the particles an expansion in the small parameter v/r_d^3, [where v is the volume per particle, r_d is the Debye radius ($1/r_d^2 = 4\pi e^2/v\theta$; e is the particle charge; $\theta = kT$; T is the absolute temperature)], was used in [1] to obtain the Debye expression for the radial function:

$$G(r) = 1 - \frac{v}{r_d^3}\frac{r_d}{r}e^{-r/r_d},$$

which is a good representation of its behavior at large distances. At small distances, however, (1) becomes negative as the correction term exceeds the principal term; this makes it necessary to improve the convergence of the expansion at small distances.

A number of attempts have been made in this direction [2]; these consist essentially of finding some way of replacing the Coulomb interaction by some other interaction which does not lead to the same difficulties. It seems to us that such attempts, although they are of some value for specific calculations, do not deal with the causes of the difficulty of constructing a radial function for systems with pure Coulomb interaction. It is our purpose here to improve the convergence of Bogoliubov's expansion at small distances.

For G(r), Bogoliubov approximated the ternary distribution function by means of the product of three binary distributions and obtained the following set of nonlinear integral equations [1]:

$$W(|q|) = \Phi(|q|) + \frac{1}{v}\int dq_1\,\{G(|q_1|) - 1\}\int\limits_{\infty}^{|q-q_1|} dr\,G(r)\frac{d\Phi(r)}{dr}; \tag{2}$$

$$G(|q|) = \exp\left\{-\frac{1}{\theta}W(|q|)\right\}$$

with respect to the functions G and W, where $\Phi(|q|) = \frac{e^2}{|q|}$.

We substitute for the unknown functions

$$G(|q|) = e^{-\bar{\Phi}(|q|)/\theta}C(|q|); \quad W(|q|) = \bar{\Phi}(|q|) + V(|q|), \tag{3}$$

where $\bar{\Phi}(r)$ is a function of which we at present require that when $r \to 0$, $\bar{\Phi}(r) \sim e^2/r$. Equation (2) then becomes

$$V(|q|) = \Phi(|q|) - \overline{\Phi}(|q|) + \\ + \frac{1}{v}\int dq_1 \{e^{-\overline{\Phi}(|q_1|)/\theta} C(|q_1|) - 1\} \int\limits_{\infty}^{|q-q_1|} dr \frac{d\Phi(r)}{dr} e^{-\overline{\Phi}(r)/\theta} C(r); \\ C(|q|) = \exp\left\{-\frac{1}{\theta} V(|q|)\right\}. \tag{4}$$

For the solution of these equations we use the "plasma" expansion [1], that is, we set

$$\frac{1}{\theta}\Phi(|q|) = v\psi(|q|); \quad \frac{1}{\theta}\overline{\Phi}(|q|) = v\overline{\psi}(|q|), \tag{5}$$

and we seek C and V as power series in v:

$$C(|q|) = C_0(|q|) + vC_1(|q|) + v^2C_2(|q|) + \ldots; \\ V(|q|) = V_0(|q|) + vV_1(|q|) + v^2V_2(|q|) + \ldots \tag{6}$$

The zero approximation equations are of the form

$$V_0(|q|) = \theta\int dq_1 \{C_0(|q_1|) - 1\} \int\limits_{\infty}^{|q-q_1|} dr \frac{d\psi(r)}{dr} C_0(r); \tag{7}$$

$$C_0(|q|) = \exp\left\{-\frac{1}{\theta} V_0(|q|)\right\}.$$

These obviously possess the solution

$$V_0(|q|) = 0; \quad C_0(|q|) = 1. \tag{8}$$

Taking account of (8) the first approximation equations are

$$V_1(|q|) = \theta\{\psi(|q|) - \overline{\psi}(|q|)\} + \\ + \theta\int dq_1 \{C_1(|q_1|) - \overline{\psi}(|q_1|)\}\psi(|q - q_1|); \\ C_1(|q|) = -\frac{1}{\theta} V_1(|q|). \tag{9}$$

Hence, we obtain for the first order correction

$$C_1(|q|) = \overline{\psi}(|q|) - \frac{1}{4\pi r_d^2}\frac{e^{-|q|/r_d}}{|q|}. \tag{10}$$

We now obtain $\overline{\psi}$ by letting the first order correction C_1 vanish; then

$$\overline{\Phi}(|q|) = \frac{e^2}{|q|} e^{-|q|/r_d}, \tag{11}$$

that is, $\overline{\Phi}(|q|)$ is a Coulomb potential with Debye screening.

The solution of the second approximation equation is

$$C_2(|q|) = -\frac{1}{2}\int dq_1' \overline{\psi}(|q-q_1|)\,\overline{\psi}^2(|q_1|) - $$

$$-\int dq_1 \overline{\psi}(|q-q_1|) \int\limits_{\infty}^{|q_1|} dr \frac{d\psi(r)}{dr} \overline{\psi}(r) +$$

$$+\int dq_2 \overline{\psi}(|q-q_2|) \int dq_1 \overline{\psi}(|q_2-q_1|) \int\limits_{\infty}^{|q_1|} dr \frac{d\psi(r)}{dr} \overline{\psi}(r). \tag{12}$$

It is easily seen that the correction C_2 is finite for all $\underline{q}$ because although the first two integrals in this equation diverge for small $\underline{q}$ they cancel each other and the last integral is finite for small $\underline{q}$.

Neglecting corrections of the second and higher approximations we obtain for the radial function the expression

$$G(r) = \exp\left\{-\frac{e^2}{\theta}\frac{1}{r} e^{-r/r_d}\right\}. \tag{13}$$

This expression for G becomes Equation (1) at large distances, and at small distances it becomes the Boltzmann equation $G(r) \sim \exp\left\{-\frac{e^2}{\theta r}\right\}$.

We shall show that (13) can be obtained directly, without use of the ternary approximation, from the set of equations for the distribution functions F_s [1]:

$$\frac{\partial F_s}{\partial q_1^\alpha} + \frac{1}{\theta}\frac{\partial U_s}{\partial q_1^\alpha} F_s + \frac{1}{\theta v}\int \frac{\partial \Phi(|q_1 - q_{s+1}|)}{\partial q_1^\alpha} F_{s+1}\, dq_{s+1} = 0 \quad (s = 1, 2, \ldots) \tag{14}$$

by observing the conditions for weakening of correlation and the normalization of the functions F_s. We substitute for the unknown functions F_s

$$F_s = e^{-\overline{U}_s/\theta} C_s, \tag{15}$$

where $\overline{U}_s = \sum\limits_{(1<i<j<s)} \overline{\Phi}(|q_i - q_j|)$; $\overline{\Phi}(r)$ for $r \to 0$ is of the order e^2/r. For C_s we obtain the equations

$$\frac{\partial C_s}{\partial q_1^\alpha} + \frac{1}{\theta}\left(\frac{\partial U_s}{\partial q_1^\alpha} - \frac{\partial \bar{U}_s}{\partial q_1^\alpha}\right) C_s + \tag{16}$$

$$+ \frac{1}{\theta v}\int \frac{\partial \Phi(|q_1 - q_{s+1}|)}{\partial q_1^\alpha} \exp\Big[-\frac{1}{\theta}\sum_{(1<i<s)} \bar{\Phi}(|q_i - q_{s+1}|)\Big] C_{s+1}\, dq_{s+1} = 0$$

with similar conditions for weakening of correlation and normalization.

Following [1] we use the "plasma" expansion for the solution of (16) and substitute accordingly

$$\frac{1}{\theta}\Phi(r) = v\psi(r); \quad \frac{1}{\theta}\bar{\Phi}(r) = v\bar{\psi}(r), \tag{17}$$

while the functions C_s are sought in the form

$$\begin{aligned} &C_1(q) = g_1(q); \\ &C_2(q_1, q_2) = g_1(q_1)\, g_1(q_2) + v g_2(q_1, q_2); \\ &C_3(q_1, q_2, q_3) = g_1(q_1)\, g_1(q_2)\, g_1(q_3) + \\ &\qquad + v\{g_2(q_1, q_2)\, g_1(q_3) + g_2(q_2, q_3)\, g_1(q_1) + g_2(q_3, q_1)\, g_1(q_2)\} + \\ &\qquad + v^2 g_3(q_1, q_2, q_3), \end{aligned} \tag{18}$$

with the g_s to be obtained as power series in v.

We note that by virtue of the spatial homogeneity of the problem $g_1(q) = 1$, $g_2(q_1, q_2) = g_2(|q_1 - q_2|)$, so that the first equation of (16) is satisfied identically. For $g_2^0(|q|)$ we obtain

$$\frac{\partial g_2^0(|q|)}{\partial q^\alpha} + \frac{\partial \psi(|q|)}{\partial q^\alpha} - \frac{\partial \bar{\psi}(|q|)}{\partial q^\alpha} + \tag{19}$$

$$+ \int dq' \, \frac{\partial \psi(|q - q'|)}{\partial q^\alpha} \left(g_2^0(|q'|) - \bar{\Psi}'(|q'|)\right),$$

with the solution

$$g_2^0(|q|) = \bar{\Phi}(|q|) - \frac{1}{4\pi r_d^2}\frac{1}{|q|} e^{-|q|/r_d}, \tag{20}$$

which agrees identically with (10) and consequently leads for the radial function to (13), neglecting corrections of the order v^2 and higher.

We can expect that these considerations can be applied with some modifications to the problem of a system of charged particles of different signs.

In conclusion we take this opportunity to thank Academician N. N. Bogoliubov for valuable discussions.

LITERATURE CITED

[1] N. N. Bogoliubov, Problems of Dynamical Theory in Statistical Physics (Moscow, 1946).

[2] A. E. Glauberman, Doklady Akad. Nauk SSSR 78, 883 (1951); A. E. Glauberman and I. R. Iukhnovskii, J. Exptl.-Theoret. Phys. (USSR) 22, 562, 572 (1952); I. R. Iukhnovskii, J. Exptl.-Theoret. Phys. (USSR) 27, 690 (1954).

V. A. Steklov Mathematics Institute,
Academy of Sciences, USSR.

Received December 14, 1956.

SOVIET PHYSICS – "DOKLADY" VOL. 2, NO. 3 May - June, 1957

(Translation of all papers in the "Physics" Sections of the Proceedings of the Academy of Sciences of the USSR, Vol. 114, Nos. 1-6, published by the American Institute of Physics, February 1958).

CONTENTS

	Page	Russian Issue No.	Russian Page
The Influence of Chemical Bonds on the Fine Structure of Titanium $K\beta$ Lines in Compounds. E. E. Vainshtein and Iu. N. Vasil'ev	207	1	53
On the Calculation of the Photoelastic Coefficient of Polymers. Iu. Ia. Gotlib	210	1	57
Energy Level Shift of Spin 1/2 Particles in a Coulomb Field. G. A. Zaitsev	214	1	61
Temperature Dependence of the g-Factor and Relaxation Time in Ferromagnetic Resonance of Some Ferrites. A. P. Komar and N. I. Krivko	217	1	64
Calculation of the Anisotropy of Diamagnetic Susceptibility of Aromatic Molecules with a Metal Molecule Model. T. K. Rebane	223	1	70
On the Relation Between the Electrical Properties of Crystals and the Lattice Parameters. V. A. Presnov and V. I. Haman	220	1	67
The Influence of Gravitation on the Propagation of Light. G. V. Skrotskii	226	1	73
On the Causes of Ultrasonic Distension of Liquid Surfaces. L. D. Rozenberg and L. O. Makarov	230	2	275
On Allowed Transformations of the Equations for Particles with Higher Spins. E. E. Fradkin and S. V. Izmailov	232	2	277
The Excitation of Hypersonic Frequencies in Quartz. K. N. Baranskii	237	3	517
The Absorption of Light by CdS Crystals. V. L. Broude, V. V. Eremenko and E. I. Rashba	239	3	520
Concentration Dependence of the Absorption Spectra of Organic Vapors. B. S. Neporent and V. P. Klochkov	242	3	524
On the Multiple Excitation of Atoms. K. I. Rozgachev and V. A. Fabrikant	246	3	528
The Relativistic Collision Integral. N. A. Chernikov	248	3	530
The Titanium $K\beta$ Group in Titanium Carbide. E. E. Vainshtein and Iu. N. Vasil'ev	251	4	741
The Luminescence of Trivalent Uranium. L. N. Galkin and P. P. Feofilov	255	4	745
An Experimental Study of the Relation Between the Speed of Highly Elastic Rupture and the Strain Rate. V. E. Gul' and G. P. Krutetskaia	258	5	973
The Luminescence of Zinc Oxide-Boric Oxide Phosphors. Iu. S. Leonov	261	5	976
The Relation Between the Number of Shower Particles and the Atomic Number of a Disintegrating Nucleus. Zh. S. Takibaev	265	5	980
On the Pulsations of a Plasma Filament. A. G. Kulikovskii	269	5	984

(continued)

CONTENTS (continued)

	Page	Russian Issue No.	Russian Page
Oscillations of an Infinite Cylinder of Gas Acted on by its Own Gravity and a Magnetic Field. I. M. Iavorskaia	273	5	988
On the Statistical Theory of Crystallization. E. A. Arinshtein	277	6	1189
The $L\beta_3$ and $L\beta_4$ Lines of Germanium. G. P. Borovikova and M. I. Korsunskii . .	281	6	1192
The Effect of Neutron Irradiation on the Martensite Transformation. A. I. Zakharov and O. P. Maksimova	283	6	1195
The Quantitative Study of Latent Image Formation by Ionizing Particles. A. L. Kartuzhanskii	287	6	1199
The Spectral Response Curves for Photoconductivity in CdS Single Crystals. V. E. Lashkarev, E. A. Sal'kov, G. A. Fedorus and M. K. Sheinkman. . . .	291	6	1203
On the Relationship Between Ordinary Space and Isotopic Spin Space. G. A. Sokolik.	294	6	1206
Distribution Functions for a Classical Electron Gas. S. V. Tiablikov and V. V. Tolmachev	299	6	1210

SIGNIFICANCE OF ABBREVIATIONS MOST FREQUENTLY ENCOUNTERED IN SOVIET PHYSICS PERIODICALS

AN SSSR	*Academy of Sciences, USSR*
FIAN	*Physics Institute, Academy of Sciences USSR*
GITI	*State Scientific and Technical Press*
GITTL	*State Press for Technical and Theoretical Literature*
GOI	*State Optical Institute*
GONTI	*State United Scientific and Technical Press*
Gosenergoizdat	*State Power Press*
Gosfizkhimizdat	*State Physical Chemistry Press*
Gozkhimizdat	*State Chemistry Press*
GOST	*All-Union State Standard*
Goztekhizdat	*State Technical Press*
GTTI	*State Technical and Theoretical Press*
GUPIAE	*State Office for Utilization of Atomic Energy*
IF KhI	*Institute of Physical Chemistry Research*
IFP	*Institute of Physical Problems*
IL	*Foreign Literature Press*
IPF	*Institute of Applied Physics*
IPM	*Institute of Applied Mathematics*
IREA	*Institute of Chemical Reagents*
ISN (Izd. Sov. Nauk)	*Soviet Science Press*
IIaP	*Institute of Nuclear Studies*
Izd	*Press (publishing house)*
KISO	*Solar Research Commission*
LETI	*Leningrad Electrotechnical Institute*
LFTI	*Leningrad Institute of Physics and Technology*
LIM	*Leningrad Institute of Metals*
LITMiO	*Leningrad Institute of Precision Instruments and Optics*
Mashgiz	*State Scientific-Technical Press for Machine Construction Literature*
MATI	*Moscow Aviation Technology Institute*
MGU	*Moscow State University*
Metallurgizdat	*Metallurgy Press*
MOPI	*Moscow Regional Institute of Physics*
NIAFIZ	*Scientific Research Association for Physics*
NIFI	*Scientific Research Institute of Physics*
NIIMM	*Scientific Research Institute of Mathematics and Mechanics*
NII ZVUKSZAPIOI	*Scientific Research Institute of Sound Recording*
NIKFI	*Scientific Institute of Motion Picture Photography*
OIIaI	*Joint Institute of Nuclear Studies*
ONTI	*United Scientific and Technical Press*
OTI	*Division of Technical Information*
OTN	*Division of Technical Science*
RIAN	*Radium Institute, Academy of Sciences of the USSR*
SPB	*All-Union Special Planning Office*
Stroiizdat	*Construction Press*
URALFTI	*Ural Institute of Physics and Technology*

NOTE: Abbreviations not on this list and not explained in the translation have been transliterated, no further information about their significance being available to us.—*Publisher.*

The expanded program of the American Institute of Physics comprises translation of four leading Soviet physics journals, as listed below. These translations, by competent, qualified scientists, provide all research laboratories and libraries with accurate and up-to-date information of the results of research in the U.S.S.R.

Soviet Physics — Technical Physics

A translation of the "Journal of Technical Physics" of the Academy of Sciences of the U.S.S.R. The translation began with the 1956 issues, and is being continued. Twelve issues per year, approximately 3,000 Russian pages. Annually $90.00 domestic, $95.00 foreign.

Soviet Physics — Acoustics

A translation of the "Journal of Acoustics" of the Academy of Sciences of the U.S.S.R. The translation began with the 1955 issues. Four issues per year, approximately 400 Russian pages. Annual price, beginning with the 1957 issues, $12.00 domestic, $14.00 foreign. Prices for each volume prior to 1957, $20.00 domestic, $22.00 foreign.

Soviet Physics — "Doklady"

A translation of the "Physics Section" of the Proceedings of the Academy of Sciences of the U.S.S.R. The translation began with the 1956 issues. Six issues per year, approximately 900 Russian pages. Annually $25.00 domestic, $27.50 foreign.

Soviet Physics — JETP

A translation of the "Journal of Experimental and Theoretical Physics" of the Academy of Sciences of the U.S.S.R. Translation began with the 1955 issues. Twelve issues per year, approximately 4,000 Russian pages. Annual price, beginning with the 1957 issues, $75.00 domestic, $79.00 foreign. Prices for back volumes may be obtained from the American Institute of Physics upon request.

Subscriptions should be addressed to the American Institute of Physics, 335 East 45th Street, New York 17, N. Y.